LEPTON FLAVOUR NON-UNIVERSALITY

FROM EFFECTIVE FIELD THEORY TO EXTENDED GAUGE MODELS

Zur Erlangung des akademischen Grades eines

DOKTORS DER NATURWISSENSCHAFTEN

von der KIT-Fakultät für Physik des
Karlsruher Instituts für Technologie (KIT)

genehmigte

DISSERTATION

von

M.Sc. Marta Moscati
aus Neapel

Tag der mündlichen Prüfung: 08.11.2019

Referent: Prof. Dr. Ulrich Nierste (Karlsruhe)
Korreferent: Prof. Dr. Thomas Schwetz-Mangold (Karlsruhe)
Betreuende Wissenschaftlerin: Dr. Monika Blanke (Karlsruhe)

This work is licensed under a Creative Commons "Attribution-NonCommercial-ShareAlike 4.0 International" license.

"*Dal* Libro del Grande Bastardo,
capitolo 7

Se vedi uno stregone con un copricapo di piume di ororoko che cammina sopra i tetti, fa volare le edicole e fa cadere polvere d'oro sui passanti, può darsi che la tua vita stia per cambiare, ma molto più probabilmente stai vedendo un video musicale. Se vedi una persona che non si rassegna alle cerimonie dei tempi, che prezioso e invisibile aiuta gli altri anche se questo non verrà raccontato in pubbliche manifestazioni, che non percorre i campi di battaglia sul bianco cavallo dell'indignazione, ma con pietà e vergogna cammina tra i feriti, ecco uno stregone."

Stefano Benni,
La compagnia dei celestini (1992)

A tutti gli stregoni.

Abstract

The experimental averages of the ratios $\mathcal{R}(D^{(*)})$, testing lepton flavour universality in the decays $B \to D^{(*)}\ell\nu$, exceed the Standard Model prediction by 1.4σ and 2.5σ respectively. Taking correlations into account, these tensions result in a combined difference above 3.1σ. This thesis focuses on analysing possible scenarios of Physics beyond the Standard Model to solve this tension, following a bottom-up approach: the first part is focused on a global analysis of the $b \to c\tau\nu$ data, including the newly released polarisation observables, in terms of an effective field theory, considering scenarios with a single additional particle mediating the decay. This analysis allows us to infer which virtual particle is more likely to be responsible of the tension with the data. Motivated by an $SO(10)$ grand unified theory with an intermediate Pati-Salam theory, we then focus on one of the scenarios preferred by the effective field theory fit, namely the one with a scalar leptoquark S_1. We update the evaluation of the effects of this particle on the coupling of leptons to the Z gauge boson, including effects coming from electroweak renormalisation, and include the Z-pole observables in the fit of the Yukawa coupling to $b \to c\ell\nu$ data. Finally, we discuss in more detail the possible UV completion of a model containing the scalar leptoquark S_1.

Acknowledgements

My first thank you goes to Ulrich Nierste, for giving me the opportunity to pursue a PhD here, in the first place, and even to prolong it to a bit more than three years. Even more, I would like to thank him for suggesting the topic of research, as well as for supervising and guiding my work, although leaving me the freedom and ease to work at my own pace.

I also want to thank Thomas Schwetz-Mangold for agreeing on being the second supervisor of this dissertation.

I am infinitely grateful to Monika Blanke, for her advise throughout these years, for the fruitful discussions, for always being there when I needed help, and finally for being a role model for me.

Thank you to Monika Blanke, Stefan de Boer, Andreas Crivellin, Teppei Kitahara, Ulrich Nierste and Ivan Nišandžić, for the intense and fruitful discussions that led to our work in References [1, 2].

I want to thank Monika, Simon and Christoph, that went through this thesis already during the draft phase. Their insight and comments were very helpful in improving this work.

A big thank you goes to my office mates – in order of appearance – Christoph, Simon, Mustafa and Abdur, for the enjoyable atmosphere during these years. With this respect, I would also like to thank the members of TTP and ITP with whom I had a good time.

I also want to thank Martina Schorn, Isabelle Junge and Barbara Lepold for the excellent administrative support.

Then there is a series of people without whom I would have gone insane after no time. First of all, the Patio family – Weinan, Jasmin, Max, Stefan, Tobi and David. Thank you for creating that magic atmosphere that reigns at our place. Thank you for all the deep and all the stupid discussions, for all the music we made and for all the music we listened to, for the daily tasty culinary festivals and for the outdoor trips.

Thanks to Simon, for cheering me up in my moments of distress, for motivating me to go a bit further than my comfort zone when I needed it and for always finding time to discuss with me – be it Physics or not.

I'd like to thank Luca for being close to me despite the kilometres separating us. A big thank you to all those that came and check how I was doing here, and provided me with numerous *pacchi da giù* – mamma, papà, Luca, Stefano, Mariantonia, Ferdinando, Antonietta, Pippo (whom I'd also like to thank for being my personal source of great reading material!), Stelvio, zia Eva and Marco. And special thanks to Bart for the frequent Franco-German cultural exchanges!

I still believe that without the early lessons on dinosaurs I would not have made it, that's why my brother Stefano deserves another thank you.

Finally, I want to thank my three *Genitori*: Dr Lorenzo Genitori, without whom everything I do would have been – if not impossible – at least extremely more painful.

And, of course, my true *Genitori*, mamma e papà. Grazie per tutto l'affetto. Grazie per tutto il supporto nelle mie scelte e per la vostra apertura nel discuterle criticamente ma senza mai mettermi sotto pressione. Il mio giudizio sarà di parte, ma ci tengo a dirvi che non avrei potuto augurarmi una mamma ed un papà migliori di voi.

Contents

1 Introduction **1**

2 Setting the scene **3**

2.1 Flavour physics in the Standard Model 3

2.2 Overview and current status of the $B \to D^{(*)}\ell\nu$ anomalies 6

2.3 Effective field theory 7

3 New physics scenarios for $b \to c\tau\nu$ data **10**

3.1 Effective field theory for $\mathcal{R}(D^{(*)})$ 10

3.2 Single-mediator scenarios of new physics 13

3.3 Fit of $b \to c\tau\nu$ data 17

3.3.1 One-dimensional scenarios 22

3.3.2 Two-dimensional scenarios 24

3.3.3 Summary of the effective field theory analysis 28

4 The scalar leptoquark S_1 **31**

4.1 Motivation 31

4.2 Leptoquark Lagrangian 33

4.3 Modification of the $Z\ell\ell$ coupling 35

4.3.1 Effects from electroweak renormalisation 36

4.4 Phenomenology 39

4.4.1 Fitting scenarios 40

4.4.2 Experimental inputs 41

4.4.3 Fit results 47

4.5 Summary 59

5 Towards a grand unified theory **61**

5.1 The Pati-Salam model 62

5.1.1 Why $SU(4)_\mathrm{c} \times SU(2)_\mathrm{L} \times SU(2)_\mathrm{R}$? 62

5.1.2 Pati-Salam gauge bosons and $\mathcal{R}(D^{(*)})$ 66

5.1.3 Pati-Salam scalars and $\mathcal{R}(D^{(*)})$ 68

5.1.4 An $SO(10)$-inspired scalar content 69

5.2 Scalar leptoquark solution to $\mathcal{R}(D^{(*)})$ within Pati-Salam 75

5.3 Summary 77

6 Conclusion **79**

A Technical details about the $B \to D^{(*)}\ell\nu$ observables **82**

A.1 Helicity amplitudes 82

A.2 Form factors 85

A.2.1 $B \to D\ell\nu$ 85

A.2.2 $B \to D^*\ell\nu$ 85

B Summary of $b \to s\ell\ell$ data **86**

Bibliography **88**

CHAPTER 1

Introduction

> "Fluctuations are aching my soul
> Expectation is taking its toll"
>
> *Tame Impala,*
> *Expectation (2010)*

The Standard Model (SM) of Particle Physics well deserves its two capital letters for the accurate description and correct predictions of data collected at experimental facilities and accelerators for decades, with its triumph in the discovery of the Higgs boson in 2012. Nonetheless it is believed not to be the end of the story, both for its inadequacy in describing some of the phenomena we observe and for some unsatisfactory conceptual aspects.

In the first category fall the description of the largest fraction of gravitationally interacting matter – namely *dark matter*, constituting more than 84% of the total matter in the Universe – as well as the description of neutrino masses, which are well established to be nonvanishing due to the oscillation of their flavour eigenstates. Another aspect of our Universe that the SM is not able to account for is the baryon-antibaryon asymmetry. Furthermore, on a more fundamental level, it does not comprise a description of Gravity in terms of a Quantum Field Theory.

In addition to its limits, some aspects of the SM are often considered to be unsatisfactory from conceptual or aesthetical points of view. For instance, this is the case for the strong CP problem – i.e. the smallness of the θ parameter in the QCD Lagrangian – , and for the so-called flavour puzzle, the observed hierarchy among fermion masses. Finally, in scenarios where the solution to the aforementioned problems involves the addition of particles with masses well above the Electroweak (EW) scale, the coupling of these particles with the SM Higgs gives rise to the hierarchy problem, i.e. the need of fine-tuning in order to get rid of

the new physics (NP) radiative corrections and keep the Higgs mass at the EW scale.

The path to establishing the presence of NP is twofold. On one side there is the possibility of observing directly the NP particles on-shell. This is the approach pursued at accelerators like the Large Hadron Collider (LHC) at CERN, by the CMS and ATLAS collaborations, and requires great technological effort in order to achieve the centre of mass energy necessary for the production of the particles.

The direct production mechanism so far has revealed nothing that the SM cannot account for. This would indicate, if we believe that the couplings of the additional particles are not very small, that the energy scale of NP lies well above the EW one, and that the additional particles are much heavier than the SM ones.

On the other side, we can establish the presence of NP by measuring, with further increasing precision, observables to which the NP particles can contribute as quantum effects, i.e. as virtual off-shell particles. Historically, the latter approach has been proven successful in at least two cases: in the prediction of the existence of a fourth quark, namely the charm quark, in order to account for the smallness of the observed flavour changing neutral currents (FCNC) through the Glashow-Iliopoulos-Maiani (GIM) mechanism and in the prediction of the existence of a third generation of quarks, needed to account for the observed CP violation in the weak interactions.

Although most of the data we collected is well in agreement with the SM predictions, there is indeed some tension in the data coming from decays of meson involving a b quark, both in the neutral-current decays $B \to K^{(*)}\ell\ell$ and in the charged-current decays $B \to D^{(*)}\ell\nu$. The interest in these disagreements, usually referred to as B anomalies, is further increased by the fact that for both processes, the tension shows up in quantities testing lepton flavour universality (LFU), i.e. the feature of the SM gauge weak interaction of having universal coupling with respect to the lepton generation.

The work presented in this thesis focuses on the description of the anomalous data in the $B \to D^{(*)}\ell\nu$ decays in terms of NP. The rest of the thesis is organised as follows. In Chapter 2 we briefly review the flavour structure of the SM, the current status of the $B \to D^{(*)}\ell\nu$ anomaly as well as introducing the tool of effective field theories (EFT). The remaining chapters represent the core results of the work.

Our initial point of view in Chapter 3 closely follows the concept of Fermi interaction: under the assumption of a heavy NP scale, we analyse and compare in terms of EFT scenarios of NP in which a single additional particle is responsible for the anomaly. The analysis assumes that this particle couples mostly to third generation fermions, and is performed by fitting all the data at our disposal for the transition $b \to c\tau\nu$. In Chapter 4 we consider one of the scenarios that seems to be favoured by the data and take it a step further towards a UV completion: we introduce a scalar leptoquark (LQ), specifying its kinetic term as well as its Yukawa couplings to SM fields, and evaluate the effect of this particle on the coupling of the Z to charged leptons, with the novel inclusion of EW renormalisation effects, previously not considered in the literature. We determine the parameter space preferred for this model, extending our fit with the inclusion of data from Z pole observables. The final part of the work, Chapter 6, is devoted to the study of an extended gauge model accounting for the existence of the LQ considered.

CHAPTER 2

Setting the scene

In this chapter we review the flavour aspects of the SM and the basic principles of EFT. We also review the current experimental status of the anomaly concerning the $b \to c\tau\nu$ transition. The chapter does not intend to give a complete description of these topics, but rather to introduce the reader to those aspects that will be needed in the rest of this work. For a more complete description, the interested reader is referred to the references within each section.

2.1 Flavour physics in the Standard Model

The SM is based on the gauge group $SU(3)_{\mathrm{c}} \times SU(2)_{\mathrm{L}} \times U(1)_Y$. Particle fields transform as representations under this group. Throughout this thesis, these representations will be marked as $(C, L)_Y$, where C is either an integer or a barred integer referring to the representation under the colour group $SU(3)_{\mathrm{c}}$, L is an integer referring to the representation under the chiral $SU(2)_{\mathrm{L}}$ group and Y is a rational number denoting the $U(1)_Y$ hypercharge.

The fermionic content of the SM comes in three different copies[1]. This feature of the SM, together with the fact that the left- and right-handed components of quarks, as well as of charged leptons, belong to different representations under the SM gauge group, is the origin of the flavour changing couplings with the W boson. Let us focus first on the quark flavour sector. Throughout this section, indices will always refer to flavour space, i.e. run through the three generations.

[1] A compact review of flavour physics in the SM can be found in Reference [3]

The quarks transform under the SM group as

$$Q_{\mathrm{L}}^{i} = \begin{pmatrix} u_L^i \\ d_L^i \end{pmatrix} \sim (3,2)_{1/6} \qquad u_{\mathrm{R}}^{i} \sim (3,1)_{2/3} \qquad d_{\mathrm{R}}^{i} \sim (3,1)_{-1/3} \tag{2.1}$$

where $i = 1, 2, 3$ is the index distinguishing the three flavour generations. These representations imply the following couplings with the charged gauge bosons

$$\mathcal{L} \supset \frac{g}{\sqrt{2}} \overline{u}_{\mathrm{L}}^{i} \gamma^{\mu} d_{\mathrm{L}}^{i} W_{\mu}^{+} + \text{h.c.}. \tag{2.2}$$

We see that each generation couples independently of the others, i.e. we are summing over equal indices i, a feature reminiscent of the fact that these couplings originate from the kinetic term of each field. Furthermore, this part of the Lagrangian of the quark sector features a global symmetry $U(3)_{Q_L} \times U(3)_{D_R} \times U(3)_{U_R}$. This means that under the transformations

$$Q_{\mathrm{L}}^{i} \to (U_Q)_{ij} Q_{\mathrm{L}}^{j}, \qquad u_{\mathrm{R}}^{i} \to (U_u)_{ij} u_{\mathrm{R}}^{j}, \qquad d_{\mathrm{R}}^{i} \to (U_d)_{ij} d_{\mathrm{R}}^{j}, \tag{2.3}$$

with $U_{Q,u,d}$ being three independent 3×3 unitary matrices, this part of the Lagrangian remains unchanged, since in each coupling the same unitary matrix appears with its hermitian conjugate.

If we now write down all the possible gauge-invariant terms including the Higgs doublet H as well, we get the Yukawa Lagrangian

$$\mathcal{L} \supset -(Y_d)_{ij} \overline{Q}_{\mathrm{L}}^{i} H d_{\mathrm{R}}^{j} - (Y_u)_{ij} \overline{Q}_{\mathrm{L}}^{i} \widetilde{H} u_{\mathrm{R}}^{j} + \text{h.c.}, \tag{2.4}$$

in which couplings among different generations are permitted by gauge invariance. After electroweak symmetry breaking (EWSB), these interactions give rise to the mass terms for quarks

$$\mathcal{L} \supset -(m_d)_{ij} \overline{d}_{\mathrm{L}}^{i} d_{\mathrm{R}}^{j} - (m_u)_{ij} \overline{u}_{\mathrm{L}}^{i} u_{\mathrm{R}}^{j} + \text{h.c.}, \tag{2.5}$$

which are not diagonal in the flavour basis, resulting in the fact that the physical particles, i.e. the mass eigenstates, do not coincide with single flavours separately. Using singular value decomposition, we can rewrite the mass terms as

$$\mathcal{L} \supset -\overline{d}_{\mathrm{L}} U_d M_d V_d^{\dagger} d_{\mathrm{R}} - \overline{u}_{\mathrm{L}} U_u M_u V_u^{\dagger} u_{\mathrm{R}} + \text{h.c.}, \tag{2.6}$$

where $U_{d,u}, V_{d,u}$ are unitary matrices in flavour space and $M_{d,u}$ are diagonal matrices. From Equation (2.6) we conclude that four unitary matrices are needed in order to obtain from the flavour eigenstates the mass eigenstates, given by

$$u'_{\mathrm{L}} = U_u^{\dagger} u_{\mathrm{L}}, \qquad d'_{\mathrm{L}} = U_d^{\dagger} d_{\mathrm{L}}, \qquad d'_{\mathrm{R}} = V_d^{\dagger} d_{\mathrm{R}}, \qquad u'_{\mathrm{R}} = V_u^{\dagger} u_{\mathrm{R}}. \tag{2.7}$$

Three out of these four transformations are unphysical, due to the global flavour symmetry of Equation (2.3). In other words we can redefine the quark fields with the substitutions

$$Q_{\mathrm{L}} \to U_d Q_{\mathrm{L}}, \qquad d_{\mathrm{R}} \to V_d d_{\mathrm{R}}, \qquad u_{\mathrm{R}} \to V_u u_{\mathrm{R}}, \tag{2.8}$$

without affecting the kinetic term. With this redefinition, the mass eigenstates are given by

$$u'_{\mathrm{L}} = U_u^\dagger U_d u_{\mathrm{L}}, \qquad d'_{\mathrm{L}} = d_{\mathrm{L}}, \qquad d'_{\mathrm{R}} = d_{\mathrm{R}}, \qquad u'_{\mathrm{R}} = u_{\mathrm{R}}. \tag{2.9}$$

This implies that in terms of mass eigenstates the gauge interaction part of the Lagrangian will be

$$\begin{aligned} \mathcal{L} \supset & \frac{g}{\sqrt{2}} \overline{u'}_{\mathrm{L}} U_u^\dagger U_d \gamma^\mu d'_{\mathrm{L}} W_\mu^+ + \text{h.c.} \\ = & \frac{g}{\sqrt{2}} \overline{u'^i}_{\mathrm{L}} (U_u^\dagger U_d)_{ij} \gamma^\mu d'^j{}_{\mathrm{L}} W_\mu^+ + \text{h.c.} \end{aligned} \tag{2.10}$$

The matrix $V_{\mathrm{CKM}} = U_u^\dagger U_d$ in Equation (2.10) is the Cabibbo-Kobayashi-Maskawa (CKM) unitary matrix, parameterising the flavour changes in the charged current weak interactions[2].

In the lepton sector the situation is different due to the absence of right-handed neutrino fields. The flavour symmetry of the kinetic Lagrangian is $U(3)_{L_L} \times U(3)_{e_R}$, while the Yukawa coupling with the Higgs reads

$$\mathcal{L} \supset -(Y_\ell)_{ij} \overline{L}_{\mathrm{L}}^i H \ell_{\mathrm{R}}^j + \text{h.c.} \tag{2.11}$$

The diagonalisation of the mass term after EWSB introduces the two matrices U_ℓ, V_ℓ

$$\mathcal{L} \supset -\overline{\ell}_{\mathrm{L}} U_\ell^\dagger M_\ell V_\ell \ell_{\mathrm{R}} + \text{h.c.} \tag{2.12}$$

If we now redefine the lepton fields as

$$L_{\mathrm{L}} \to U_\ell L_{\mathrm{L}}, \qquad \ell_{\mathrm{R}} \to V_\ell \ell_{\mathrm{R}}, \tag{2.13}$$

we see that the unitary matrices U_ℓ, V_ℓ drop out from both the Yukawa and the gauge part of the Lagrangian, hence leading to a unit matrix in the couplings with the gauge bosons. This feature of the SM gauge interactions is often referred to as lepton flavour universality, and can be summarised by saying that in the SM the only feature that distinguishes charged leptons is their masses.

It is worth noticing that this pattern is only valid in absence of neutrino masses. The established presence of neutrino oscillations implies that the actual coupling with charged currents involves a matrix called the Pontecorvo-Maki-Nakagawa-Sakata (PMNS) matrix, analogous to the CKM matrix[3]. Throughout this thesis the neutrino fields will always indicate the flavour eigenstates, implicitly implying the presence of the PMNS matrix if one writes the coupling in the mass basis. Since the flavour of the neutrino in weak interactions is unobserved and the neutrino masses are irrelevant for the kinematics, this treatment is

[2]Our choice corresponds to the so-called down basis, in which flavour and mass eigenstates coincide for the down-type quarks. Analogously, in the up-type basis $Q_{\mathrm{L}} \to U_u Q_{\mathrm{L}}$. The two descriptions are physically completely equivalent.

[3]Depending on the actual mechanism underlying the generation of neutrino masses, the PMNS matrix may be not unitary.

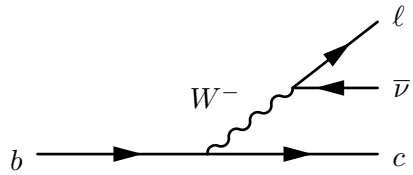

Figure 2.1: Feynman diagram for the tree-level $b \to c\ell\nu$ transition in the Standard Model.

not contradictory.

2.2 Overview and current status of the $B \to D^{(*)}\ell\nu$ anomalies

The charged weak interactions of the SM mediate at tree level the process[4] $b \to c\ell\nu$, as shown in Figure 2.1. As commented in Section 2.1, lepton flavour universality (LFU) is expected in the SM processes mediated by a W boson, which implies that the differences between the channels with $\ell = e, \mu, \tau$ arise only from phase space or helicity effects. Comparing the branching ratios for channels with different leptons constitutes, then, a test of LFU and a measurement of nonuniversal effects would be a clear sign of NP.

Due to colour confinement, the process $b \to c\tau\nu$ can only be observed in bound states of mesons, as in the decays $B \to D^{(*)}\ell\nu$, or baryons, as in the decays $\Lambda_b \to \Lambda_c\ell\nu$, in which the other quark(s) acts as a spectator quark(s). This implies the need of describing the hadronic transition, e.g. $B \to D$, in order to predict branching ratios. The hadronic part of the process is parameterised in terms of form factors.

In the case of the $B \to D^{(*)}$ transitions within the SM, the part of the decay rate which is not helicity-suppressed by the insertion of a m_ℓ^2 turns out to be independent of the lepton [4,5]. This implies that the dependence on hadronic form factors is significantly reduced if one considers the ratios

$$\mathcal{R}(D^{(*)}) \equiv \frac{\mathrm{BR}(B \to D^{(*)}\tau\nu)}{\mathrm{BR}(B \to D^{(*)}\ell\nu)} \tag{2.14}$$

instead of considering the individual branching ratios. Furthermore, each of the three branching ratios is proportional to the squared absolute value of the CKM matrix element, $|V_{cb}|^2$. In taking the ratio, this proportionality cancels out, hence resulting in a more precise prediction [4–11], not involving the uncertainties on V_{cb}.

The SM predictions of the two ratios have been evaluated by several authors; their computations differ in two aspects:

- the parameterisation used for the form factors, depending on the theory input used, such as the use or not of heavy quark effective theory (HQET) and the order of the

[4]Throughout the thesis, we will refer as $b \to c\ell\nu$ to both the processes $b \to c\ell^-\overline{\nu}$ and $\overline{b} \to \overline{c}\ell^+\nu$.

$\Lambda_{\rm QCD}/m_{b,c}$ expansion, or such as the use or not of QCD sum rules,

- the fitting procedure, namely if the form factor parameters are fitted to experimental data, to lattice data or to both.

A brief summary of these evaluations can be found in Reference [12], while for the single evaluations we refer the reader to References [5–8] for $\mathcal{R}(D)$, to References [4, 9] for $\mathcal{R}(D^*)$ and to References [10, 11] for combined predictions. The arithmetic average of these predictions gives [12]

$$\mathcal{R}_{\rm SM}(D) = 0.299 \pm 0.003, \qquad \mathcal{R}_{\rm SM}(D^*) = 0.258 \pm 0.005, \tag{2.15}$$

where the errors originate from the form factor uncertainty, neglecting the contribution from theoretical approximations such as the truncation of the HQET expansion.

The BaBar and Belle collaborations performed combined measurements of the two ratios, using hadronic or semileptonic tagging [13–19]; the LHCb collaboration measured $\mathcal{R}(D^*)$ using different decay modes to identify the τ [20–22]. The average of these measurements gives [12]

$$\mathcal{R}(D) = 0.340 \pm 0.027 \pm 0.013, \qquad \mathcal{R}(D^*) = 0.295 \pm 0.011 \pm 0.008, \tag{2.16}$$

where the uncertainties reflect the statistical and the systematic uncertainty respectively.

The average of the SM predictions in Equation (2.15) and the average of the experimental results in Equation (2.16) are in tension with each other, at 1.4σ for $\mathcal{R}(D)$ and at 2.5σ for $\mathcal{R}(D^*)$. Despite the fact that these tensions alone are not striking when considered separately, taking into account the correlation between them results in a difference of about[5] 3.1σ. Furthermore, several experiments have contributed to the anomaly and every individual measurement lies above the SM prediction. These considerations, together with the fact that LFU would be a clear sign of NP, attracted the attention of the community on these anomalies.

The Heavy Flavour Averaging Group [12] provides a plot that summarises most of the aspects considered in this Section. This plot is displayed in Figure 2.2.

2.3 Effective field theory

This section is a short introduction to the tool of EFT, used in Chapter 3. It is based on References [25–27], in which the reader can find a more detailed description.

EFTs are a tool to address problems where multiple energy scales are present. The underlying idea is that for a process at energy scale μ, short-distance contributions mediated by virtual particles of mass $M \gg \mu$ induce contributions that can be parameterised in terms of local interactions, obtained from an expansion in μ/M. The order $\mathcal{O}(\mu/M)$ at which the

[5] The authors of Reference [23] recently updated the SM predictions of the $\mathcal{R}(D^{(*)})$ ratios with the inclusion of all the $\mathcal{O}(1/m_c^2)$ terms of the HQET expansion. The tension of the experimental values with this updated theory prediction is at the level of 3.9σ [24].

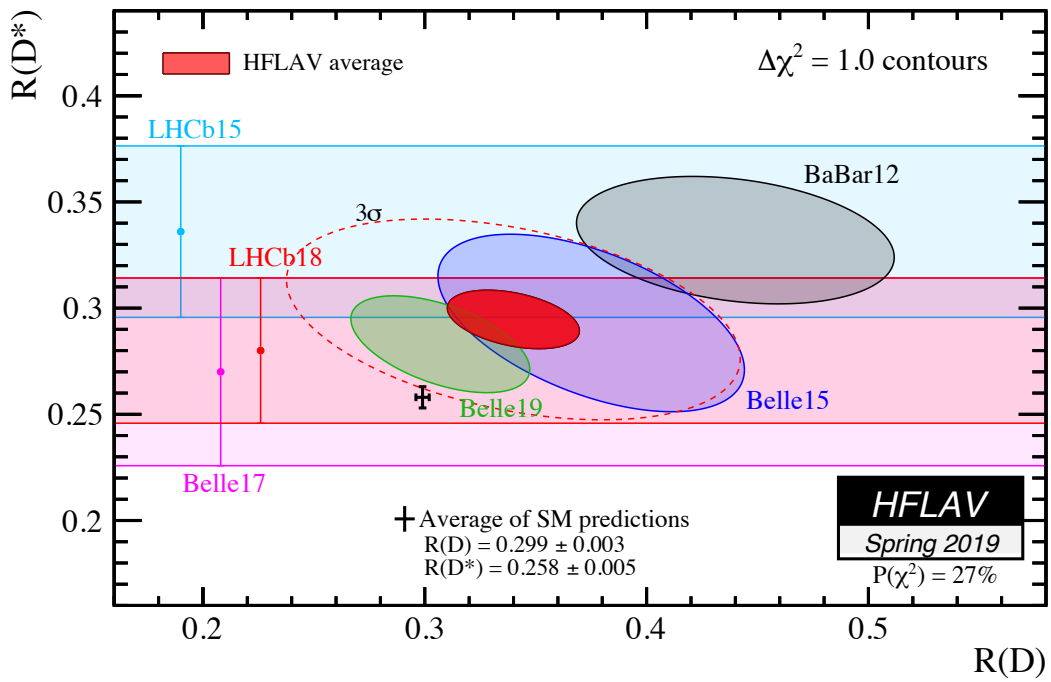

Figure 2.2: HFLAV [12] summary plot of the current status of the $\mathcal{R}(D^{(*)})$ Standard Model predictions and experimental results. The red ellipse shows the $\chi^2 = 1$ contour from experiments, while the black point with error bars represent the Standard Model predictions.

expansion is truncated is chosen accordingly to the precision required. Let us illustrate the use of EFT with an example.

Consider the Lagrangian

$$\mathcal{L} = \overline{\psi} i \partial\!\!\!/ \psi - m\overline{\psi}\psi + \frac{1}{2}(\partial_\mu \phi)^2 - \frac{M^2}{2}\phi^2 - g\phi\overline{\psi}\psi, \tag{2.17}$$

in which the fermion field is much lighter than the scalar one, i.e. $m \ll M$, and consider experiments performed at energy scales much below the scalar mass, $\mu \ll M$. In this regime, the initial and final states cannot involve scalar particles, since there is not enough energy to produce them on-shell. Nonetheless, the scalars can contribute as virtual off-shell intermediate state particles to processes having only fermions in the initial and final states.

With a formal approach in terms of path integrals, one can integrate over the ϕ field configurations. The resulting Lagrangian, written in terms of ψ fields only, contains nonlocal interactions. Assuming $M \gg m, \mu$, these interactions can be expanded up to arbitrary order, and this expansion brings us back to local operators. The coefficients of these operators are referred to as Wilson coefficients (WC). Higher order terms correspond to operators of higher mass dimension, with further increasing suppressions of $m, \mu/M$. We will not describe this procedure in detail, but it can be found in [25–27].

An equivalent procedure, closer to the one we will follow in Chapter 3, does not require

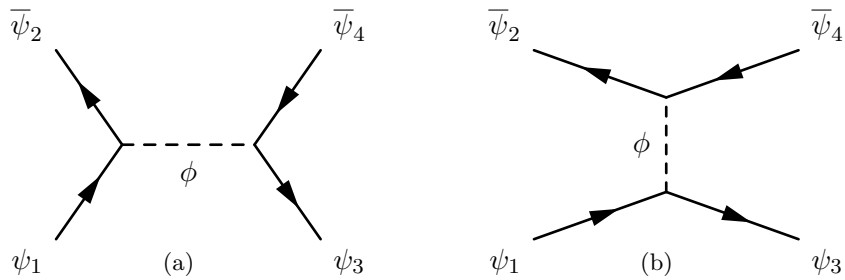

Figure 2.3: Feynman diagram for the scattering $\psi\overline{\psi} \to \psi\overline{\psi}$ in the full theory.

the formalism of path integrals. It is instead based on building a Lagrangian using only the fields that we are interested in, i.e. those that can be present in the initial and final states, and that respects the symmetries that have to be preserved at the energy scale of the process under consideration. Depending on the precision required, this is done up to operators of a specific mass dimension, i.e. having coefficients up to a specific order in $m, \mu/M$.

For the Lagrangian in Equation 2.17, our building block is the field ψ. We require the effective Lagrangian to be Lorentz invariant. Furthermore, the full Lagrangian has a global $U(1)$ symmetry, i.e. it is invariant under $\psi \to e^{i\theta}\psi$. We want to focus on the effects of ϕ that are leading in the expansion $m, \mu/M$. There are no operators of dimension five that respect the required symmetry. Instead, for operators of dimension six we can have the structures $(\overline{\psi}\Gamma\psi)(\overline{\psi}\Gamma\psi)$, where $\Gamma = 1, \gamma^\alpha, \sigma^{\alpha\beta}$ indicates a generic Lorentz structure. To determine which structures are actually induced by ϕ, and with which couplings, we compare the scattering process $\psi\overline{\psi} \to \psi\overline{\psi}$ in the full and the effective theory.

In the full theory, ϕ contributes to $\psi\overline{\psi}$ scattering via the diagrams in Figure 2.3. Expanding the propagators of the ϕ, we get the matrix element

$$\mathcal{M}_{\text{full}} \sim \frac{g^2}{M^2}(\overline{\psi}_3\psi_4)(\overline{\psi}_2\psi_1) + \frac{g^2}{M^2}(\overline{\psi}_3\psi_1)(\overline{\psi}_2\psi_4), \tag{2.18}$$

so we see that only scalar Lorentz structures, $\Gamma = 1$, arise. Up to dimension six, the effective Lagrangian will be

$$\mathcal{L} = \overline{\psi}i\partial\!\!\!/\psi - m\overline{\psi}\psi + \frac{c}{M^2}(\overline{\psi}\psi)(\overline{\psi}\psi). \tag{2.19}$$

In the EFT, the matrix element will be

$$\mathcal{M}_{\text{EFT}} \sim \frac{2c}{M^2}[(\overline{\psi}_3\psi_4)(\overline{\psi}_2\psi_1) + (\overline{\psi}_3\psi_1)(\overline{\psi}_2\psi_4)]; \tag{2.20}$$

comparing with Equation (2.18) we find $c = g^2/2$.

This simple example illustrates the procedure we will follow in the next Chapter to describe possible effects of a NP particle in $b \to c\tau\nu$ processes. A final remark is in order: as explained in [25, 27], if we build an effective Lagrangian using SM fields, interacting strongly and/or electroweakly, the higher order corrections of these interactions can give rise to additional tensor structures, and to mixing among these structures under renormalisation.

CHAPTER 3

New physics scenarios for $b \to c\tau\nu$ data

This chapter is based on References [1, 2] and focuses on the study of several scenarios of NP, each of which might be responsible for the $\mathcal{R}(D^{(*)})$ anomaly. The NP effects are analysed with the EFT formalism introduced in the previous chapter. We first comment on the different effects that each effective operator has on $b \to c\tau\nu$ observables. We then focus on those EFT scenarios that can arise from the introduction of a single additional particle to the SM content. After defining the statistical approach followed in the analysis, we fit the coefficients of each of the scenarios to the $b \to c\tau\nu$ data at our disposal, including limits from B_c lifetime and from collider searches. From the results of the fit we are able to make predictions for observables that are not yet available from experiments: $P_\tau(D)$ and $\mathcal{R}(\Lambda_c)$. We analyse the correlation of these observables with the anomalous ones, i.e. $\mathcal{R}(D^{(*)})$.

3.1 Effective field theory for $\mathcal{R}(D^{(*)})$

The enhancement observed in the $\mathcal{R}(D^{(*)})$ ratios with respect to their SM predictions can be traced back to an enhancement of the channel $b \to c\tau\nu$ and/or a suppression of the channels $b \to cl\nu$, with $l = e, \mu$. Ratios analogous to $\mathcal{R}(D^{(*)})$ but comparing the μ and the e channels, $\mathcal{R}_{\mu/e}(D)$ and $\mathcal{R}_{e/\mu}(D^*)$, have been measured by the Belle Collaboration [28–30]. As explained in Section 2.2, due to the smallness of the muon and electron mass, this ratio

is predicted to be 1 in the SM, up to corrections of order (m_l^2/m_B^2). The experiments give

$$\begin{aligned}
&\frac{\mathrm{BR}(B \to D\mu\nu_\mu)}{\mathrm{BR}(B \to De\nu_e)} = 0.995 \pm 0.022 \pm 0.039, \\
&\frac{\mathrm{BR}(\overline{B}^0 \to D^{*+}e^-\overline{\nu}_e)}{\mathrm{BR}(\overline{B}^0 \to D^{*+}\mu^-\overline{\nu}_\mu)} = 1.04 \pm 0.05 \pm 0.01, \\
&\frac{\mathrm{BR}(B^0 \to D^{*-}e^+\nu_e)}{\mathrm{BR}(B^0 \to D^{*-}\mu^+\nu_\mu)} = 1.01 \pm 0.01 \pm 0.03,
\end{aligned} \tag{3.1}$$

well in agreement with the SM prediction. This would indicate that, if the $\mathcal{R}(D^{(*)})$ ratios are a hint of NP, the additional contributions are either coupling mostly to the τ, or coupling to the electron and the μ in the same way. Furthermore, the BaBar and Belle analyses of the angular distributions in $B \to D^{(*)}l\nu$, with $l = e, \mu$ [29], showed consistency with the SM predictions. For these reasons, in this chapter we start our analysis assuming that NP modifies only the $b \to c\tau\nu$ transition.

Furthermore, due to the charges of the particles taking part in the quark-level process, if NP contributes to the process at tree-level, the additional mediator must necessarily be electrically charged. The limits posed by experiments on the existence of charged particles beyond those of the SM push the masses of these particles to scales well above the mass of the B mesons. For instance, the CMS search for W' bosons coupling mostly to third generation fermions [31] sets a lower limit of the order of hundreds of GeV on the mass of the W'. This lower bound depends on the specific model in which the W' arises, and can also reach $\mathcal{O}(\mathrm{TeV})$. An analogous search for LQs coupled to third-generation quarks [32] sets a lower limit of the order of $\mathcal{O}(\mathrm{TeV})$, the exact value depending on the branching fractions of the LQ.

Since the mass of the additional NP particle contributing to $b \to c\tau\nu$ lies well above $m_B \simeq 5.3\,\mathrm{GeV}$, which is the typical scale of energy exchanged in the decays we are interested in, we are in the position of describing its effects in terms of an EFT. The most general effective Hamiltonian contributing to $b \to c\tau\nu$, assuming for simplicity the neutrinos in the final state to be left-handed and SM-like, is

$$\mathcal{H}_{\mathrm{eff}} = 2\sqrt{2}G_F V_{cb}\left[(1 + C_V^L)O_V^L + C_V^R O_V^R + C_S^R O_S^R + C_S^L O_S^L + C_T O_T\right], \tag{3.2}$$

with the dimension six operators

$$\begin{aligned}
&O_V^L = (\bar{c}\gamma^\mu P_L b)\,(\bar{\tau}\gamma_\mu P_L \nu_\tau)\,, \qquad && O_V^R = (\bar{c}\gamma^\mu P_R b)\,(\bar{\tau}\gamma_\mu P_L \nu_\tau)\,, \\
&O_S^R = (\bar{c}P_R b)\,(\bar{\tau}P_L \nu_\tau)\,, && O_S^L = (\bar{c}P_L b)\,(\bar{\tau}P_L \nu_\tau)\,, \\
&O_T = (\bar{c}\sigma^{\mu\nu}P_L b)\,(\bar{\tau}\sigma_{\mu\nu}P_L \nu_\tau)\,.
\end{aligned} \tag{3.3}$$

In fact, if the NP we are considering lies well above the EW scale, the NP degrees of freedom can be integrated out already in the EW unbroken phase. This means that the

operators of Equation (3.5) originate from dimension six operators that are invariant under the SM group $SU(3)_\mathrm{c} \times SU(2)_\mathrm{L} \times U(1)_Y$, i.e. from operators of the so-called SM effective field theory (SMEFT) [33]. In terms of SMEFT, the operator O_V^R can only arise from the SMEFT operator $i\widetilde{H}^\dagger D_\mu H \bar{c}\gamma^\mu P_R b$ after integrating out the W boson [34–37]. For this reason, O_V^R will always give lepton flavour universal contributions, and hence we will not include it in our analysis.

Our effective Hamiltonian will then be

$$\mathcal{H}_\mathrm{eff} = 2\sqrt{2}G_F V_{cb}[(1+C_V^L)O_V^L + C_S^R O_S^R + C_S^L O_S^L + C_T O_T]\,, \tag{3.4}$$

with nonvanishing WCs for the operators

$$\begin{aligned} O_V^L &= (\bar{c}\gamma^\mu P_L b)\,(\bar{\tau}\gamma_\mu P_L \nu_\tau)\,, \qquad & O_S^R &= (\bar{c}P_R b)\,(\bar{\tau}P_L\nu_\tau)\,, \\ O_S^L &= (\bar{c}P_L b)\,(\bar{\tau}P_L\nu_\tau)\,, & O_T &= (\bar{c}\sigma^{\mu\nu}P_L b)\,(\bar{\tau}\sigma_{\mu\nu}P_L\nu_\tau)\,. \end{aligned} \tag{3.5}$$

Analyses of the $\mathcal{R}(D^{(*)})$ anomalies in terms of an EFT have already been performed [38–64]. The novelty of our analysis consists not only in the inclusion of the most recent data released by experiments on the two ratios, but also in the inclusion of data on the angular distributions of the particles in the decay $B \to D^*\tau\nu$. These data contain information that is important in distinguishing the properties of spin and charge of the particle mediating the decay. Intuitively, this can be understood from the fact that the colour, charge and spin conservation at the vertices where the virtual particle interacts imply a specific spin configuration of the particles in the final state, and hence a specific angular distribution.

We can illustrate this in the case of the $B \to D^*(\to D\pi)\tau\nu$ decay [65, 66]. We define the coordinate system as in Figure 3.1, adapted from Reference [66]. The full angular distribution reads [65]

$$\frac{d^5\Gamma}{dq^2 dm_{D\pi}^2 d\cos\theta_D d\cos\theta_\ell d\chi} = \frac{\sqrt{\lambda_{BD^*}(q^2)}}{256(2\pi)^6 m_B^3}\left(1-\frac{m_\ell^2}{q^2}\right)\frac{|\boldsymbol{p}_D|}{m_{D\pi}}\sum_{\lambda_\ell}\left|\sum_{\lambda_{D^*}}\mathcal{M}^{\lambda_{D^*},\lambda_\ell}(\overline{B}\to D\pi\ell\overline{\nu}_\ell)\right|^2, \tag{3.6}$$

where q^2 is the invariant mass squared of the lepton-neutrino system, $m_{D\pi}^2$ is the invariant mass squared of the $D-\pi$ system, $\boldsymbol{p}_D$ is the three-momentum of the D in the rest frame of the $D\pi$ system, $\lambda_{BD^*}(q^2) = m_B^4 + m_{D^*}^4 + q^4 - 2\left(m_B^2 m_{D^*}^2 + m_B^2 q^2 + m_{D^*}^2 q^2\right)$, while the sums run over the possible spin states of the intermediate D^* and of the lepton in the final state. The angles $\theta_{D,\ell}, \chi$ are displayed in Figure 3.1. θ_ℓ is the angle between ℓ and B in the (virtual) W rest frame, χ is the angle between the dilepton and the D^* decay planes while θ_D is the angle between D and B in the D^* rest frame. The distribution of the final state particles with respect to this angle depends on the polarisation state of the D^*. If we introduce the fraction of longitudinally polarised D^*

$$F_L(D^*) \equiv \frac{\Gamma(B\to D_L^*\tau\nu)}{\Gamma(B\to D^*\tau\nu)}, \tag{3.7}$$

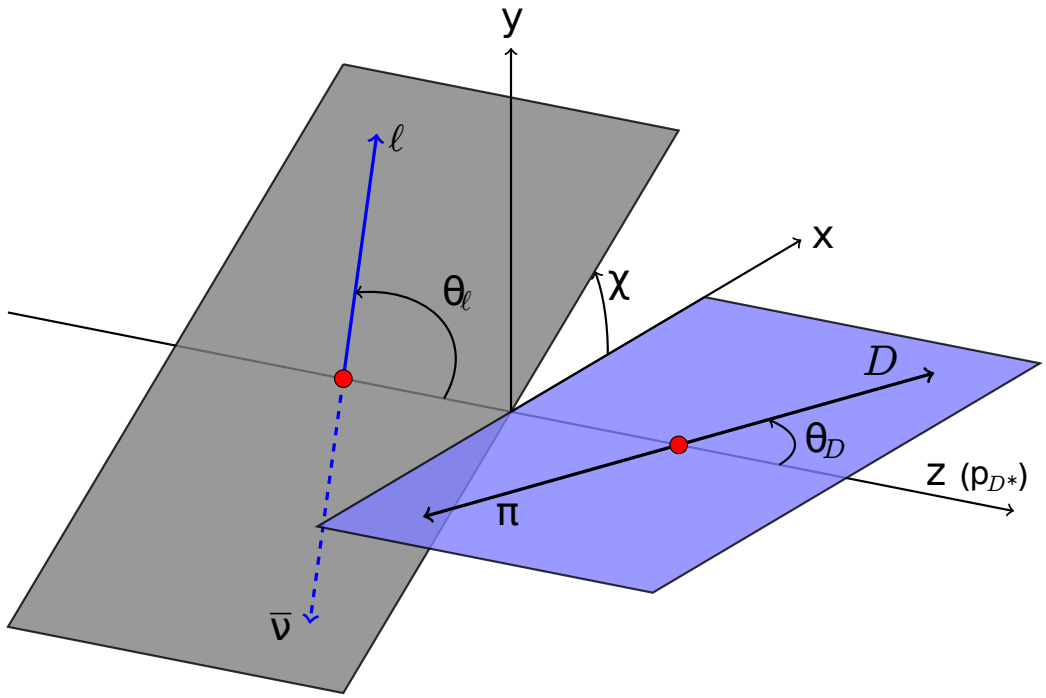

Figure 3.1: Kinematics of $B \to D^*(\to D\pi)\tau\nu$. Figure adapted from Reference [66]

it can be shown [67] that the angular distribution in the $D^* \to D\pi$ decay is given by

$$\frac{1}{\Gamma}\frac{d\Gamma}{d\cos\theta_D} = \frac{3}{4}[2F_L(D^*)\cos^2\theta_D + (1 - F_L(D^*))\sin^2\theta_D]. \tag{3.8}$$

This dependence allows for a measurement of $F_L(D^*)$.

We can show the model-discriminating power of $F_L(D^*)$ by plotting $\frac{1}{\Gamma}\frac{d\Gamma}{d\cos\theta_D}$ as a function of θ_D and assuming only one of the NP contributions to the WCs of Equation (3.5) to be nonvanishing, and equal to one for simplicity. The plot is displayed in Figure 3.2. Although these plots correspond to arbitrary values of the WCs, we see that the shape of the angular dependence can change significantly when different WCs come into play. On the contrary, the possibility of having the same differential distribution with different nonvanishing WCs is not excluded, depending on the specific value of the individual coefficients.

3.2 Single-mediator scenarios of new physics

As mentioned above, in our analysis we make the assumption that only one NP particle is responsible for the $\mathcal{R}(D^{(*)})$ anomaly. Let us then determine which combinations of WCs can arise from each of these mediators.

We illustrate the procedure by considering the effective four-fermion coupling displayed in Figure 3.3, for a vector coupling with left-handed quarks, O_V^L. The procedure for the other

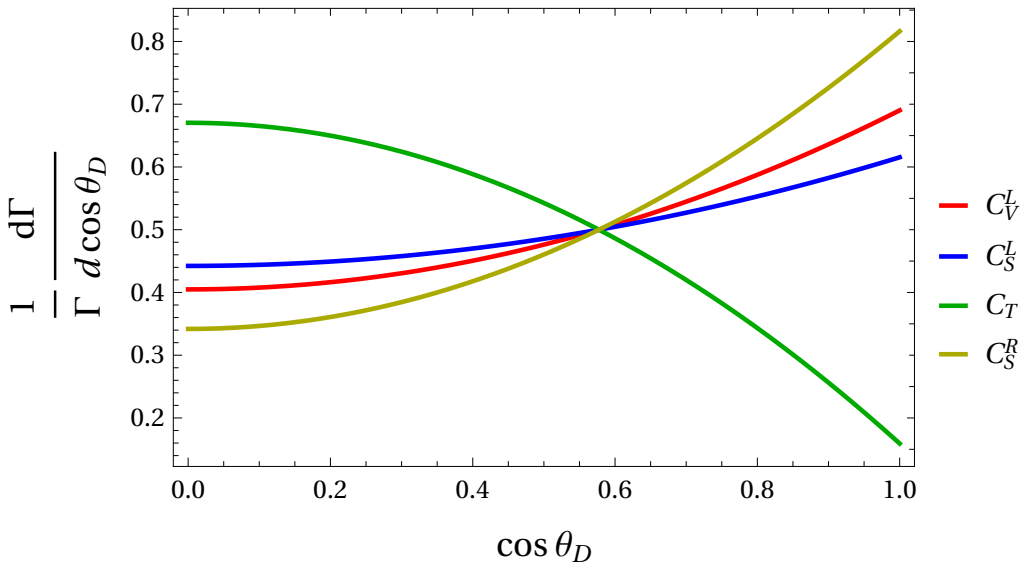

Figure 3.2: $\frac{1}{\Gamma}\frac{d\Gamma}{d\cos\theta_D}$ as a function of θ_D for different nonvanishing Wilson coefficients.

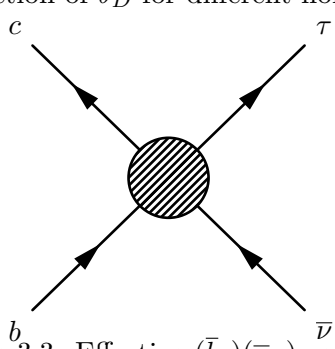

Figure 3.3: Effective $(\overline{b}c)(\overline{\tau}\nu)$ coupling.

tensor structures is analogous.

We can classify the possible mediators depending on how the additional particle gets exchanged, i.e. in the s, t or u channel. These channels can be visualised by imagining to stretch the effective vertex of Figure 3.3 by pulling two of the four lines together. We are left with the three possibilities displayed in each row of Table 3.1. Furthermore, since two fermions are interacting at each vertex, the addition of angular momentum implies that the mediator can have either spin zero or spin one. We are left with the six possibilities of Table 3.1.

In the first row of the table, each vertex involves either only quarks or only leptons. The mediator is, then, a colour-singlet with electric charge -1. Depending on its spin, it can be either a charged Higgs or a charged vector boson W'. However, the couplings with the scalar particle would not include any Dirac matrix other than the projectors, hence not giving rise to the O_V^L operator we are analysing in this example. The W', on the other

Spin 0	Spin 1
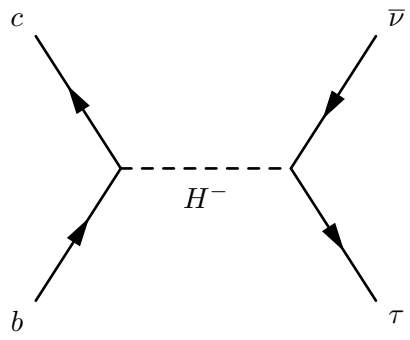	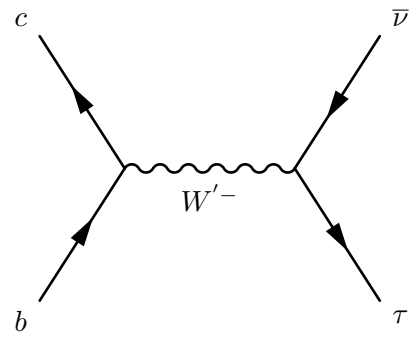
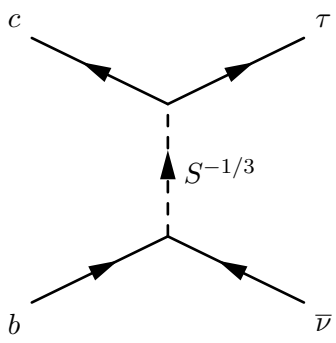	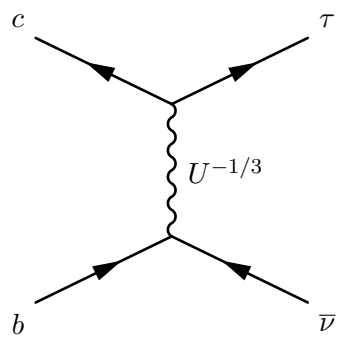
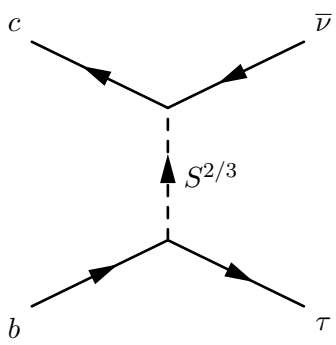	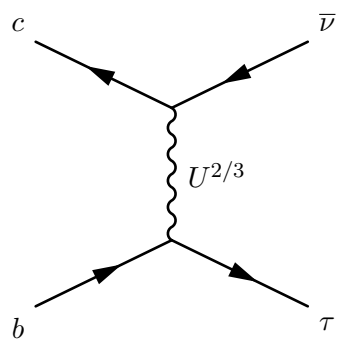

Table 3.1: Possible new physics mediators of the effective coupling. S and U indicate scalar and vector leptoquarks respectively.

hand, would generate a vector operator – analogously as in the SM – and can hence give rise to the O_V^L structure.

In the remaining two rows, each vertex involves both a quark and a lepton[1]. The hypothetical NP particles mediating these kinds of interactions are called leptoquarks. These particles are a prediction of grand unified theories (GUTs) [31,68–71], and can also arise in other scenarios beyond the SM. An extensive review of their phenomenology can be found in Reference [72], of which we assume the labelling of the particles, indicating scalar and vector LQs as S and U respectively.

Due to colour conservation, LQs are necessarily colour triplets. From the conservation of electric charge we can deduce the charge assignment of each particle. Finally, we are looking at the effective coupling with left-handed fermions, which are components of $SU(2)_\mathrm{L}$. This implies that at each vertex, their $SU(2)_\mathrm{L}$ indices can be arranged as a singlet or a triplet, resulting from the decomposition $2 \otimes 2 = 1 \oplus 3$, and hence that the LQ can be either an $SU(2)_\mathrm{L}$ singlet or triplet. We can now compare these eight possibilities with the ones listed in Reference [72] and cross out those that do not give rise to the required couplings. As an illustrative example, let us consider the $SU(2)_\mathrm{L}$-triplet case of the vector LQ in the second row of Table 3.1. In order for the vertex to conserve electric charge, the LQ must have charge $-1/3$. From Reference [72] we see that the only triplet vector-LQ is $U_3 = (\mathbf{3}, \mathbf{3}, 2/3)$. This triplet does indeed have a component with charge $-1/3$ which couples to fermions as

$$\mathcal{L}_{-1/3} \propto \overline{d}_L \gamma^\mu U^{-1/3} \nu_L. \tag{3.9}$$

The LQ does not couple up-type quarks to charged leptons, and furthermore it does not have the required structure involving charge conjugation, hence there is no contribution to O_V^L from the vector LQ $U^{-1/3}$ depicted in Table 3.1.

We can proceed analogously for the remaining cases Table 3.1 and for the effective coupling with a different tensor structure. This leads to the mediators listed in Table 3.2.

For each of these particles, one can write down the most general set of Yukawa couplings and then integrate out the particle using the procedure outlined in Section 2.3, as done for instance in Reference [47]. As a result, in each scenario at most two of the WCs of Equation (3.5) are nonvanishing and independent. The nonvanishing WCs corresponding to each particle are shown in Table 3.2. These are given at the NP scale, which we assume to be $\Lambda_\mathrm{NP} \sim 1\,\mathrm{TeV}$, as motivated by collider constraints. This is also the scale at which we will quote our results in the rest of this work. The relations among the WCs at the scale m_b are obtained by evolving those at the scale Λ_NP via renormalisation group (RG) evolution. We do this by using the results at three-loop QCD and one-loop in QED and EW from Reference [73]. These effects are not relevant for the vector coupling C_V^L, which does not evolve in QCD [25] and does not mix with the other operators [74], hence we assume $C_V^L(\Lambda_\mathrm{NP}) = C_V^L(m_b)$. The evolution of the other coefficients can be summarised in

[1] In the second row of the table, the fermion flow gets inverted at each vertex. This results from interactions involving charge conjugation.

$SU(3)$	**Scalar**	**Vector**
1	Charged Higgs $H^- \sim (\mathbf{1}, \mathbf{2}, 1/2)$ (C_S^R, C_S^L)	Charged vector boson $W'^- \sim (\mathbf{1}, \mathbf{3}, 0)$ C_V^L
3	Scalar LQ • $S_1 \sim (\overline{\mathbf{3}}, \mathbf{1}, 1/3)$ $(C_V^L, C_S^L = -4C_T)$ • $S_3 \sim (\overline{\mathbf{3}}, \mathbf{3}, 1/3)$ C_V^L • $R_2 \sim (\mathbf{3}, \mathbf{2}, 7/6)$ $C_S^L = 4C_T$	Vector LQ • $U_1 \sim (\mathbf{3}, \mathbf{1}, 2/3)$ (C_V^L, C_S^R) • $U_3 \sim (\mathbf{3}, \mathbf{3}, 2/3)$ C_V^L • $V_2 \sim (\overline{\mathbf{3}}, \mathbf{2}, 5/6)$ C_S^R

Table 3.2: Possible new physics mediators and corresponding nonvanishing Wilson coefficients. S and U indicate scalar and vector leptoquarks respectively.

the following expressions, obtained from Reference [73]:

$$\begin{aligned} C_V^L(m_b) &= C_V^L(1\,\text{TeV}), \\ C_S^R(m_b) &= 1.737 C_S^R(1\,\text{TeV}), \\ \begin{pmatrix} C_S^L(m_b) \\ C_T(m_b) \end{pmatrix} &= \begin{pmatrix} 1.752 & -0.287 \\ -0.004 & 0.842 \end{pmatrix} \begin{pmatrix} C_S^L(1\,\text{TeV}) \\ C_T(1\,\text{TeV}) \end{pmatrix}. \end{aligned} \tag{3.10}$$

3.3 Fit of $b \to c\tau\nu$ data

Let us summarise the experimental data used as inputs for our fits.

The most relevant inputs are the anomalous ratios $\mathcal{R}(D^{(*)})$ in Equation (2.16), which include the average of the results of the three experiments, BaBar, Belle and LHCb.

An analogous ratio, but related to the decay $B_c \to J/\Psi \ell\nu$, hence differing from $B \to D^{(*)}\ell\nu$ only in the spectator quark, has been measured by the LHCb Collaboration, giving [75]

$$\mathcal{R}(J/\Psi) \equiv \frac{\text{BR}(B_c \to J/\Psi\tau\nu)}{\text{BR}(B_c \to J/\Psi\mu\nu)} = 0.71 \pm 0.17 \pm 0.18, \tag{3.11}$$

where the uncertainties refer to the statistical and systematic ones respectively. The SM

prediction of this ratio is not as precise as the one for the $B \to D^{(*)}\ell\nu$, due to the large theory uncertainty on the form factors. The larger uncertainty compared to the $B \to D^{(*)}\ell\nu$ case arises from the presence of two heavy quarks and from the restricted dataset available for fitting the form factor parameters. The SM prediction can be computed with different modelling of the form factors, and the typical range in which the central value lies is [76–82] $0.25 \lessapprox \mathcal{R}(J/\Psi) \lessapprox 0.28$. The most precise determination, released after the completion of our analysis, uses the form factors computed exploiting LQCD data, dispersion relations and HQET, and gives [83] $\mathcal{R}_{\rm SM}(J/\Psi) = 0.25(3)$. Although the experimental value is indeed in tension with these predictions, the large uncertainty on the theory predictions available when our work was completed prevented us from including this quantity in our statistical analysis.

As we pointed out in Section 3.2, useful information for discriminating NP scenarios comes from the angular distribution of the particles in the final state, which can be expressed in terms of the polarisation observables. The polarisation of the D^* in the decay $B \to D^*\tau\nu$, defined in Equation (3.7), is predicted in the SM to be [48, 63]

$$F_{L,\,\rm SM}(D^*) = 0.46 \pm 0.04, \tag{3.12}$$

where the uncertainty comes from the form factors. This observable has been measured by the Belle Collaboration [57, 67], obtaining

$$F_L(D^*) = 0.60 \pm 0.08 \pm 0.04, \tag{3.13}$$

the first uncertainty being statistical and the second systematic. The value agrees with the SM prediction at 1.4σ.

As in the case of the D^*, in both the decays $B \to D^{(*)}\tau\nu$ we can introduce an angular observable for the τ, measuring the polarisation asymmetry along the longitudinal directions of the τ lepton, i.e.

$$P_\tau(D^{(*)}) = \frac{\Gamma(B \to D^{(*)}\tau^{\lambda=+1/2}\nu) - \Gamma(B \to D^{(*)}\tau^{\lambda=-1/2}\nu)}{\Gamma(B \to D^{(*)}\tau\nu)}. \tag{3.14}$$

For a two-body hadronic decay of the τ, these quantities can be measured via the differential decay rate

$$\frac{d\Gamma}{d\cos\theta_2} = \frac{1}{2}(1 + \alpha P_\tau(D^{(*)})\cos\theta_2), \tag{3.15}$$

where θ_2 is the angle formed by the momentum of the meson resulting from the decay of the τ, and the direction opposite to the momentum of the virtual W in the rest frame of the τ. The parameter α depends on the decay channel of the τ, and is $\alpha = 1.0$ for $\tau \to \pi\nu$ and $\alpha = 0.45$ for $\tau \to \rho\nu$. This value arises from the average over the unobserved polarisation of the ρ [84]. The SM prediction of the τ polarisations in the decays $B \to D^{(*)}\tau\nu$ is [40, 85]

$$P_{\tau,\,\rm SM}(D) = 0.325 \pm 0.009, \qquad P_{\tau,\,\rm SM}(D^*) = -0.497 \pm 0.013. \tag{3.16}$$

The Belle Collaboration [15, 17, 86] measured this quantity for the decay $B \to D^*\tau\nu$, ob-

taining

$$P_\tau(D^*) = -0.38 \pm 0.51^{+0.21}_{-0.16}, \tag{3.17}$$

the first uncertainty being statistical and the second systematic. This measurement is well in agreement with the SM prediction.

BaBar and Belle also provide the binned q^2 differential decay rate [21,22] for $B \to D^{(*)}\tau\nu$. However, due to the large uncertainty on each bin, reaching and even exceeding 100% for some of them, this data would not add any significant information to the fit. For this reason we do not include it in our analysis.

The effective vertex of Figure 3.3 can also mediate the decay $B_c \to \tau\nu_\tau$. In terms of the WCs, the branching ratio $\mathrm{BR}(B_c \to \tau\nu_\tau)$ is given by [87]

$$\mathrm{BR}(B_c \to \tau\nu_\tau) = \tau_{B_c} \frac{m_\tau^2 m_{B_c} f_{B_c}^2 G_{\mathrm{F}}^2 |V_{cb}|^2}{8\pi} \left(1 - \frac{m_\tau^2}{m_{B_c}^2}\right)^2 \left|1 + C_V^L + \frac{m_{B_c}^2}{m_\tau(m_b + m_c)}(C_S^R - C_S^L)\right|^2. \tag{3.18}$$

where f_{B_c} is the B_c decay constant[2]. The branching ratio $\mathrm{BR}(B_c \to \tau\nu_\tau)$ is sensitive to the vector C_V^L and pseudoscalar $C_P \equiv C_S^R - C_S^L$ NP contributions, the latter sensitivity being enhanced by the mass ratio m_{B_c}/m_τ. It would then be reasonable to include $\mathrm{BR}(B_c \to \tau\nu_\tau)$ in the fit of those scenario having at least one nonvanishing WC among C_V^L, C_P. Data on B_c mesons are available from their production at the Large Electron-Positron Collider (LEP), Tevatron and at LHC [31]. The production rate of B_c at LHC is suppressed by a factor of $\sim 10^{-2} - 10^{-3}$ with respect to the production of B mesons [77], of $\sigma \sim 0.1\mu$b and [89] $\sigma \sim 10\mu$b respectively. This is due to the need of either two gluons splitting into heavy-quark pairs, or of a heavy-antiquark fragmentation with the heavy quark originating from the parton distribution function, relevant at large transverse momenta of the B_c, $p_T \gg M_{B_c}$. Furthermore, in the SM the leptonic decay $B_c \to \tau\nu_\tau$ proceeds via the annihilation of the two quarks in the meson state via weak interactions, and the branching ratio shows a helicity suppression of m_τ^2. The resulting branching ratio expected in the SM is $\sim 2\%$. This mode has also a low experimental efficiency due to the large hadronic background for the decay of the τ. Due to all these reasons, there is no measurement of the $\mathrm{BR}(B_c \to \tau\nu_\tau)$ branching ratio so far, which prevents us from including it in our statistical analysis. Nonetheless, one can put constraints on the NP contribution to $\mathrm{BR}(B_c \to \tau\nu_\tau)$ by requiring that this channel does not saturate or exceed the total decay rate. This *naive* limit implies $\mathrm{BR}(B_c \to \tau\nu_\tau) < \mathrm{BR}(B_c \to \tau\nu_\tau)_{\mathrm{MAX}} = 100\%$. It is reasonable to assume a lower value for $\mathrm{BR}(B_c \to \tau\nu_\tau)_{\mathrm{MAX}}$, as stated for instance in References [87,90], setting $\mathrm{BR}(B_c \to \tau\nu_\tau)_{\mathrm{MAX}} = 10, 30\%$ respectively. However, these upper values require a critical revision. The stronger 10% upper bound was inferred by using the data from LEP, referred to $B_{u,c}$ mesons resulting from the b quarks produced from the decay of Z bosons, and subsequently decaying as $B_{u,c} \to \tau\nu$. The measured quantity is

$$\mathrm{BR}_{\mathrm{eff}} \equiv \mathrm{BR}(B_u \to \tau\nu)\left(1 + \frac{N_c}{N_u}\right), \tag{3.19}$$

[2]In our analysis we take the value of f_{B_c} calculated with LQCD in Reference [88].

where N_c/N_u represents the relative fraction of $\tau\nu$ final states coming from B_c and B_u [91]. If the $B_{u,c}$ originate from the hadronisation of a b quark, the ratio N_c/N_u can be rewritten in terms of the fragmentation functions $f_{u,c}$, representing the transition probabilities of a b quark hadronising to a $B_{u,c}$, as

$$\frac{N_c}{N_u} = \frac{f_c}{f_u} \frac{\mathrm{BR}(B_c \to \tau\nu)}{\mathrm{BR}(B_u \to \tau\nu)}. \tag{3.20}$$

The 10% limit is obtained by using the experimental value of $f_c/f_u \sim \mathcal{O}\left(10^{-3}\right)$ [2], obtained as an average of the results from CMS and LHCb. This procedure has several pitfalls. First of all, the productions of $B_{u,c}$ mesons at LHC and at LEP involve different mechanisms, both of them explained above. Furthermore, the ratio f_c/f_u depends on the p_T of the B meson, as it is the case for $B_{d,s}$ mesons. This is evident from the fact that the ratio f_c/f_u assumes different values at CMS and LHCb, for which the kinematic variable p_T is different, and has been recently confirmed by the ATLAS Collaboration [92]. Moreover, the p_T dependence of f_c/f_u indicates that fragmentation alone does not explain the production of B_c mesons for low p_T, and hence that the estimate of $\mathrm{BR}(B_c \to \tau\nu_\tau)$ via equation (3.19) averaging the values of f_c/f_u from CMS and LHCb values is incorrect.

Let us now discuss the limit $\mathrm{BR}(B_c \to \tau\nu_\tau)_{\mathrm{MAX}} = 30\%$ stated in Reference [87]. This limit is obtained by comparing the measured lifetime of B_c, $\tau_{B_c}^{\mathrm{exp}} = (0.510 \pm 0.009)$ ps [31], with the value predicted within the SM in Reference [93], 0.4 ps $< \tau_{B_c}^{\mathrm{SM}} <$ 0.7 ps. This estimate is obtained by assuming τ_{B_c} to be dominated by the decay of one of the two heavy quarks, keeping the other as a spectator. It makes use of HQET, expanding in the ratio of the energy release in the decay of the quark with respect to the energy exchanges in the bound state, as well as NRQCD, expanding in $p/m_{b,c}$, where p is the typical three momentum of the quark in the B_c meson. The uncertainty quoted on the result arises from the large dependence on the charm pole mass, varying the latter in the range $1.4\,\mathrm{GeV} \leq m_c \leq 1.6\,\mathrm{GeV}$. The value relevant for constraining the NP effects in $\mathrm{BR}(B_c \to \tau\nu_\tau)$ by requiring the theory prediction of τ_{B_c} to agree with the experimental value is the upper value $\tau_{B_c}^{\mathrm{SM}} < 0.7$ ps, since it corresponds to a lower contribution of the SM to the total decay width, which could then be saturated (compared to the experimental value) by NP. The 30% limit is inferred with the $\tau_{B_c}^{\mathrm{SM}} < 0.7$ ps upper limit, which is sensitive to m_c. Since the latter is not well defined in a leading order QCD calculation, and since this uncertainty includes only the one originating from m_c, it is reasonable to further soften the 30% limit.

In view of the above considerations, the fit for each NP particle was performed in three scenarios differing in the $\mathrm{BR}(B_c \to \tau\nu_\tau)$ limit imposed, assuming $\mathrm{BR}(B_c \to \tau\nu_\tau)_{\mathrm{MAX}} = 10, 30, 60\%$ respectively. This limit was set as a hard cut on the parameter space allowed for the fit, i.e. by varying the WCs in the region such that $\mathrm{BR}(B_c \to \tau\nu_\tau) < \mathrm{BR}(B_c \to \tau\nu_\tau)_{\mathrm{MAX}}$.

Additional information about the region allowed for the WCs comes from the data collected at colliders. As we already commented, the direct searches through on-shell production push the mass of the NP particles to scales $\Lambda_{\mathrm{NP}} \sim$ TeV. However, as analysed in Reference [94], even for NP scales lying above the reach of on-shell production, the effective couplings of Equation (3.5) can still be probed in proton-proton collisions due to their contribution to the scattering $b\bar{c} \to \tau^-\bar{\nu}$, with the two quarks being sea partons of the colliding protons,

hence having a signature on $pp \to \tau\nu + X$. These considerations are valid for NP particles contributing in the t or u channel to $b\bar{c} \to \tau^-\bar{\nu}$. The limits coming from this signature, analysed in Reference [94], are not imposed as a hard constraint to our fit. Instead, we checked that the regions preferred by the fit still lie in the region allowed by the colliders.

Statistical methodology

Our statistical methodology follows the one of Reference [95], restricting the parameter space to $\mathrm{BR}(B_c \to \tau\nu_\tau) < \mathrm{BR}(B_c \to \tau\nu_\tau)_{\mathrm{MAX}}$. The fitting parameters are the (real and imaginary parts of the) WCs of Equation (3.5) and the best-fit point is obtained by minimising the $\chi^2(C_k)$, defined as

$$\chi^2(C_k) = \sum_{ij}^{N_{\mathrm{obs}}} [\mathcal{O}_i^{\mathrm{exp}} - \mathcal{O}_i^{\mathrm{th}}(C_k)]\mathcal{C}_{ij}^{-1}[\mathcal{O}_j^{\mathrm{exp}} - \mathcal{O}_j^{\mathrm{th}}(C_k)]. \tag{3.21}$$

where $\mathcal{O}_i^{\mathrm{exp}} = F_L(D^*), P_\tau(D^*), \mathcal{R}(D), \mathcal{R}(D^*)$ represent the experimental values of the observables. The covariance matrix $\mathcal{C}_{ij}^{-1}$ includes the experimental errors of Equations (3.13), (3.17), (2.16) and the correlation between $\mathcal{R}(D), \mathcal{R}(D^*)$ quoted by Reference [12]. The goodness of fit is quantified in terms of the p-value, defined as

$$p\text{-value} = 1 - F_{N_{\mathrm{obs}}-N_{\mathrm{par}}}(\chi^2_{\mathrm{min}}), \tag{3.22}$$

where F_n stands for the cumulative distribution function of a χ^2-distributed random variable with n degrees of freedom, $N_{\mathrm{obs}} = 4$ is the number of fitted observables and N_{par} is the number of fitted parameters. This quantity can be interpreted as the probability that a measurement of the observables distributed normally around the value predicted at the best fit point leads, due to statistical fluctuations, to a χ^2 equal or greater than the one actually observed.

We can quantify the $\chi^2(x)$ as a function of the parameters x in terms of σ as

$$s(x) = \sqrt{F_1^{-1}(F_{N_{\mathrm{par}}}(\chi^2(x) - \chi^2_{\mathrm{min}}))}, \tag{3.23}$$

which allows us to determine the boundaries of the N sigma regions, x_s, around the best-fit points by requiring that $s(x_N) = N$. The meaning of this region is the following. Under the assumption that the scenario under consideration is the one realised in Nature, with an unknown fixed true value of the parameter, if we repeat the experiments many times, in $F_1(1) \simeq 68\%(F_2(4) \simeq 95\%)$ of the times the 1σ (2σ) region will contain the true value. When $s(x_s)$ is evaluated at the SM point, i.e. $s(0)$, it represents the SM-pull, quantifying how much the best-fit point is favoured over the SM point (considered as the limiting case of the scenario under consideration).

The remaining sections of this chapter display the results of our analysis, separating them depending on the number of fitted parameters. As we observed at the beginning of this chapter, a single NP particle contributes at most to two nonvanishing combinations of WCs. Each of these scenarios is analysed under the further assumption that the contributions of the NP particle are CP-conserving, i.e. assuming all WCs to be real numbers for simplicity,

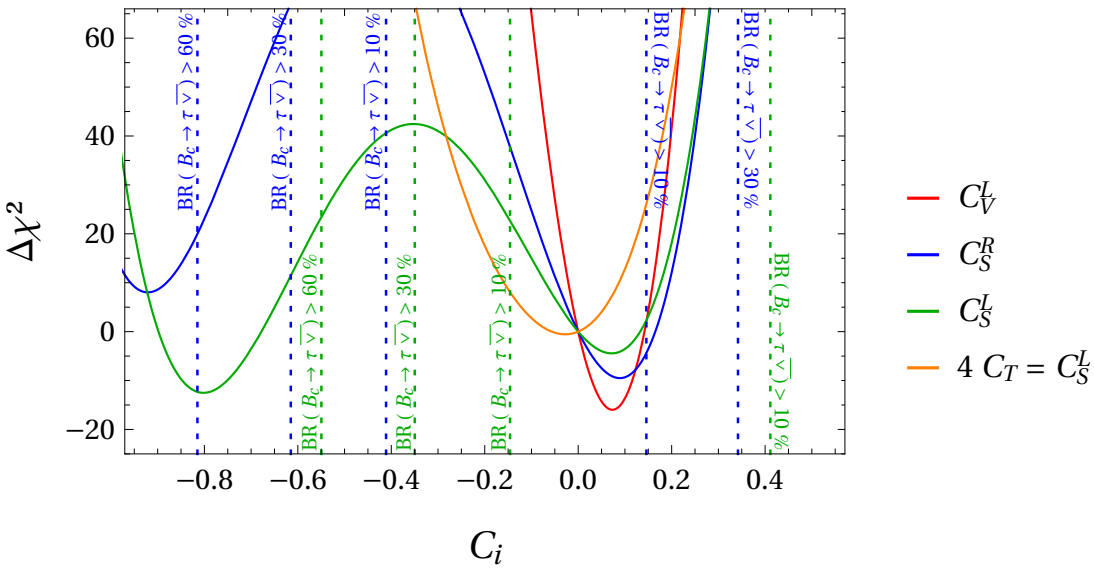

Figure 3.4: $\Delta\chi^2$ for the four one-dimensional (1D) scenarios, with Wilson coefficients at the scale $\mu = 1\,\text{TeV}$. The dashed vertical lines correspond to the limit on $C_S^{L,R}$ from $\text{BR}(B_c \to \tau\nu)$, excluding the region in which the label of the line lies. The plot is adapted from Reference [2].

since the analysis of most scenarios is not sensitive to the imaginary part of the WCs. The only scenario for which complex coefficients are allowed is the one with a scalar LQ R_2, since this scenario does not provide a good fit to the $\mathcal{R}(D^{(*)})$ anomaly for real couplings but it does for complex ones [96]. As a result, each scenario requires the fitting of either one or two parameters only.

3.3.1 One-dimensional scenarios

As we see from Table 3.2, the W', S_3, U_3 generate contributions to C_V^L only, R_2 to $C_S^L = 4C_T$ and U_2 to C_S^R. In addition to these one-dimensional scenarios, we consider a scenario with nonvanishing WC C_S^L, which can arise from a charged Higgs H^- if the flavour structure suppresses the C_S^R coupling.

The results of the fit are summarised in Figures 3.4 and 3.5, as well as in Table 3.3 at the end of the chapter. In Figure 3.4 we show the value of $\Delta\chi^2 = \chi^2(C_i) - \chi^2_{\text{SM}}$ as a function of the WC(s). Plotting this quantity allows us to visualise how much the description of the data improves in NP scenarios with respect to the SM. The dashed vertical lines represent the limits imposed by $\text{BR}(B_c \to \tau\nu_\tau)$, excluding the region in which the label of the line lies. This limit is only displayed for the $C_S^{L,R}$ scenario, since it turns out not to be relevant in the other two scenarios. The WCs are referred to the NP scale $\Lambda_{\text{NP}} = 1\,\text{TeV}$.

We see that the limit on $\text{BR}(B_c \to \tau\nu_\tau)$ challenges the scenario with nonvanishing C_S^L, since each of the three $\text{BR}(B_c \to \tau\nu_\tau)_{\text{MAX}}$ bounds rules out the absolute minimum. The minima

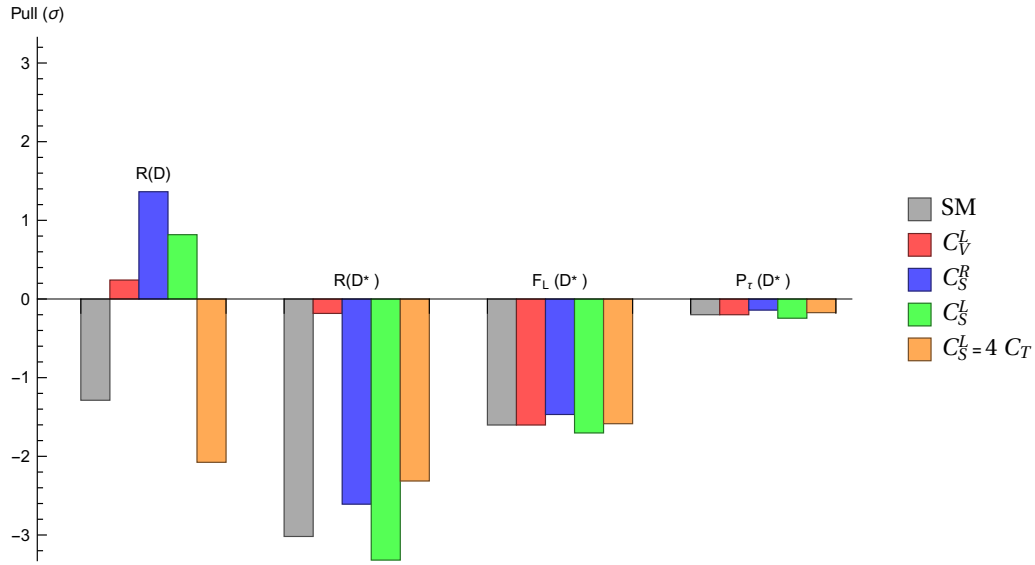

Figure 3.5: Pulls of the measured observables in the Standard Model and at the best-fit points of the 1D scenarios with $\mathrm{BR}(B_c \to \tau\nu_\tau)_{\mathrm{MAX}} = 60\%$.

of the scenarios C_S^R, $C_S^L = 4C_T$, as well as the relative minimum of C_S^L that is not ruled out by $\mathrm{BR}(B_c \to \tau\nu_\tau)$, do not describe the data significantly better with respect to the SM, while this is the case for the scenario C_V^L. These results are also visualised in Table 3.3 at the end of the chapter, in which we display the best-fit point, together with its 1 and 2σ ranges, the p-value and the SM pull, defined as in Section 3.3. The last six columns display the value of $\mathcal{R}(D), \mathcal{R}(D^*), F_L(D^*), P_\tau(D^*), P_\tau(D), \mathcal{R}(\Lambda_c)$ at the best-fit point. For the observables that have already been measured, we also quote the pull with respect to the experimental value, defined as

$$\mathrm{d}_{\mathcal{O}_i} = \frac{\mathcal{O}_i^{\mathrm{NP}} - \mathcal{O}_i^{\mathrm{exp}}}{\sigma^{\mathcal{O}_i^{\mathrm{exp}}}}. \tag{3.24}$$

These are also displayed in Figure 3.5 together with the pulls of the same observables in the SM, and assuming $\mathrm{BR}(B_c \to \tau\nu_\tau)_{\mathrm{MAX}} = 60\%$ for all the scenarios.

The low p-value of the scenarios $C_S^{L,R}$, $C_S^L = 4C_T$ reflects the high $\Delta\chi^2$. From the table we see that this is due to the very marginal improvement of these scenarios in the description of $\mathcal{R}(D^{(*)})$. From the table and from Figure 3.5 we see that none of the 1D scenarios significantly improves the agreement with the experimental value of $F_L(D^*)$, showing that this angular observable has a marginal impact in the discrimination of 1D scenarios. However, as we can observe from Table 3.3, a measurement of $P_\tau(D)$ will allow to further discriminate these scenarios, since the predicted value depends significantly on the scenario assumed.

3.3.2 Two-dimensional scenarios

We consider the scenarios S_1, U_1, H^- with two nonvanishing combinations of WCs (see Table 3.2). In addition, we consider the scenario $C_S^L = 4C_T$ with complex WC, i.e. we fit ($\mathrm{Re}[C_S^L = 4C_T]$, $\mathrm{Im}[C_S^L = 4C_T]$). The best-fit points and their 2σ regions are visualised in Figure 3.6, assuming either $\mathrm{BR}(B_c \to \tau\nu_\tau)_{\mathrm{MAX}} = 10\%$ or 60%. We also display the collider limits and the limits from $\mathrm{BR}(B_c \to \tau\nu_\tau)$. These limits are taken from the EFT analysis in Reference [94], which does not work for mediators exchanged in the s channel. For this reason, these constraints are shown as a dashed line for the charged Higgs scenario. The WCs are referred to the NP scale $\Lambda_{\mathrm{NP}} = 1\,\mathrm{TeV}$.

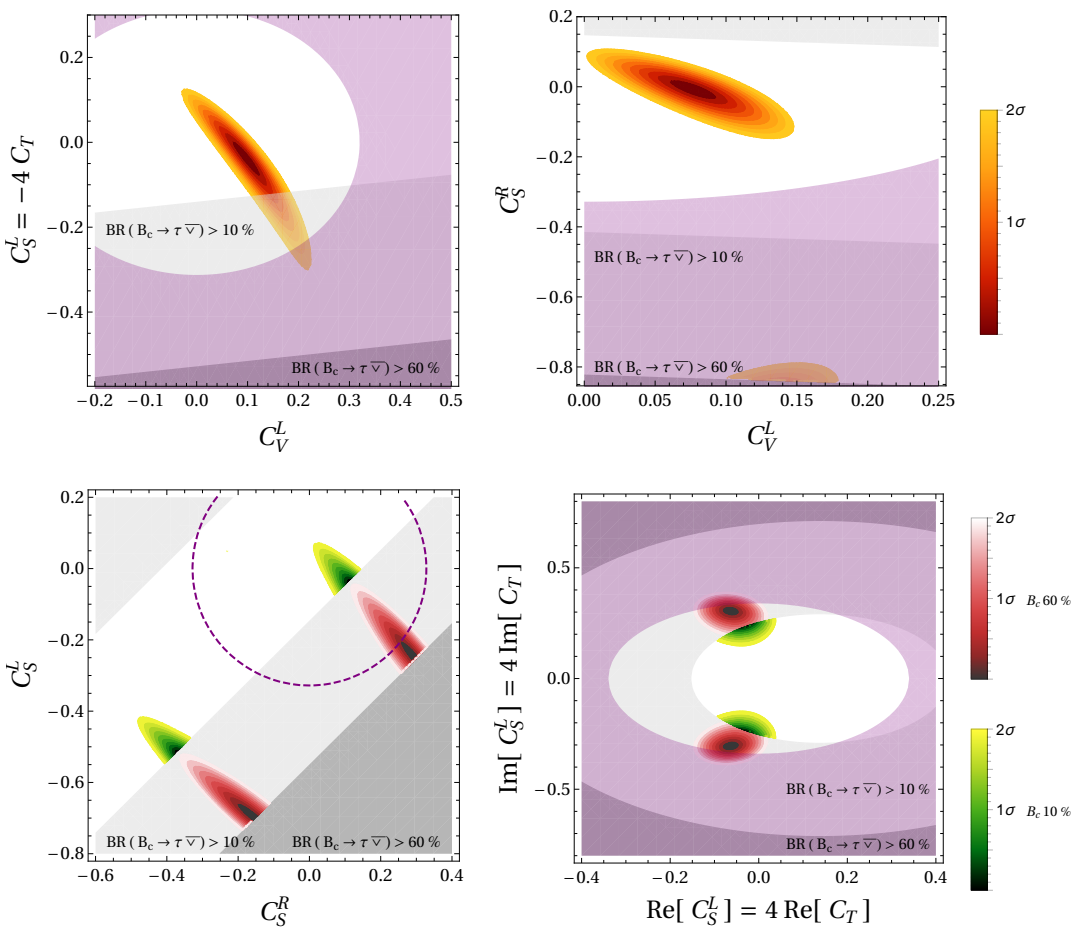

Figure 3.6: 2σ regions of the 2D fits, with Wilson Coefficients at the scale $\mu = 1\,\mathrm{TeV}$. The $\mathrm{BR}(B_c \to \tau\nu_\tau)$ constraints exclude the grey regions. The collider bounds from Reference [94] exclude the purple regions at $2\,\sigma$ level. For the charged Higgs scenario this bound is displayed as a dashed line. The plots are adapted from Reference [2].

As a first remark, we observe that the scenarios (C_S^R, C_S^L) and ($\mathrm{Re}[C_S^L = 4C_T]$, $\mathrm{Im}[C_S^L = 4C_T]$) are challenged by the $\mathrm{BR}(B_c \to \tau\nu_\tau)_{\mathrm{MAX}} = 10\%$ limit, since the best-fit points obtained with $\mathrm{BR}(B_c \to \tau\nu_\tau)_{\mathrm{MAX}} = 60\%$ (in red) predict $\mathrm{BR}(B_c \to \tau\nu_\tau) > 10\%$. As a

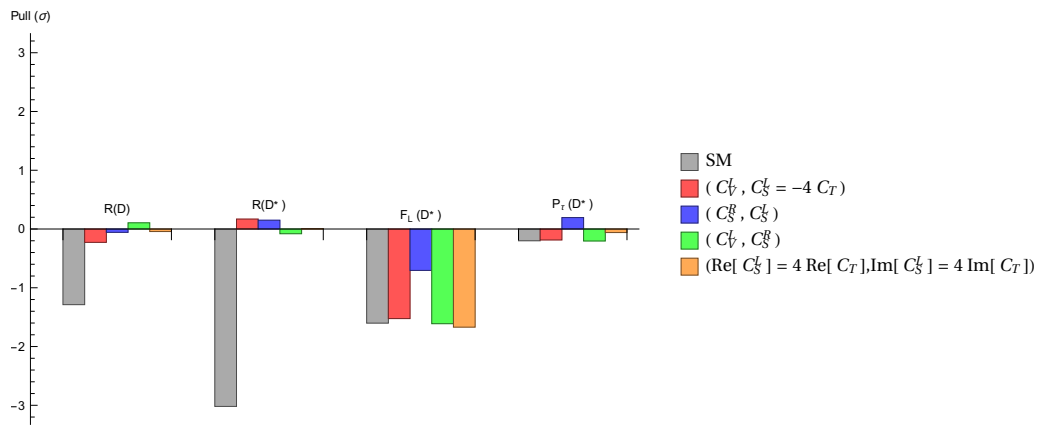

Figure 3.7: Pulls of the measured observables in the Standard Model and at the best-fit points of the 2D scenarios with $\mathrm{BR}(B_c \to \tau\nu_\tau)_{\mathrm{MAX}} = 60\%$.

result, these points move to the boundary of the $\mathrm{BR}(B_c \to \tau\nu_\tau) < 10\%$ region as soon as this constraint is imposed. This shift implies a drastic worsening of the description of the data, as encoded in the sharp decrease of the p-value, displayed in Table 3.4. Phenomenologically, this encodes the strict correlation between $\mathcal{R}(D^{(*)})$ and $\mathrm{BR}(B_c \to \tau\nu_\tau)$, and implies that if either of these scenarios is responsible of the $\mathcal{R}(D^{(*)})$ anomalies, a measurement of $\mathrm{BR}(B_c \to \tau\nu_\tau)$ will give $\mathrm{BR}(B_c \to \tau\nu_\tau) > 10\%$. The fit of the other two scenarios is not affected by the $\mathrm{BR}(B_c \to \tau\nu_\tau)$ constraint.

From Table 3.4 and from the pull plot in Figure 3.7 we also observe that the unconstrained (C_S^R, C_S^L), generated by a charged Higgs, is the one preferred by the current data, i.e. with the highest p-value. This is a result of the better fit allowed by this scenario to $F_L(D^*)$, whose pull is lowered below 1σ only in this scenario. As for the 1D scenario, we observe from Table 3.4 that the predicted value of $P_\tau(D)$ depends significantly on the scenario assumed. On the contrary, the value of the ratio $\mathcal{R}(\Lambda_c)$, comparing the τ and μe branching ratios in the baryon decay $\Lambda_b \to \Lambda_c \ell\nu$ and predicted in the SM to be [97]

$$\mathcal{R}_{\mathrm{SM}}(\Lambda_c) = 0.33 \pm 0.01, \tag{3.25}$$

is enhanced in all the scenarios.

Correlations between observables

In this section we investigate in more detail the correlation between the $\mathcal{R}(D^{(*)})$ anomaly and the polarisation observables, $F_L(D^*), P_\tau(D), P_\tau(D^*)$, as well as $\mathcal{R}(\Lambda_c)$. Here, we consider all the 2D scenarios with the $\mathrm{BR}(B_c \to \tau\nu_\tau)_{\mathrm{MAX}} = 60\%$ limit. For each of them, we project the 1σ region resulting from the fit in planes having as axes the two observables of which we want to study the correlation.

Let us start from the correlations between polarisation observables, displayed in Figure 3.8. We see that the 1σ regions of the different scenarios clearly separate in these planes. This

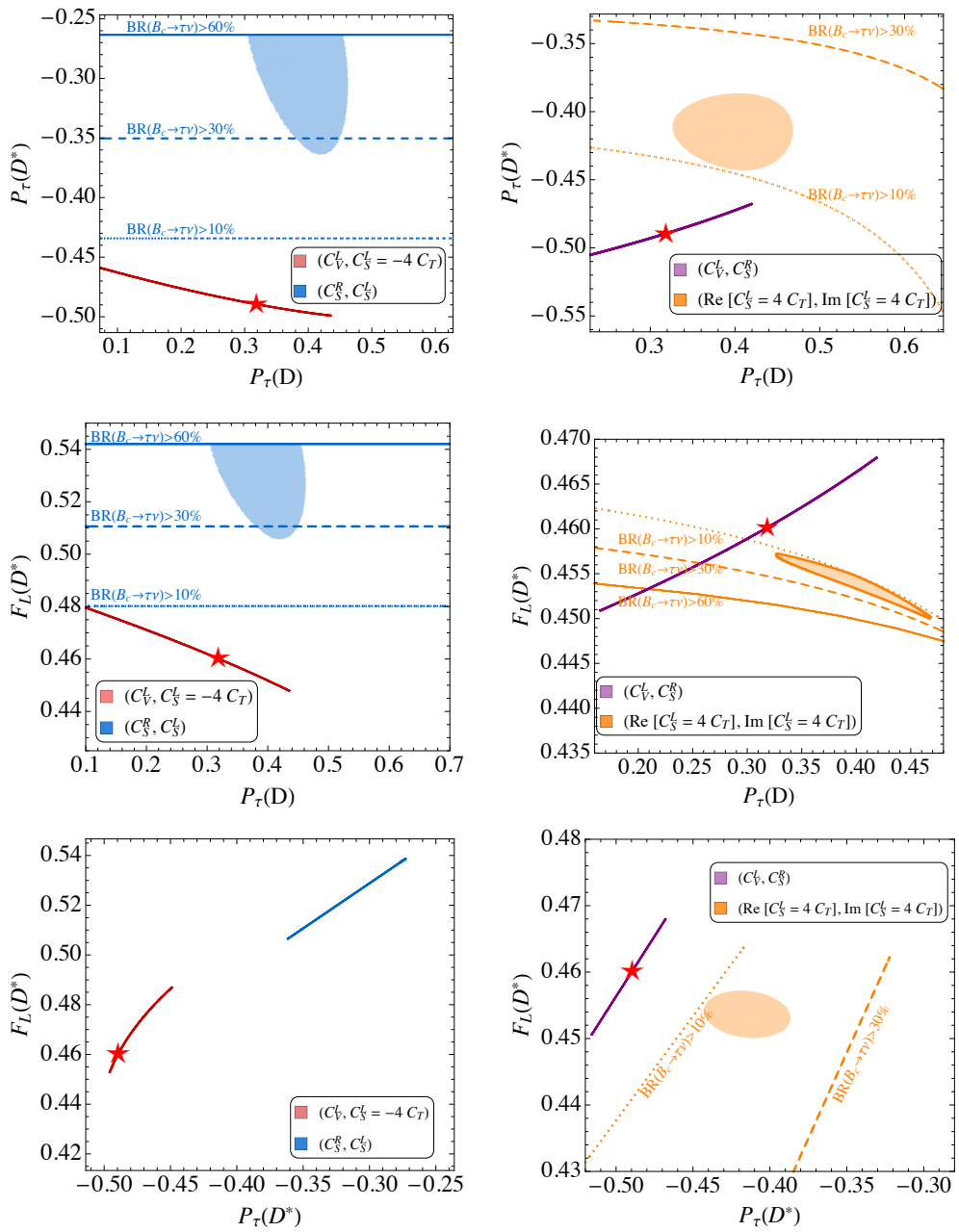

Figure 3.8: Projection of the $1\,\sigma$ regions from the 2D fits with $\mathrm{BR}(B_c \to \tau\nu_\tau)_{\mathrm{MAX}} = 60\%$ in the $P_\tau(D) - P_\tau(D^*)$, $P_\tau(D) - F_L(D^*)$ and $P_\tau(D^*) - F_L(D^*)$ planes. Each colour refers to a different scenario, and the red star represents the Standard Model prediction. The dashed and dotted lines represent respectively the limits $\mathrm{BR}(B_c \to \tau\nu_\tau)_{\mathrm{MAX}} = 30, 10\%$, excluding the region on which the label of the line lies. The plots correspond to those in Reference [2].

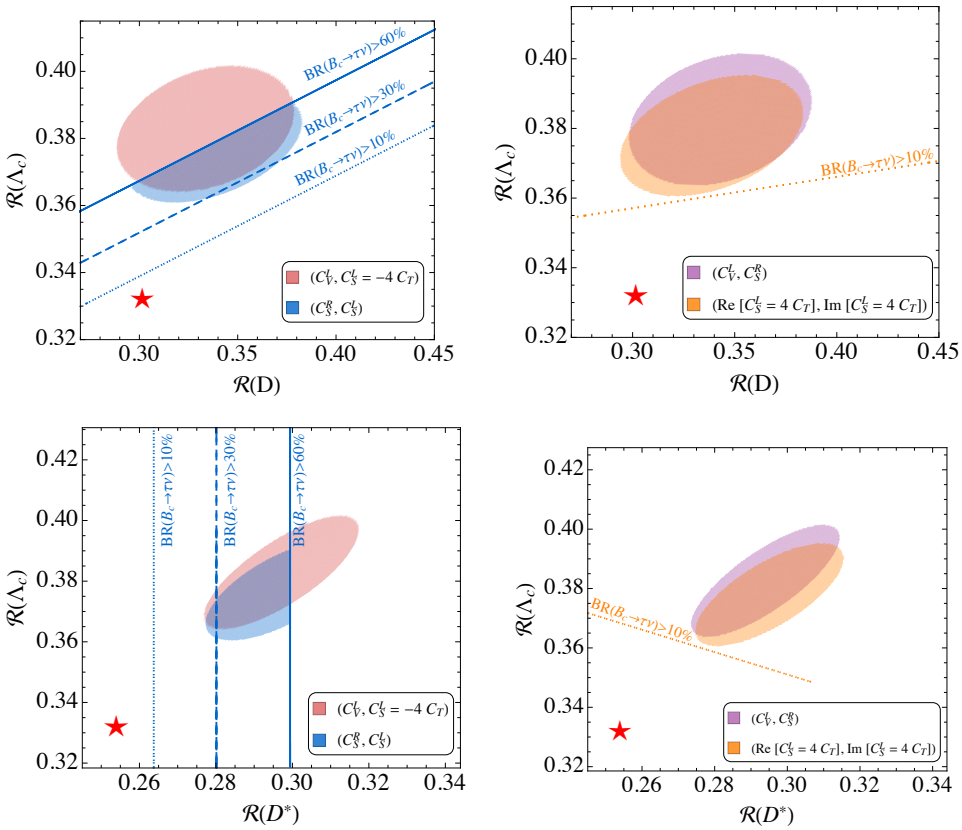

Figure 3.9: Projection of the $1\,\sigma$ regions from the 2D fits with $\mathrm{BR}(B_c \to \tau\nu_\tau)_{\mathrm{MAX}} = 60\%$ in the $\mathcal{R}(D^{(*)})$–$\mathcal{R}(\Lambda_c)$ plane. Each colour refers to a different scenario, and the red star represents the Standard Model prediction. The dashed and dotted lines represent respectively the limits $\mathrm{BR}(B_c \to \tau\nu_\tau)_{\mathrm{MAX}} = 30, 10\%$. The plots correspond to those in Reference [2].

implies that a precise knowledge of all the three polarisation observables is important in assessing which scenario of NP is responsible for the $\mathcal{R}(D^{(*)})$ anomaly. In other words, a (precise enough) experimental measurement of all the three polarisations will correspond to a point (up to uncertainties) in each of these planes, and due to the separation of the 1σ regions, these points will favour one of the scenarios considered. We also observe that in some scenarios the projection of the 1σ regions onto polarisation planes results in a line. This occurs whenever the two observables are independent on one of the two WCs, so that there is only one parameter defining the implicit dependence of the two observables on each other. In these plots, the theoretical uncertainties coming from the form factors are neglected; the lines would broaden to regions (and the regions would be broader) if theoretical uncertainties were taken into account.

Let us now consider the correlation between $\mathcal{R}(\Lambda_c)$ and the anomalous ratios $\mathcal{R}(D^{(*)})$, displayed in Figure 3.9. In these plots, the 1σ regions of the different scenarios always

overlap. The regions, which always lie above the SM prediction of $\mathcal{R}(D^{(*)})$ due to their current experimental value, also lie above the SM prediction of $\mathcal{R}(\Lambda_c)$. This tells us that an enhancement of $\mathcal{R}(D^{(*)})$ always implies an enhancement of $\mathcal{R}(\Lambda_c)$, irrespective of the NP responsible for it.

The ratio $\mathcal{R}(\Lambda_c)$ has not yet been measured. The overlap of the regions in Figure 3.9 implies that a measurement of $\mathcal{R}(\Lambda_c)$ can serve as a cross-check for the presence of NP in $\mathcal{R}(D^{(*)})$. Furthermore, we find that the correlation between $\mathcal{R}(D^{(*)})$ and $\mathcal{R}(\Lambda_c)$ can be traced back to the numerical relation

$$\frac{\mathcal{R}(\Lambda_c)}{\mathcal{R}_{\rm SM}(\Lambda_c)} \simeq 0.262 \frac{\mathcal{R}(D)}{\mathcal{R}_{\rm SM}(D)} + 0.738 \frac{\mathcal{R}(D^*)}{\mathcal{R}_{\rm SM}(D^*)}, \tag{3.26}$$

with no dependence on any of the WCs. Substituting the current experimental averages of $\mathcal{R}(D^{(*)})$ we get

$$\begin{aligned} \mathcal{R}(\Lambda_c) =& \mathcal{R}_{\rm SM}(\Lambda_c)\,(1.15 \pm 0.04) \\ =& 0.38 \pm 0.01 \pm 0.01, \end{aligned} \tag{3.27}$$

where the first error arises from the experimental uncertainty of $\mathcal{R}(D^{(*)})$, while the second error comes from the form factors.

3.3.3 Summary of the effective field theory analysis

Under the assumptions of NP coupling mostly to third generation fermions and of absence of light right-handed neutrinos, we identified NP particles that can contribute to the process $b \to c\tau\nu$ and hence modify the anomalous ratios $\mathcal{R}(D^{(*)})$. Motivated by collider constraints, we assumed their mass to be of $\mathcal{O}$(TeV) and analysed their effects in terms of an EFT. We fitted the WCs of each scenarios to the $b \to c\tau\nu$ data.

- We included the yet unmeasured $\mathrm{BR}(B_c \to \tau\nu_\tau)$ as a hard cut on the parameter space; in some of the scenarios (charged Higgs H^-, scalar LQ R_2) this limit is saturated at the best-fit point. This implies that a solution of the $\mathcal{R}(D^{(*)})$ anomaly in terms of one of these particle would come with the distinctive sign of an enhanced $\mathrm{BR}(B_c \to \tau\nu_\tau)$.

- We included the polarisation observables of the $B \to D^*\tau\nu$ channel in the fit and observed that the current central value of the D^* polarisation favours the charged Higgs scenario.

- We analysed how pairs of observables related to the process $b \to c\tau\nu$ are correlated in each model. In this analysis we included the yet-unmeasured τ polarisation in the D channel and the ratio $\mathcal{R}(\Lambda_c)$. We concluded that

  - correlations between polarisation observables are different for different NP models; hence these observables contain important information for inferring which NP scenario is responsible for the $\mathcal{R}(D^{(*)})$ anomaly.

– The ratio $\mathcal{R}(\Lambda_c)$ shows the same correlation with $\mathcal{R}(D^{(*)})$, irrespective of the NP model assumed. The current experimental values of $\mathcal{R}(D^{(*)})$ would imply an enhancement of $\mathcal{R}(\Lambda_c)$ with respect to its SM prediction. For this reason, this ratio can be seen as a test of the presence of NP in the anomalous ratios $\mathcal{R}(D^{(*)})$.

Table 3.3: Results of the 1D fits, with the Wilson coefficients defined at the scale $\mu = 1\,\text{TeV}$. The table is taken from Reference [1].

1D hyp.	best-fit	$1\,\sigma$ range	$2\,\sigma$ range	p-value (%)	pull_{SM}	$\mathcal{R}(D)$	$\mathcal{R}(D^*)$	$F_L(D^*)$	$P_\tau(D^*)$	$P_\tau(D)$	$\mathcal{R}(\Lambda_c)$
C_V^L	0.07	[0.05, 0.09]	[0.04, 0.11]	44	4.0	0.347 $+0.2\,\sigma$	0.292 $-0.2\,\sigma$	0.46 $-1.6\,\sigma$	-0.49 $-0.2\,\sigma$	0.32	0.38
C_S^R	0.09	[0.06, 0.11]	[0.03, 0.14]	2.7	3.1	0.380 $+1.4\,\sigma$	0.260 $-2.6\,\sigma$	0.47 $-1.5\,\sigma$	-0.46 $-0.1\,\sigma$	0.46	0.36
C_S^L	0.07	[0.04, 0.10]	$[-0.00, 0.13]$	0.26	2.1	0.364 $+0.8\,\sigma$	0.250 $-3.3\,\sigma$	0.45 $-1.7\,\sigma$	-0.51 $-0.2\,\sigma$	0.44	0.35
$C_S^L = 4C_T$	-0.03	$[-0.07, 0.01]$	$[-0.11, 0.04]$	0.04	0.7	0.278 $-2.1\,\sigma$	0.263 $-2.3\,\sigma$	0.46 $-1.6\,\sigma$	-0.47 $-0.2\,\sigma$	0.27	0.33

Table 3.4: Results of the 2D fits, with the Wilson coefficients defined at the scale $\mu = 1\,\text{TeV}$. The table is taken from Reference [1].

2D hyp.	best-fit	p-value (%)	pull_{SM}	$\mathcal{R}(D)$	$\mathcal{R}(D^*)$	$F_L(D^*)$	$P_\tau(D^*)$	$P_\tau(D)$	$\mathcal{R}(\Lambda_c)$
$(C_V^L,\, C_S^L = -4C_T)$	$(0.10, -0.04)$	29.8	3.6	0.333 $-0.2\,\sigma$	0.297 $+0.2\,\sigma$	0.47 $-1.5\,\sigma$	-0.48 $-0.2\,\sigma$	0.25	0.38
$\left(C_S^R,\, C_S^L\right)\Big\vert_{60\%}$	$(0.29, -0.25)$ $(-0.16, -0.69)$	75.7	3.9	0.338 $0.1\,\sigma$	0.297 $+0.1\,\sigma$	0.54 $-0.7\,\sigma$	-0.27 $+0.2\,\sigma$	0.39	0.38
$\left(C_S^R,\, C_S^L\right)\Big\vert_{30\%}$	$(0.21, -0.15)$ $(-0.26, -0.61)$	30.9	3.6	0.353 $+0.4\,\sigma$	0.280 $-1.1\,\sigma$	0.51 $-1.0\,\sigma$	-0.35 $0.0\,\sigma$	0.42	0.37
$\left(C_S^R,\, C_S^L\right)\Big\vert_{10\%}$	$(0.11, -0.04)$ $(-0.37, -0.51)$	2.6	2.9	0.366 $+0.9\,\sigma$	0.263 $-2.3\,\sigma$	0.48 $-1.4\,\sigma$	-0.44 $-0.1\,\sigma$	0.44	0.36
$(C_V^L,\, C_S^R)$	$(0.08, -0.01)$	26.6	3.6	0.343 $+0.1\,\sigma$	0.294 $-0.1\,\sigma$	0.46 $-1.6\,\sigma$	-0.49 $-0.2\,\sigma$	0.31	0.38
$(\text{Re}[C_S^L = 4C_T],\, \text{Im}[C_S^L = 4C_T])\Big\vert_{60,30\%}$	$(-0.06, \pm 0.31)$	25.0	3.6	0.339 $0.0\,\sigma$	0.295 $0.0\ \sigma$	0.45 $-1.7\,\sigma$	-0.41 $-0.1\,\sigma$	0.41	0.38
$(\text{Re}[C_S^L = 4C_T],\, \text{Im}[C_S^L = 4C_T])\Big\vert_{10\%}$	$(-0.03, \pm 0.24)$	5.9	3.2	0.330 $-0.3\,\sigma$	0.275 $-1.4\,\sigma$	0.46 $-1.6\,\sigma$	-0.45 $-0.1\,\sigma$	0.38	0.36

CHAPTER 4

The scalar leptoquark S_1

So far we analysed new physics scenarios contributing to $\mathcal{R}(D^{(*)})$ in terms of an effective field theory and focusing only on the effective couplings relevant for the τ contributions. This allowed us to estimate and compare the potential of each particle in resolving the anomaly. In this chapter we extend the analysis of one of the solutions, the scalar leptoquark $S_1 \sim (\overline{\mathbf{3}}, \mathbf{1}, 1/3)$, no longer focusing on the effective $b \to c\tau\nu$ coupling only, but building the Lagrangian for the leptoquark field and constraining its couplings by requiring agreement with experimental data. The analysis is motivated by the fact that the particle is among those favoured by the effective field theory analysis, and by the attention that this particle received as a solution of the anomaly [47, 98–102], as well as by the need to update some of the constraints on its parameter space, as we will explain below. We will review the main works present in the literature concerning the solution of the anomaly with this particle and reconsider one of the constraints that are most relevant for this scenario, the coupling of the Z boson to charged leptons. The effects of the leptoquark on these couplings are reevaluated with the inclusion of electroweak renormalisation effects. We analyse the impact of these additional effects on the description of $b \to c\tau\nu$ data by fitting the leptoquark couplings on experimental data and considering two scenarios: a scenario in which the only nonvanishing couplings are those needed to obtain Wilson coefficients for $\mathcal{R}(D^{(*)})$ with the same structure of those considered in Chapter 3 in the scalar leptoquark scenario. In a second step, we consider a scenario in which more couplings are allowed to be nonvanishing.

4.1 Motivation

Our interest in resolving the $\mathcal{R}(D^{(*)})$ anomaly with the scalar LQ S_1 is justified by two observations. First of all, as we notice from Table 3.3, this particle is among the palatable solutions of the anomaly, having a relatively high p-value, $p = 29.8\%$, compared to the

other solutions. The only model doing significantly better is the charged Higgs scenario with the mild limit $\mathrm{BR}(B_c \to \tau\nu_\tau)_{\mathrm{MAX}} = 60\%$ ($p = 75.7\%$). As we saw in the previous chapter, a description of $\mathcal{R}(D^{(*)})$ in terms of S_1 is not affected by the constraint posed on $\mathrm{BR}(B_c \to \tau\nu_\tau)$. For this reason, the S_1 solution would be favoured with respect to the charged Higgs one, in case of a low $\mathrm{BR}(B_c \to \tau\nu_\tau)$. In addition, S_1 has been largely discussed in the literature [47,98–102] as a possible solution to the $\mathcal{R}(D^{(*)})$ anomalies. The interest increased when the authors of Reference [99] attempted a simultaneous description of $\mathcal{R}(D^{(*)})$, of the anomalous magnetic moment of the muon Δa_μ and of the data from $B \to K^{(*)}\mu\mu$ decays – from now on generically referred to as $R_{K^{(*)}}$ anomalies. These three (sets of) observables are in tension with their SM prediction and the confirmation of any of them would imply NP with LFNU. This explanation of the anomalies was criticised by the authors of Reference [100], pointing out that the analysis in Reference [99] neglects some of the constraints from leptonic meson decays and that some of the constraints included are imposed as conditions that are necessary but not sufficient for guaranteeing agreement with the experimental data. In their analysis, the authors of Reference [100] find that the region of parameters allowing for a description of $R_{K^{(*)}}$ and simultaneously passing all flavour constraints from leptonic decays predicts a value of $\mathcal{R}(D^{(*)})$ below the experimental average, and predicts too large effects on the μ channel, implying disagreement with the experimental value of the $\mathcal{R}(D)_{\mu/e}$ and $\mathcal{R}(D^*)_{e/\mu}$ ratios. The scenario with a S_1 was analysed again in Reference [101], pointing out that although a simultaneous solution of the $R_{K^{(*)}}$ and $\mathcal{R}(D^{(*)})$ anomalies is indeed challenged by current flavour constraints, the solution of only one of the two tensions is still viable. In other words, if one of the two anomalies turns out to be due to a statistical fluctuation, the LQ is among the favoured candidates for the remaining one. The focus of our work is on $\mathcal{R}(D^{(*)})$ only, for which S_1 is hence still a viable candidate.

In analysing which region of the parameter space of S_1 is allowed for the explanation of the anomaly, the authors of Reference [101] found the constraint imposed on the effects of S_1 on the $Z\ell\ell$ couplings to be decisive. However, their bounds are set by using an expression which neglects terms of order $\mathcal{O}(m_Z^2/m_t^2)$. These corrections were later evaluated in Reference [103] but only analysed in a scenario with two scalar LQs, S_1 and S_3. Furthermore, none of the references takes into account that the LQ also gives contributions to the $\mu \to e\nu\overline{\nu}$ decay, which is used to precisely measure the Fermi constant G_{F}. This means that the measured value of G_{F} includes both the SM and the LQ contribution. This effect is further related to the $Z\ell\ell$ coupling via $SU(2)$, giving an additional contribution to the $Z\ell\ell$ couplings via the counterterm for the g coupling. To refine the analysis of the NP scenario with S_1, in this chapter we include both these effects and analyse their impact on a possible explanation of $\mathcal{R}(D^{(*)})$ in terms of S_1. We will start by writing down the Lagrangian for S_1, then we will analyse in detail the effects of the LQ on the $Z\ell\ell$ coupling and conclude with a phenomenological analysis, fitting the $b \to c\tau\nu$ data together with the $Z\ell\ell$ ones, as well as including other flavour observables that are affected as soon as we start assuming a nontrivial Yukawa structure, with couplings not only to third generation fermions.

Throughout the whole chapter, we will simplify our notation and refer to the scalar LQ as $\Delta \sim S_1^\dagger \sim (3, 1, -1/3)$, adopting the notation of Reference [100].

4.2 Leptoquark Lagrangian

In this section we review the NP model including a scalar LQ Δ. The description is analogous to the ones in References [99–101].

The kinetic term and the interaction of the scalar LQ Δ with the SM Higgs doublet Φ read

$$\mathcal{L} \supset (D_\mu \Delta)^\dagger D^\mu \Delta - M_\Delta^2 |\Delta|^2 - g_{\Phi\Delta} |\Delta|^2 |\Phi|^2 + \text{h.c.}. \tag{4.1}$$

Since we are interested in meson decays, the part of the Lagrangian that is most relevant for us is the Yukawa interaction of the scalar LQ with fermions. Writing down all the possible renormalisable interactions that can be built with Δ and SM fermion fields requiring Lorentz and gauge invariance under the SM group, one gets [72]

$$\begin{aligned} \mathcal{L} \supset & y^L_{ij} \overline{Q^c_i} i\tau_2 L_j \Delta^\dagger + y^R_{ij} \overline{u^c_{Ri}} \ell_{Rj} \Delta^\dagger + \\ & + z^L_{ij} \overline{Q^c_i} \Delta i\tau_2 Q_j + z^R_{ij} \overline{Q^c_{Ri}} \Delta d_{Rj} + \text{h.c.}, \end{aligned} \tag{4.2}$$

where the indices $i, j = 1, 2, 3$ refer to flavour space, τ_2 is the Pauli matrix in $SU(2)_\text{L}$ space and $\Psi^c = C\overline{\Psi}^\text{T} = i\gamma^2\gamma^0\overline{\Psi}^\text{T}$ are charge-conjugated spinors. Throughout our analysis, we will assume the di-quark couplings $z^{L,R}$ to be vanishing, and hence neglect the second line of Equation (4.2). This assumption is motivated by the fact that the presence of both di-quark and LQ couplings implies possible contributions of Δ to proton decay. The experimental lower bound on the lifetime of the proton, which is $\mathcal{O}(10^{29})$ years [31], would push the $z^{L,R}$ couplings to negligible values. As we will see in the following chapter, from a theoretical point of view the vanishing of the $z^{L,R}$ couplings can be motivated by imposing an additional symmetry on the Lagrangian. We will neglect this issue for the time being, and just set $z^{L,R} = 0$ on a phenomenological basis, in agreement with Reference [72]. With vanishing $z^{L,R} = 0$, the Yukawa Lagrangian we will consider is then

$$\mathcal{L} \supset y^L_{ij} \overline{Q^c_i} i\tau_2 L_j \Delta^\dagger + y^R_{ij} \overline{u^c_{Ri}} \ell_{Rj} \Delta^\dagger + \text{h.c.}. \tag{4.3}$$

Writing down the $SU(2)_\text{L}$ components explicitly, we get

$$\mathcal{L} \supset y^L_{ij} (\overline{u^c_{Li}} \ell_{Lj} - \overline{d^c_{Li}} \nu_j) \Delta^\dagger + y^R_{ij} \overline{u^c_{Ri}} \ell_{Rj} \Delta^\dagger + \text{h.c.}. \tag{4.4}$$

The fields in Equation (4.4) are written in the interaction basis. To obtain the expressions for physical observables we must use the mass basis instead. If we use the down-quark basis, the change of basis leads to the Lagrangian

$$\begin{aligned} \mathcal{L} \supset & y^L_{ij} (V^*_{\text{CKM}ki} \overline{u'^c_{Lk}} \ell_{Lj} - \overline{d'^c_{Li}} \nu_j) \Delta^\dagger + y^R_{ij} \overline{u'^c_{Ri}} \ell'_{Ri} \Delta^\dagger + \text{h.c.} \\ \equiv & \left(y^L_{u\ell}\right)_{ij} \overline{u'^c_{Lj}} \ell_{Lj} \Delta^\dagger - \left(y^L_{d\nu}\right)_{ij} \overline{d'^c_{Li}} \nu_j \Delta^\dagger + \left(y^R_{u\ell}\right)_{ij} \overline{u'^c_{Ri}} \ell'_{Ri} \Delta^\dagger + \text{h.c.}, \end{aligned} \tag{4.5}$$

where we introduced the coupling matrices $y^L_{d\nu} = y^L$, $y^R_{u\ell} = y^R$ and $y^L_{u\ell} = V^*_\text{CKM} y^L = V^*_\text{CKM} y^L_{d\nu}$. All the fields in Equation (4.5) apart from the neutrino ones are now written in the mass basis. As in the analysis of Chapter 3, the neutrino fields are kept in the flavour

basis. To simplify our notation, we will remove the apex in what follows; all the unprimed fields u, d, ℓ will denote the mass eigenstates while ν will denote the flavour eigenstates.

In our analysis we will assume the mass of the LQ to be fixed to $M_\Delta = 1\,\text{TeV}$, this value being in the mass range expected for a solution to the $\mathcal{R}(D^{(*)})$ anomalies. A lower value of this mass is challenged by direct searches at colliders, as mentioned in the previous sections. A higher value would require larger couplings for fitting the anomalous ratios, and could possibly exceed the perturbative unitarity limit[1] [104]. The free parameters of our model are hence given by

$$y^L_{d\nu} = \begin{pmatrix} y^L_{11} & y^L_{12} & y^L_{13} \\ y^L_{21} & y^L_{22} & y^L_{23} \\ y^L_{31} & y^L_{32} & y^L_{33} \end{pmatrix}, \qquad y^R_{u\ell} = \begin{pmatrix} y^R_{11} & y^R_{12} & y^R_{13} \\ y^R_{21} & y^R_{22} & y^R_{23} \\ y^R_{31} & y^R_{32} & y^R_{33} \end{pmatrix}. \tag{4.6}$$

However, possible effects of BSM particles on processes involving first generation fermions are severely constrained by experimental data. In particular, flavour changing processes with down-type quarks are constrained by light meson data such as those from the decays $K \to \pi\nu\nu$ and from $K - \overline{K}$ mixing [31], while lepton flavour violation (LFV) involving light leptons is severely constrained from experiments on μ–e conversion in muonic atoms [105]. For this reason, as in References [99, 101], we assume the following structure

$$y^L_{d\nu} = \begin{pmatrix} 0 & 0 & 0 \\ 0 & y^L_{s\mu} & y^L_{s\tau} \\ 0 & y^L_{b\mu} & y^L_{b\tau} \end{pmatrix}, \qquad y^R_{u\ell} = \begin{pmatrix} 0 & 0 & 0 \\ 0 & y^R_{c\mu} & y^R_{c\tau} \\ 0 & y^R_{t\mu} & y^R_{t\tau} \end{pmatrix}. \tag{4.7}$$

Nonetheless, couplings with the up quark are still generated via the switch to the mass basis, i.e.

$$y^L_{u\ell} = V^*_{\text{CKM}} y^L = \begin{pmatrix} 0 & y^L_{u\mu} & y^L_{u\tau} \\ 0 & y^L_{c\mu} & y^L_{c\tau} \\ 0 & y^L_{t\mu} & y^L_{t\tau} \end{pmatrix} = \begin{pmatrix} 0 & V^*_{us} y^L_{s\mu} + V^*_{ub} y^L_{b\mu} & V^*_{us} y^L_{s\tau} + V^*_{ub} y^L_{b\tau} \\ 0 & V^*_{cs} y^L_{s\mu} + V^*_{cb} y^L_{b\mu} & V^*_{cs} y^L_{s\tau} + V^*_{cb} y^L_{b\tau} \\ 0 & V^*_{ts} y^L_{s\mu} + V^*_{tb} y^L_{b\mu} & V^*_{ts} y^L_{s\tau} + V^*_{tb} y^L_{b\tau} \end{pmatrix}. \tag{4.8}$$

Compared to Reference [100] we include nonvanishing entries in the coupling matrix $y^R_{u\ell}$. As we will see, the novelty of our analysis with respect to those in References [99–101] is the inclusion of the EW renormalisation effects on the $Z\ell\ell$ couplings. Furthermore, the methodology followed will be different, since where possible we will include the observables affected by the scalar LQ in a fit of its parameters, rather than performing a scan in the parameter space. Finally, our analysis also includes the polarisation observables of the $B \to D^*\tau\nu$, as was the case for the EFT analysis of the previous chapter.

[1] The leading order LQ contributions to $\mathcal{R}(D^{(*)})$ are tree-level processes. For this reason, if we neglect LQ effects of higher orders, the $\mathcal{R}(D^{(*)})$ data only allow to constrain ratios of couplings over the mass of the LQ. Fixing one parameter hence amounts in a rescaling of the others.

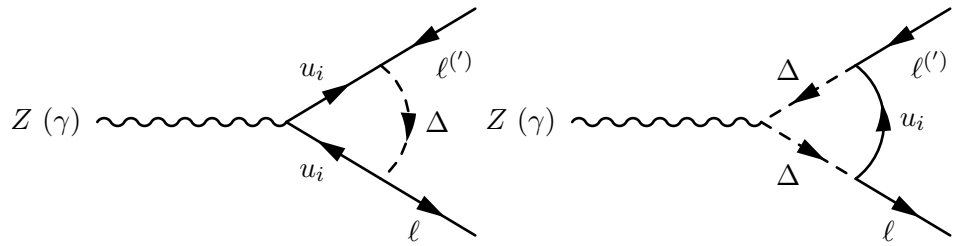

Figure 4.1: Vertex diagrams contributing to the $Z\ell\ell$ couplings and to the magnetic moment of leptons. For different lepton flavours and for γ as a gauge boson, these are the same diagrams contributing to $\tau \to \mu\gamma$.

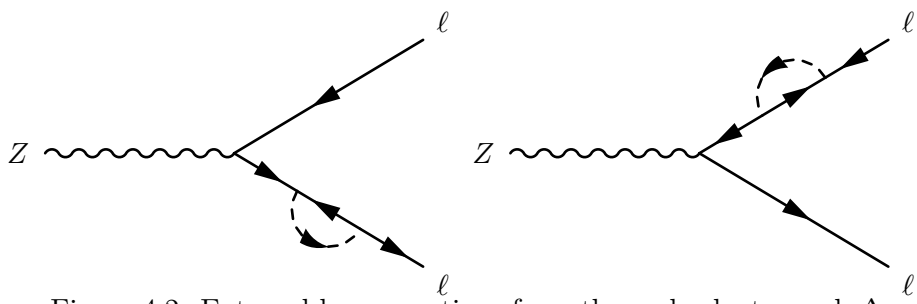

Figure 4.2: External leg corrections from the scalar leptoquark Δ.

4.3 Modification of the $Z\ell\ell$ coupling

For the evaluation of the matrix elements needed for the analysis in this chapter, the Feynman rules for Δ involving fermion number violation have been obtained following References [106, 107]. For the evaluation of the loop integrals we used the Mathematica packages FeynCalc [108, 109] and PackageX [110].

Direct one-loop contributions of Δ to the right- and left-handed couplings of charged leptons to the Z boson arise from the diagrams in Figure 4.1, with the additional external leg corrections of Figure 4.2. The evaluation of these contributions is simplified by some considerations on the energy scales at play. The $Z\ell\ell$ couplings were measured at LEP, colliding e^+e^- at energies close to the Z mass. The external momenta have, then, four momentum squared of the order $\sim m_Z^2$. If no approximations are made, there are three energy scales relevant for this process: the masses of the virtual particles in the loop m_u, M_Δ, and the external momenta $\sim m_Z$. First of all, we can separate the contributions from diagrams with light quarks in the internal loop from those with a top quark. In the first case one can get rid of one of the mass scales by setting $m_{u,c} \simeq 0$. The top effects were evaluated in Reference [99] getting rid of one of the mass scales by neglecting terms of order $\mathcal{O}(m_Z^2/m_t^2)$. Since $m_Z \simeq 91\,\text{GeV}$ and $m_t \simeq 173\,\text{GeV}$, there is clearly room for improvement on this. The terms of order $\mathcal{O}(m_Z^2/m_t^2)$ were recently evaluated in Reference [103], and we recomputed them, in order to later include the EW renormalisation effects.

To include terms of order $\mathcal{O}(m_Z^2/m_t^2)$ we used the following expansion of the LQ propagators

with respect to the ratios of external momenta over the LQ mass $p^2/M_\Delta^2 \sim m_Z^2/M_\Delta^2$:

$$\frac{1}{(l+p)^2 - M_\Delta^2} = \frac{1}{l^2 - M_\Delta^2}\left[1 - \frac{-p^2 + 2l\cdot p}{l^2 - M_\Delta^2} + \frac{4\,(l\cdot p)^2}{(l^2 - M_\Delta^2)^2}\right] + \mathcal{O}\left(\frac{p}{M_\Delta}\right)^4, \tag{4.9}$$

where l denotes the loop momentum, and used partial fraction decomposition to rewrite the products of propagators as

$$\frac{1}{(l^2 - m_t^2)(l^2 - M_\Delta^2)} = \frac{1}{(M_\Delta^2 - m_t^2)}\left[\frac{1}{l^2 - M_\Delta^2} - \frac{1}{l^2 - m_t^2}\right]. \tag{4.10}$$

Recursively applying these substitutions, and restricting to the leading term in the decoupling limit, i.e. neglecting terms of order $\sim 1/M_\Delta^4$ and higher, we obtained the light quarks contributions to the right- and left-handed couplings

$$\begin{aligned}
\Delta g_{Z\ell\ell}^{L,u,c} =& \frac{1}{16\pi^2}\frac{m_Z^2}{M_\Delta^2}\sum_{q=u,c}\left|y_{q\ell}^L\right|^2\left[\left(\log\frac{m_Z^2}{M_\Delta^2} - i\pi\right)\left(\frac{1}{2} - \frac{2}{3}\sin^2\theta\right) - \frac{1}{6} + \frac{5}{6}\sin^2\theta\right],\\
\Delta g_{Z\ell\ell}^{R,u,c} =& -\frac{1}{288\pi^2}\frac{m_Z^2}{M_\Delta^2}\sin^2\theta\sum_{q=u,c}\left|y_{q\ell}^R\right|^2\left[12\log\frac{m_Z^2}{M_\Delta^2} - 12i\pi - 5\right].
\end{aligned} \tag{4.11}$$

Proceeding analogously, for the top-quark contributions we get

$$\begin{aligned}
\Delta g_{Z\ell\ell}^{L,t} =& \left|y_{t\ell}^L\right|^2\Bigg[-\frac{3}{32\pi^2}\frac{m_t^2}{M_\Delta^2}\left(\log\frac{m_t^2}{M_\Delta^2} + 1\right) +\\
&+ \frac{1}{192\pi^2}\frac{m_Z^2}{M_\Delta^2}\left(5\cos(2\theta) + 2(2\cos(2\theta)+1)\log\frac{m_t^2}{M_\Delta^2} + 6\right)\Bigg],\\
\Delta g_{Z\ell\ell}^{R,t} =& \left|y_{t\ell}^R\right|^2\left[\frac{3}{32\pi^2}\frac{m_t^2}{M_\Delta^2}\left(\log\frac{m_t^2}{M_\Delta^2} + 1\right) - \frac{1}{192\pi^2}\frac{m_Z^2}{M_\Delta^2}\left(2(5 + 4\log\frac{m_t^2}{M_\Delta^2})\sin^2\theta + 3\right)\right].
\end{aligned} \tag{4.12}$$

Both results in Equations (4.11) and (4.12) are in agreement with Reference [103].

4.3.1 Effects from electroweak renormalisation

As a matter of fact, not all effects on the $Z\ell\ell$ couplings are included in Equations (4.11) and (4.12), which are missing the effects of EW renormalisation, as we now briefly explain. These effects were previously neglected in the literature.

Since the EW theory has two coupling constants, we can express the couplings with the W, Z and γ gauge bosons in terms of two parameters. The most convenient choice is to use the weak $SU(2)$ coupling g and the electromagnetic coupling e. The value of the first one is determined via a measurement of the Fermi constant $G_F^{SM}/\sqrt{2} = g^2/8m_W^2$ via the muon lifetime [111], i.e. via the decay $\mu \to e\nu\nu$. For the electromagnetic coupling e, the

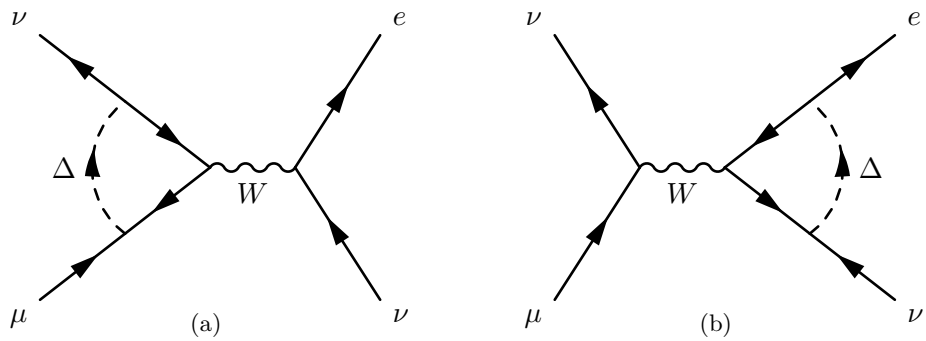

Figure 4.3: Leptoquark contribution to $\mu \to e\nu\nu$ decay. Since Δ does not couple to electrons, the contribution of the right panel vanishes. External leg corrections are not shown here.

value of the electromagnetic fine structure constant $\alpha = e^2/4\pi$ is fixed at $q^2 = 0$ to the one measured in atomic, condensed-matter and low-energy particle physics, providing independent measurements of the constant. These choices are convenient since these measurements provide a high precision. For reference, the values quoted by the Particle Data Group are $G_{\mathrm{F}} = 1.1663787(6) \times 10^{-5}\,\mathrm{GeV}^{-2}$ and $\alpha = 1/137.035999139(31)$ [31].

NP particles can also contribute to the processes used to determine the values of the couplings. This implies that in presence of NP, the actual values of the EW parameters differ from the ones extracted by assuming the SM as underlying theory, since a share in the processes used to measure them is actually to be accounted to the NP contribution. The simplest way to account for this is to require the values of the parameters of the EW theory at the scale of the experiment used to measure them to remain unvaried with respect to the SM ones. After the inclusion of the NP virtual corrections, this is equivalent to setting the finite part of the counterterm of the bare parameter such that it cancels the NP effects. This additional finite part of the conunterterm will have to be taken into account when considering observables expressed in terms of the EW parameters.

Let us illustrate this in the case of the Fermi constant. As mentioned above, this quantity is measured via the muon decay constant, in the decay $\mu \to e\nu\nu$. When including the NP effects, we require that the relation $G_{\mathrm{F}}/\sqrt{2} = g^2/8m_W^2$ still holds after the introduction of Δ. Since $g^2/8m_W^2$ is by definition the contribution of the SM to $G_{\mathrm{F}}/\sqrt{2}$, this requirement can be satisfied by requiring that the finite part of the counterterm δg cancels the effects of the NP particles.

In our model, Δ contributes to the μ decay via the diagrams in Figure 4.3. Since we assumed Δ not to couple with electrons, as can be seen in Equation (4.8), there are no contributions such as those in Figure 4.3b. We can hence set $G_{\mathrm{F}}/\sqrt{2} = g^2/8m_W^2$ by requiring the contributions of the diagram in Figure 4.3a and of the external leg corrections to be cancelled by δg. In other words, we set

$$-\delta g^{\mathrm{NP}} =$$

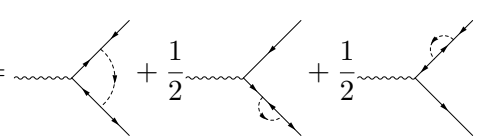

$$+\frac{1}{2}$$

$$+\frac{1}{2}$$

(4.13)

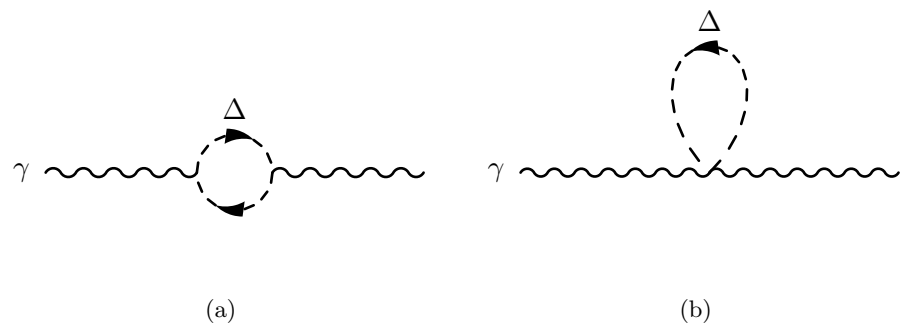

Figure 4.4: Leptoquark contributions to the vacuum polarisation of the photon.

Concerning the electromagnetic coupling[2], the renormalised fine-structure constant is given by

$$\alpha(q^2) = \frac{\alpha_0}{1 - [\Pi(q^2) - \Pi(0)]}, \tag{4.14}$$

where $\Pi(q^2)$ is the vacuum polarisation of the photon, stripped of the tensor structure fixed by the Ward identity. Analogously to the case of the Fermi constant, fixing the finite part of the counterterm such that it cancels the NP contributions to the vacuum polarisation of the photon at $q^2 = 0$ sets the finite part of the counterterm for the electromagnetic coupling to

$$\delta e^{\mathrm{NP}} = -\frac{e}{2}\left[\Pi_{\mathrm{NP}}(q^2) - \Pi_{\mathrm{NP}}(0)\right]. \tag{4.15}$$

In our model, the NP contributions to $\Pi(q^2)$ in Equation (4.15) come from the LQ effects displayed in Figure 4.4.

Let us now look at how δg^{NP} and δe^{NP} affect the $Z\ell\ell$ coupling. If we choose as parameters the $SU(2)$ coupling g and the weak mixing angle θ, which relates the g and the electromagnetic coupling e as $\sin\theta = e/g$, the coupling of $Z\ell\ell$ reads

$$ig_{Z\ell\ell}\gamma_\mu = i\frac{g}{\cos\theta}\gamma_\mu\left(\frac{1}{2}\tau_\ell^3 - Q_\ell \sin^2\theta - \frac{1}{2}\tau_\ell^3\gamma_5\right), \tag{4.16}$$

where τ_ℓ^3 stands for the third generator of the $SU(2)_L$ representation of the particle considered. The terms from Equations (4.13) and (4.15) can be included in the $Z\ell\ell$ couplings in Equation (4.16) using the relation $\sin\theta = e/g$ and obtaining the counterterm for $g_{Z\ell\ell}$ as

$$\delta g_{Z\ell\ell} = \frac{\partial g_{Z\ell\ell}}{\partial g}\delta g + \frac{\partial g_{Z\ell\ell}}{\partial e}\delta e. \tag{4.17}$$

When these effects are taken into account, the modification of Δ on the $Z\ell\ell$ couplings read

[2]The procedure is analogous to the one used in Reference [112] to take into account the leading logarithms coming from the light fermions in the charge renormalisation

$$g^R_{Z\ell\ell} = \frac{g}{\cos\theta}\Bigg[\frac{g^2}{3456\pi^2}\frac{m_Z^2}{M_\Delta^2}\sin^2\theta\,(\cos(2\theta)+2)\tan^2\theta + \\ + \frac{3}{128\pi^2}\frac{\left|y^L_{t\mu}\right|^2}{\cos^2\theta}\frac{m_t^2}{M_\Delta^2}\left(2\log\frac{m_t^2}{M_\Delta^2}+1\right) + \\ + \sum_{q=u,c,t}\Delta g^{R,q}_{Z\ell\ell}\Bigg], \tag{4.18}$$

$$g^L_{Z\ell\ell} = \frac{g}{\cos\theta}\Bigg[\frac{g^2}{3456\pi^2}\frac{m_Z^2}{M_\Delta^2}\sin^2\theta\,(\cos(2\theta)+2)\tan^2\theta + \\ + \frac{3}{128\pi^2}\frac{\left|y^L_{t\mu}\right|^2}{\cos^2\theta}\frac{m_t^2}{M_\Delta^2}\left(2\log\frac{m_t^2}{M_\Delta^2}+1\right) + \\ + \sum_{q=u,c,t}\Delta g^{L,q}_{Z\ell\ell}\Bigg], \tag{4.19}$$

where we split the contribution to the left- and right-handed leptons. The first lines in Equations (4.18) and (4.19) come from the photon polarisation, the second ones from the g counterterm. The third lines are the *direct* effects of Equations (4.11) and (4.12). Interestingly, the EW renormalisation effects imply that even the coupling of Z to electrons receives contributions from Δ, although Δ does not couple to the electron directly. This can be seen by noting that the first two lines of Equations (4.18) and (4.19) do not depend on the couplings with the electron. The EW renormalisation effects are tiny in the case of δe, but can be significant for δg which, however, only arises for nonvanishing couplings with the muons $y^L_{t\mu} \neq 0$. This will be shown explicitly in the analysis in the next section.

4.4 Phenomenology

In this section we analyse the impact of including the results in Equations (4.18) and (4.19) on the explanation of the $\mathcal{R}(D^{(*)})$ data in terms of the scalar LQ Δ. Our approach will be different from the one followed in Reference [101], where the authors require the $Z\ell\ell$ couplings to agree at 95% confidence level with the results of the fit to EW precision observables (EWPO) [113] assuming LFU. Since the scalar LQ implies the presence of LFNU, this approach only requires the scalar LQ not to have a large impact on each of the $Z\ell\ell$ couplings. Instead, once the hypothesis of LFU is dropped, we allow the LQ to modify these couplings, each of them independently, and include in our fits the individual $Zee, Z\mu\mu, Z\tau\tau$ couplings measured at LEP. Those couplings are displayed as ellipses in

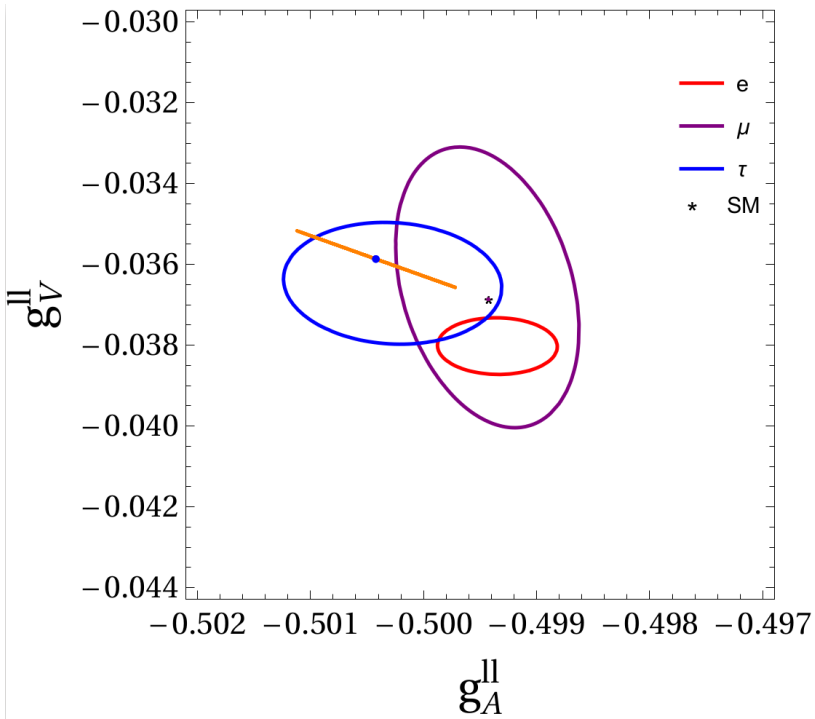

Figure 4.5: $Z\ell\ell$ couplings. The ellipses correspond to the 1σ experimental values [31], the black star to the Standard Model prediction. The coloured dots represent the values predicted at the best-fit point of the scenario with simplified couplings. The orange line represents the values of the $Z\tau\tau$ couplings obtained varying the Yukawa couplings $y^L_{b\tau}, y^R_{c\tau}$ in the 1σ region of the 2D scenario. The values of the $Z\mu\mu$ and Zee couplings overlap with the SM prediction.

Figure 4.5 in terms of the vector and axial couplings $g^{V,A}_{Z\ell\ell} = (g^R_{Z\ell\ell} \pm g^L_{Z\ell\ell})/2$. From this figure we see that the central experimental values for the three leptons are indeed slightly different, and that the SM coupling obtained from fitting EWPO, represented by the black star, is in slight tension with the electron one.

4.4.1 Fitting scenarios

Compared to Chapter 3, in which the WCs were fitted, the analysis in this chapter is performed by fitting the parameters of the LQ Lagrangian. In order to simplify the analysis and to have a reduced number of parameters to fit, we assume the Yukawa couplings of Equation (4.7) to be real.

The impact of the $Z\ell\ell$ effects will be analysed in two benchmark scenarios. In a first scenario only the two Yukawa couplings needed to reproduce the effective scenario of Chapter 3 are assumed to be nonvanishing, namely $y^L_{b\tau}, y^R_{c\tau} \neq 0$ The Yukawa structure assumed in this

scenario is then

$$y^L_{d\nu} = \begin{pmatrix} 0 & 0 & 0 \\ 0 & 0 & 0 \\ 0 & 0 & y^L_{b\tau} \end{pmatrix}, \qquad y^R_{u\ell} = \begin{pmatrix} 0 & 0 & 0 \\ 0 & 0 & y^R_{c\tau} \\ 0 & 0 & 0 \end{pmatrix}, \qquad y^L_{u\ell} = \begin{pmatrix} 0 & 0 & V^*_{ub} y^L_{b\tau} \\ 0 & 0 & V^*_{cb} y^L_{b\tau} \\ 0 & 0 & V^*_{tb} y^L_{b\tau} \end{pmatrix} \tag{4.20}$$

Since we are assuming real couplings, this scenario results in a two-dimensional (2D) fit. With the values $y^L_{b\tau} = -1.3, y^R_{c\tau} = 0.3$, this scenario corresponds to the one considered as a solution of the $\mathcal{R}(D^{(*)})$ anomalies in Reference [101]. Since Equation (4.20) implies no coupling to μ, the only EW renormalisation effect will arise from the photon polarisation; for this reason this scenario will allow us to analyse the impact of the latter.

In a second step, we assume the general texture of Equation (4.7), hence resulting in a 8D fit. Compared to the 2D scenario, the additional couplings will require us to include more experimental input and, since this time the couplings with μ are nonvanishing, they will allow us to understand the impact of EW renormalisation effects from G_{F}.

The scenarios analysed are summarised in Table 4.1, in which we list the observables included in each analysis. Their inclusion is briefly explained in the following section.

	$\mathcal{R}(D^{(*)})$	$F_L(D^*)$	$P_\tau(D^*)$	$g^{V,A}_{\ell\ell}$	$\mathcal{R}_{\mu/e}(D), \mathcal{R}_{e/\mu}(D^*)$	$B_s - \overline{B}_s$	$R_{\nu\nu}$	$\tau \to \mu\gamma$	$D^0 \to \mu\mu$	LFU ratios	Δa_μ
# observables	2	1	1	6	2	1	1	1	1	3	1
2D	✓	✓	✓	✓	∅	∅	∅	∅	∅	∅	∅
$8\mathrm{D}_{\mathrm{simple}}$	✓	✓	✓	✓	✓	$\leq$	$\leq$	$\leq$	$\leq$	✗	✗
$8\mathrm{D}_{\mathrm{LFU}}$	✓	✓	✓	✓	✓	$\leq$	$\leq$	$\leq$	$\leq$	✓	✗
$8\mathrm{D}_{a_\mu}$	✓	✓	✓	✓	✓	$\leq$	$\leq$	$\leq$	$\leq$	✗	✓

Table 4.1: Observables included in the leptoquark fits. A ✓(✗) indicates an observable (not) included in the χ^2, a ∅ indicates observables receiving no contribution, a $\leq$ indicates a hard cut on the parameter space.

4.4.2 Experimental inputs

In this Section we briefly review the observables included in our analysis.

$\mathcal{R}_{e/\mu}(D^*)$ and angular distributions for light leptons

With nonvanishing couplings to e, μ, the LQ can also affect the $B \to D^{(*)}\mu\nu$ modes, hence modifying the ratios $\mathcal{R}_{\mu/e}(D), \mathcal{R}_{e/\mu}(D^*)$. These couplings are 0 in the 2D scenario, while the 8D texture allows for couplings to μ. For the latter scenario, we include the experimental values quoted in Equation (3.1) in the fit.

Although the Belle Collaboration provides the kinematic distribution of the decays $B \to D^{(*)}\ell\nu$ with light leptons in the final state [28,29], these data are already implicitly included, since they are used for fitting the form factors [10]. For this reason we do not include them in the fit.

As mentioned in Chapter 3 however, the angular data of the light lepton channels are in good agreement with their SM predictions, and this was one of the reasons that motivated

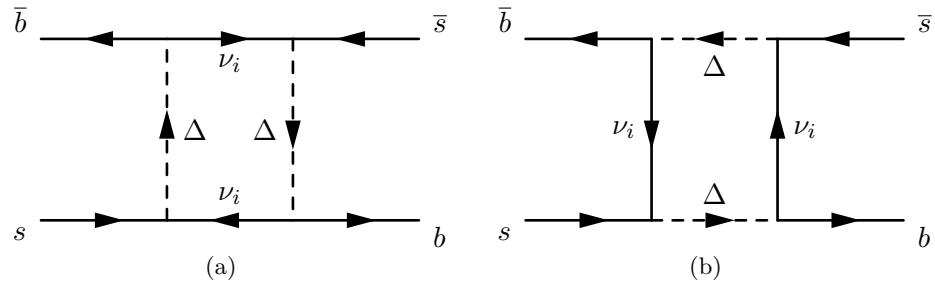

Figure 4.6: Leptoquark contributions to $B_s - \overline{B}_s$ mixing.

our minimal choice in the EFT analysis, assuming NP to couple only to τ. We will check the impact of the μ couplings of the 8D scenario on the angular distributions by plotting and comparing the measured angular distribution with the distribution predicted in the SM and with the distribution predicted at the best-fit point of the 8D fit.

$B_s - \overline{B}_s$ mixing

The mixing of the neutral B_s meson is a loop process in the SM, and as such constitutes a good probe for the presence of NP effects. The experimental limit on these effects can be set on the ratio comparing the difference between the heavy and light B_s mass eigenstates, Δm_{B_s}, with NP and within the SM. The mass difference in the SM is given by [114]

$$\Delta m_{B_s}^{\mathrm{SM}} = \frac{G_{\mathrm{F}}^2}{12\pi^2} |V_{tb} V_{ts}^*| {m_W}^2 \eta_B S_0(\frac{m_t^2}{m_W^2}) B f_{B_s}^2 M_{B_s}, \tag{4.21}$$

where the short distance information is encoded in the product $\eta_B S_0(m_t^2/m_W^2)$, in which $S_0(m_t^2/m_W^2) \simeq 2.35$ is the Inami-Lim function from the 1-loop box diagrams in the SM and $\eta_B = 0.8393 \pm 0.0034$ comprises perturbative 2-loop QCD corrections [114]. The bag parameter B and the decay constant f_{B_s} encode the nonperturbative hadronic contributions to the mixing, which can be determined with the use of sum rules in HQET or with LQCD. Using the value obtained using HQET sum rules, the SM prediction gives [115]

$$\Delta m_{B_s}^{\mathrm{SM}} = (18.5^{+1.2}_{-1.5})\mathrm{ps}^{-1}, \tag{4.22}$$

where the largest uncertainty comes from the nonperturbative parameters, and cannot be interpreted as statistical, since it comes from the theoretical approximations used for the computation.

Nonvanishing couplings to s, b quarks imply that Δ contributes to the $B_s - \overline{B}_s$ mixing through the box diagrams in Figure 4.6. The ratio of mass differences within the LQ model and in the SM reads [100]

$$\frac{\Delta m_{B_s}^{\mathrm{NP}}}{\Delta m_{B_s}^{\mathrm{SM}}} = 1 + \frac{\eta_1 \left(y^L \cdot y^L\right)_{bs}^2}{32 G_{\mathrm{F}}^2 {m_W}^2 |V_{tb} V_{ts}^*| \eta_B S_0(\frac{m_t^2}{m_W^2}) M_\Delta^2}, \tag{4.23}$$

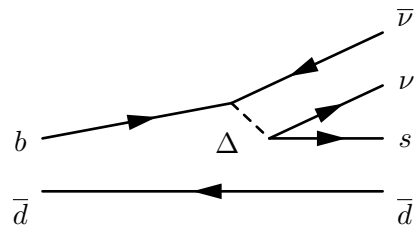

Figure 4.7: Tree-level contribution of the leptoquark Δ to $B \to K^{(*)}\nu\nu$.

where the factor $\eta_1 = 0.82(1)$ encodes the QCD running from the LQ to the b mass scale. The effects on $B_s - \overline{B}_s$ mixing are vanishing in the 2D scenario with couplings (4.20), since $y^L_{s\ell} = 0$ for all neutrino flavours $\ell = e, \mu, \tau$.

This ratio has to be compared with the ratio $\Delta m^{\rm exp}_{B_s}/\Delta m^{\rm SM}_{B_s}$, for which the experimental value $\Delta m^{\rm exp}_{B_s}$ is measured with a high precision to be $\Delta m^{\rm exp}_{B_s} = 17.76(0.02)\text{ps}^{-1}$ [31]. With the SM prediction ranging in the one from Equation (4.22), we get[3]

$$\frac{\Delta m^{\rm exp}_{B_s}}{\Delta m^{\rm SM}_{B_s}} \in [0.90, 1.04]. \tag{4.24}$$

Since the uncertainty on the theory prediction dominates the uncertainty on the ratio in Equation (4.24), and since this uncertainty cannot be interpreted as statistical, we do not include the ratio in the χ^2 of our fit, but require its value to be within the quoted interval. Furthermore, since the NP contribution in Equation (4.24) is nonnegative, this corresponds to requiring $\Delta m^{\rm NP}_{B_s}/\Delta m^{\rm SM}_{B_s} < 1.04$.

$B \to K\nu\nu$

The scalar LQ Δ couples down-type quarks to neutrinos. For this reason, in the 8D scenario with a nonvanishing coupling to the s quark, Δ mediates at tree-level the decay $B \to K^{(*)}\nu\nu$, corresponding at quark-level to the transition $b \to s\nu\nu$, as shown in Figure 4.7. Relative to the SM, the effects of the LQ read [100]

$$\begin{aligned} R_{\nu\nu} = 1 &+ \frac{1}{6C_L^{\rm SM}} {\rm Re}\left[\frac{(y^L \cdot y^{L\dagger})_{sb}}{M_\Delta^2}\right] \frac{\sqrt{2}\pi}{G_{\rm F}\alpha_{\rm em} V_{tb}V_{ts}^*} + \\ &+ \frac{1}{48(C_L^{\rm SM})^2} \frac{(y^L \cdot y^{L\dagger})_{ss}(y^L \cdot y^{L\dagger})_{bb}}{{M_\Delta}^4} \frac{2\pi^2}{G_{\rm F}^2\alpha_{\rm em}^2 |V_{tb}V_{ts}^*|^2}, \end{aligned} \tag{4.25}$$

[3]This range depends on which value is used for the SM prediction. As stated above, we use the result obtained with the use of HQET sum rules [114]. Using the average of lattice results provided by the FLAG Collaboration [116–120], mostly dominated by the 2016 result of the MILC collaboration [119], would make this range smaller, allowing for smaller NP effects. Using the recent lattice result from the HPQCD Collaboration [121] would broaden ths range, allowing for larger NP effects.

where $C_L^{\rm SM} = -6.38(6)$ encodes the SM contribution [122]. The most stringent limit on this ratio is set by the BaBar Collaboration in the decay $B^+ \to K^+\nu\overline{\nu}$, for which the upper limit on the branching fraction is $\mathrm{BR}(B^+ \to K^+\nu\overline{\nu}) < 1.7 \times 10^{-5}$ at 90% C.L. [123]. Translated in terms of $R_{\nu\nu}$, this limit reads $R_{\nu\nu} < 2.7$ [124]. This limit is set as a hard constraint on the values allowed for the fitting parameters.

Lepton flavour violation: $\tau \to \mu\gamma$ and $\tau \to \mu\mu\mu$

In the 8D scenario, the scalar LQ couples to both μ and τ. Hence the model is strongly constrained by the LFV processes $\tau \to \mu\gamma$ and $\tau \to \mu\mu\mu$.

The contribution of Δ to $\tau \to \mu\gamma$, arising from the loop-level diagrams in Figure 4.1 when the two ℓ differ in flavour, reads [100]

$$\mathrm{BR}(\tau \to \mu\gamma) = \frac{\alpha_{\rm em}(m_\tau^2 - m_\mu^2)^3}{4m_\tau^3\Gamma_\tau}(|\sigma_L|^2 + |\sigma_R|^2), \tag{4.26}$$

where Γ_τ is the decay width of the τ and with

$$\sigma_{L(R)} = -i\frac{3m_\tau}{192\pi^2 M_\Delta^2}\left\{y_{t\tau}^{R(L)}y_{t\mu}^{R(L)*} - \frac{m_t}{m_\tau}y_{t\tau}^{L(R)}y_{t\mu}^{R(L)*}\left[14 + 8\log\frac{m_t^2}{M_\Delta^2}\right]\right\}. \tag{4.27}$$

The upper limit set on this branching fraction by the BaBar Collaboration [125] is $\mathrm{BR}(\tau \to \mu\gamma) < 4.4 \times 10^{-8}$ at 90% confidence level (C.L.). This limit is imposed as a hard cut in the region of parameters allowed for the 8D fit.

The constraints from the LFV decay $\tau \to \mu\mu\mu$ for a scenario with scalar LQ Δ was found to be weaker than $\tau \to \mu\gamma$ in Reference [126]. For this reason we do not include this decay in our analysis.

Rare leptonic decay $D^0 \to \mu\mu$

The decay $D^0 \to \mu\mu$ is mediated by a flavour changing neutral current (FCNC) and as such is strongly suppressed in the SM. The current experimental limit on this decay is $\mathrm{BR}(D^0 \to \mu\mu) < 6.2 \times 10^{-9}$ at 90% C.L. [31]. Neglecting the SM contribution, which is estimated to be $\mathcal{O}(10^{-11})$, the branching ratio in presence of the scalar LQ, contributing through the diagrams in Figure 4.8 and including those with a spin-flip of one of the fermion lines, is [99]

$$\begin{aligned}\mathrm{BR}(D^0 \to \mu\mu) = \frac{f_D^2 m_D^3}{256\pi {M_\Delta}^4\Gamma_D}\left(\frac{m_D}{m_c}\right)^2\beta_\mu\Bigg[\beta_\mu^2\left|y_{c\mu}^L y_{u\mu}^{R*} - y_{c\mu}^R y_{u\mu}^{L*}\right|^2 + \\ + \left|y_{c\mu}^L y_{u\mu}^{R*} + 2\frac{m_\mu m_c}{m_D^2}(y_{c\mu}^L y_{u\mu}^{L*} + y_{c\mu}^R y_{u\mu}^{R*})\right|^2\Bigg],\end{aligned} \tag{4.28}$$

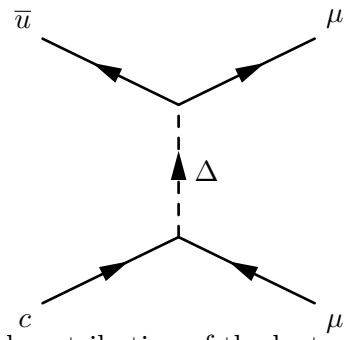

Figure 4.8: Tree-level contribution of the leptoquark Δ to $D^0 \to \mu\mu$.

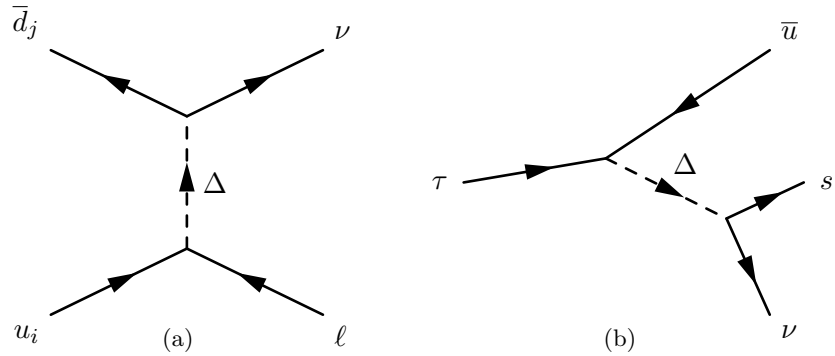

Figure 4.9: Tree-level contributions of the leptoquark Δ to leptonic meson decays and to the decay $\tau \to K\nu$.

where $\beta_\mu = \sqrt{1 - 4m_\mu^2/m_D^2}$. As for the other observables listed so far, this contribution vanishes in the 2D scenario, and is set as a hard limit in the 8D case.

Leptonic K, D, D_s, B decays, $\tau \to K\nu$ and LFU ratios

Analogously to the decay $B_c \to \tau\nu$ discussed in the effective analysis of Chapter 3, the leptonic decays of charged mesons $K \to \mu\nu$, $D_s \to \mu\nu$, $D_s \to \tau\nu$, $B \to \tau\nu$, as well as the τ decay $\tau \to K\nu$, can be mediated at tree-level by the scalar LQ Δ. The Feynman diagrams for these meson and τ decays are shown in Figure 4.9. The expressions of the branching ratios of the mesons are analogous to the one of $\mathrm{BR}(B_c \to \tau\nu_\tau)$ in Equation (3.18), with appropriate replacement of quark and lepton masses, meson decay constants as well as flavours of the implicit indices of the WCs. For the τ decay, the branching ratio reads [101]

$$\begin{aligned}\mathrm{BR}(\tau \to K\nu) = \frac{G_\mathrm{F}^2 |V_{us}^2|}{16\pi\gamma_\tau} f_K^2 m_\tau^3 \left(1 - \frac{m_K^2}{m_\tau^2}\right)^2 \times \\ \times \sum_i \left| \delta_{3i} + C_{V,3i}^L + \frac{m_K^2}{m_\tau(m_u + m_s)} (C_{S,3i}^R - C_{S,3i}^L) \right|^2 .\end{aligned} \tag{4.29}$$

where the index i refers to the flavour of the neutrino in the final state, and f_K is the decay constant of the K^+ meson.

Although the experimental values of the branching ratios for the individual decays are available [31], these data are used for estimating the value of the CKM matrix elements appearing in the expressions of the branching ratios. For this reason we do not include them in our fit[4].

However, large LQ contibution to these branching ratios would imply a modification of the CKM element fitted to the corresponding decay, and could eventually result in a deviation from the well-tested CKM unitarity. Hence we use these branching fractions to check that our model complies with the CKM unitarity in two ways. In a first step we check that the NP contribution to the branching ratios is negligible compared to the experimental uncertainty. In a second step we include in the fit also ratios of leptonic branching fractions in which the CKM matrix elements drop out. In this way, we are not running into the problem of implicitly including the same data twice in our analysis, via the already fitted CKM element. We then compare the fit with and without the LFU ratios, and verify that their inclusion has a negligible impact on the fit.

The ratios we considered are [101]

$$r_K^{e/\mu} = \frac{\mathrm{BR}(K \to e\nu)}{\mathrm{BR}(K \to \mu\nu)}, \qquad r_K^{\tau/\mu} = \frac{\mathrm{BR}(\tau \to K\nu)}{\mathrm{BR}(K \to \mu\nu)}, \qquad r_{D_s}^{\tau/\mu} = \frac{\mathrm{BR}(D_s \to \tau\nu)}{\mathrm{BR}(D_s \to \mu\nu)}. \tag{4.30}$$

A remark concerning the evolution of the WCs is in order for decays involving K, D_s and D mesons. For these mesons, the reference scale used to compute the form factors on the lattice is 2 GeV, so this is the scale to which the WCs must be evolved. The evolution from $\Lambda_{\mathrm{NP}} = 1\,\mathrm{TeV}$ to 2 GeV at three-loop QCD and one-loop in QED and EW, analogously to Equation (3.10), is [73]

$$\begin{aligned} C_V^L(2\,\mathrm{GeV}) &= C_V^L(1\,\mathrm{TeV}), \\ C_S^R(2\,\mathrm{GeV}) &= 2.047 C_S^R(1\,\mathrm{TeV}), \\ \begin{pmatrix} C_S^L(2\,\mathrm{GeV}) \\ C_T(2\,\mathrm{GeV}) \end{pmatrix} &= \begin{pmatrix} 2.064 & -0.341 \\ -0.003 & 0.791 \end{pmatrix} \begin{pmatrix} C_S^L(1\,\mathrm{TeV}) \\ C_T(1\,\mathrm{TeV}) \end{pmatrix}. \end{aligned} \tag{4.31}$$

Anomalous magnetic moment of the muon

The anomalous magnetic moment of the muon, a_μ, is defined to be the difference of the gyromagnetic ratio, g_μ, with its prediction from the Dirac equation, $g_\mu^{\mathrm{Dirac}} = 2$,

$$a_\mu = \frac{g_\mu - 2}{2}. \tag{4.32}$$

This difference arises from loop effects. Including five loops QED corrections, two loops EW corrections and nonperturbative hadronic effects, the value predicted in the SM is $a_\mu^{\mathrm{SM}} = 16591823(1)(34)(26) \times 10^{-11}$ [31].

[4] An exhaustive analysis would require to fit the CKM elements and the LQ parameters simultaneously. This analysis is beyond the scope of our work.

This quantity is measured via the precession of muons in a constant external magnetic field, and experiments give $a_\mu^{\rm exp} = 11659209.1(5.4)(3.3) \times 10^{-10}$ where the first error is statistical and the second systematic [31].

The difference between the SM prediction and the experimental result, $\Delta a_\mu = a_\mu^{\rm exp} - a_\mu^{\rm SM} = 268(63)(43) \times 10^{-11}$ shows a 3.5σ discrepancy. This tension further increases the interest in NP models predicting LFNU, hence it is interesting to analyse to which extent the model we are looking at is able to account for both the $\mathcal{R}(D^{(*)})$ and the Δa_μ anomalies.

The LQ Δ contributes at loop-level to a_μ via diagrams such as those shown in Figure 4.1. These effects are expressed by [99]

$$\Delta a_\mu^{\rm LQ} = \sum_{q=t,c} \frac{m_\mu m_q}{4\pi^2 M_\Delta^2} \left(\log \frac{M_\Delta^2}{m_q^2} - \frac{7}{4} \right) {\rm Re}\left[y_{q\mu}^R y_{q\mu}^{L*} \right] - \frac{m_\mu^2}{32\pi^2 M_\Delta^2} \left[(y_{ue}^{L\dagger} \cdot y_{ue}^L)_{\mu\mu} + (y^{R\dagger} \cdot y^R)_{\mu\mu} \right] . \tag{4.33}$$

where y_{ue}^L stands here for the matrix in Equation (4.8), and not for its individual element. The contribution in Equation (4.33) is vanishing in the 2D model, in which couplings to μ are vanishing.

To determine the interplay of $\mathcal{R}(D^{(*)})$ and the Δa_μ anomalies within the 8D scenario, we will perform our fit twice, once without the data on Δa_μ and once including Δa_μ.

Remark on neutrino flavours

The flavour of the neutrinos is indistinguished at the experiments measuring the observables we are considering. For this reason, in the 8D scenario with couplings as in Equation 4.7, when considering the NP contributions to processes with at least one neutrino in the final states, we must sum incoherently over the channels with different neutrino flavours. For processes with two leptons in the final state, the only term that can interfere with the SM contribution is the one in which the two flavours coincide.

4.4.3 Fit results

Let us analyse the fit results in the 2D and 8D scenarios. The statistical approach and definitions are the same as in Chapter 3.

Minimal couplings scenario (2D)

As summarised in Table 4.1, our 2D fit includes the $b \to c\tau\nu$ data, i.e. $\mathcal{R}(D^{(*)})$, $F_L(D^*)$, $P_\tau(D^*)$, as well as the three vector and three axial $Z\ell\ell$ couplings. However, the $Z\tau\tau$ couplings depend on the fitting parameters $y_{b\tau}^L, y_{c\tau}^R$, while the Zee and $Z\mu\mu$ receive a correction only through δe, which does not depend on either of the fitting Yukawas. We are hence fitting $y_{b\tau}^L, y_{c\tau}^R$ to six observables.

The best fit point is located at $(y_{b\tau}^L, y_{c\tau}^R) \simeq (1.98, 0.02)$ with $\chi^2_{\rm bf} = 3.4$. For $N_{\rm obs} = 6$ and $N_{\rm par} = 2$, resulting in 4 d.o.f., this corresponds to a p-value of 50%. The one and two

sigma regions in the $(y^L_{b\tau}, y^R_{c\tau})$ plane are displayed in Figure 4.10a, and in Figure 4.10b these regions are projected[5] on the plane of WCs $(C^L_V, C^L_S = -4C_T)$. The cut on the negative values of C^L_V results from the fact that $C^L_V \propto \left|y^L_{b\tau}\right|^2 \geq 0$.

Comparing the projection of the 2σ region in the WCs plane with the 2σ region obtained with the EFT approach, i.e. the upper left plot of Figure 3.6, we see that these essentially coincide. This is resulting from the fact that the fit is mostly driven by $\mathcal{R}(D^{(*)})$ data[6].

It is interesting to observe that the best fit point corresponds to the scenario discarded by the authors of Reference [101] in light of the constraint from the $Z\tau\tau$ coupling. The reason is clear if we look at the values of these couplings at the best-fit point, displayed in blue in Figure 4.5. The values for the τ couplings shift significantly from the SM LFU point, which is the one used for the constraints in Reference [101]. However, the agreement with its measured value increases. The orange line represents the projection of the 1σ region of the Yukawa couplings into the $(g^A_{Z\tau\tau}, g^V_{Z\tau\tau})$ plane; this (apparent) linear dependence, crossing the SM prediction if prolonged, is due to the fact that the dependence on $y^L_{b\tau}$ is enhanced by a factor m_t^2/m_Z^2 with respect to the dependence on $y^R_{c\tau}$.

The improved agreement with the $Z\tau\tau$ coupling is displayed in the bar plot of Figure 4.11, in which the pulls defined as in Section 3.3 are compared with the SM ones. In the same plot we observe a significant decrease of the tension in the $\mathcal{R}(D^{(*)})$ observables and no substantial difference for what concerns the polarisation observables $F_L(D^*)$and $P_\tau(D^*)$, as we expected from the analysis in Chapter 3.

From Figures 4.5 and 4.11 we also observe that the effects on the Z couplings to light leptons is negligible. Numerically, we get a relative effect of the order $\mathcal{O}(10^{-7})$. Due to the assumed Yukawa structure, these effects arise only from the photon polarisation contributions, hence we conclude that the latter are negligible and do not significantly affect NP scenarios when addressing the $\mathcal{R}(D^{(*)})$ anomaly.

In the 2D scenario, the only leptonic branching ratio receiving a contribution is $B \to \tau\nu$. This branching ratio is of particular interest due to the current tension between the measurements of the corresponding CKM element V_{ub} from exclusive and inclusive semileptonic decays, giving respectively [31]

$$\left|V^{\text{excl}}_{ub}\right| = (3.67 \pm 0.09 \pm 0.12) \times 10^{-3}, \qquad \left|V^{\text{incl}}_{ub}\right| = (4.49 \pm 0.16^{+0.16}_{-0.17} \pm 0.17) \times 10^{-3}. \quad (4.34)$$

The SM prediction and the prediction at the best-fit points using either V^{incl}_{ub} or V^{excl}_{ub} are reported in the two lines of Table 4.3. We observe that the prediction making use of V^{excl}_{ub} is lower than the lower boundary of the 1σ interval of the experimental measurement. For this reason, the model in the 2D scenario favours the value of V^{incl}_{ub}.

[5]This projection does not represent the 1 and 2σ region in the statistical sense discussed in the previous chapter.

[6]This is also confirmed by the agreement of the σ regions in the Yukawa couplings plane with Figure 2 of Reference [102], where the 2σ regions for $\mathcal{R}(D^{(*)})$ are shown.

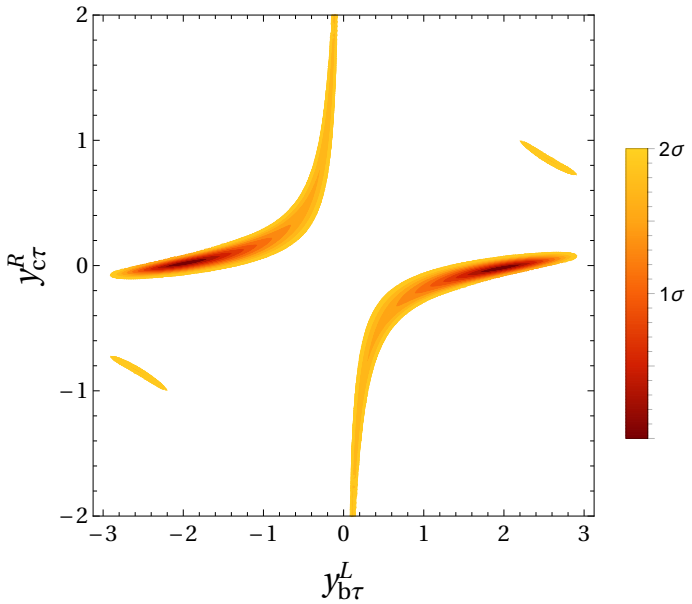

(a)

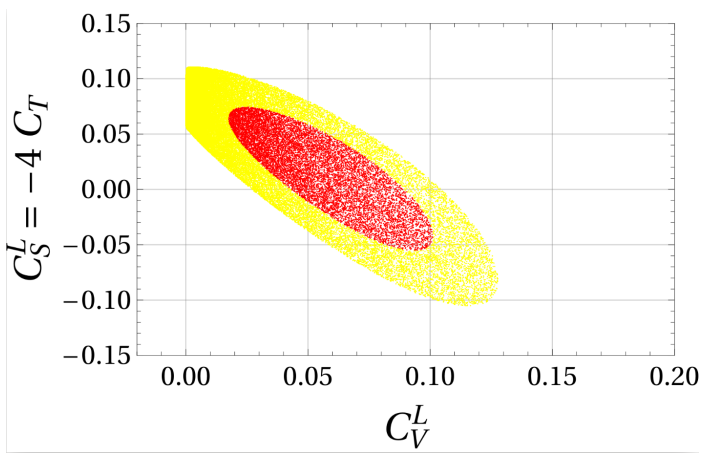

(b)

Figure 4.10: Figure (a) displays the 2σ region in the $(y^L_{b\tau}, y^R_{c\tau})$ plane for the 2D scenario assuming only two nonvanishing couplings. Figure (b) is a projection of that region into the Wilson coefficients plane.

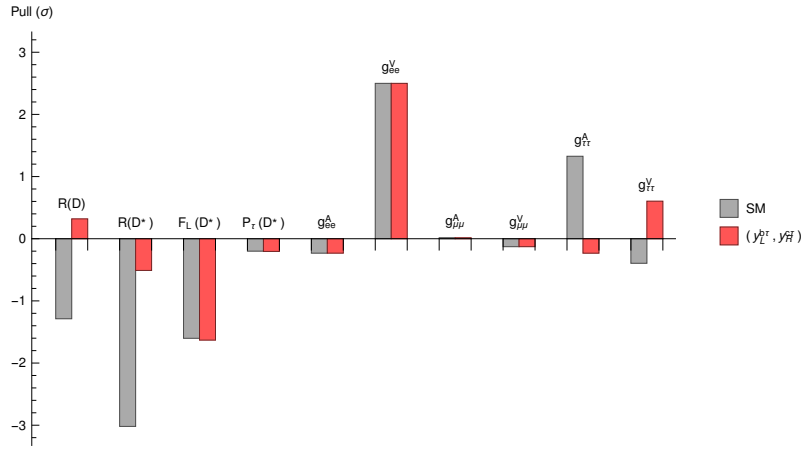

Figure 4.11: Pulls in the scenario assuming only two nonvanishing couplings for a fit including the polarisation observables and the $Z\ell\ell$ couplings with electroweak renormalisation effects taken into account.

Extended Yukawa structure (8D)

As we mentioned before and as displayed in Table 4.1, the analysis of the model with extended couplings is performed by considering separately three fitting scenarios. This will allow us to establish the interplay of the different observables within this LQ model. All the scenarios include the same *hard cut* constraints, whose value at the best-fit point is reported in Table 4.2.

	$\mathrm{BR}(B_c \to \tau\nu_\tau)$	$\Delta m_{B_s}^{\mathrm{th}}/\Delta m_{B_s}^{\mathrm{SM}}$	$\mathrm{BR}(\tau \to \mu\gamma)$	$R_{\nu\nu}$	$\mathrm{BR}(D^0 \to \mu\mu)$
Upper limit	10×10^{-2}	1.04	4.4×10^{-8}	2.7	6.2×10^{-9}
SM	2×10^{-2}	1	0	1	$\mathcal{O}(10^{-11})$
$8\mathrm{D}_{\mathrm{simple}}$	2×10^{-2}	1.01	4.4×10^{-8}	2.7	$\mathcal{O}(10^{-11})$
$8\mathrm{D}_{\mathrm{LFU}}$	2×10^{-2}	1.01	4.4×10^{-8}	2.7	$\mathcal{O}(10^{-11})$
$8\mathrm{D}_{a_\mu}$	5×10^{-2}	1.04	4.4×10^{-8}	2.7	$\mathcal{O}(10^{-10})$

Table 4.2: Values of the flavour observables imposed as a hard constraint on the fit. The values are given in the Standard Model and at the best-fit points of the three 8D scenarios.

Let us start from the scenario marked as $8\mathrm{D}_{\mathrm{simple}}$, which does not include either the LFU ratios nor Δa_μ.

The best-fit point is attained with the Yukawa matrices[7]

$$y^L_{d\nu} = \begin{pmatrix} 0 & 0 & 0 \\ 0 & -2.5\times 10^{-2} & 1.2\times 10^{-3} \\ 0 & 1.0 & -1.9 \end{pmatrix}, \qquad y^R_{u\ell} = \begin{pmatrix} 0 & 0 & 0 \\ 0 & -1.9\times 10^{-2} & 2.9\times 10^{-2} \\ 0 & 1.6\times 10^{-11} & 6.7\times 10^{-4} \end{pmatrix},$$
$$y^L_{u\ell} = V^*_{\rm CKM} y^L = \begin{pmatrix} 0 & (-4.3-i3.8)\times 10^{-3} & (-2.2-i7.2)\times 10^{-3} \\ 0 & 1.8\times 10^{-2} & 8.1\times 10^{-2} \\ 0 & 1.0 & 2.0 \end{pmatrix}, \tag{4.35}$$

with $\chi^2_{\rm bf} = 7.4$. With $N_{\rm obs} = 12$ and $N_{\rm par} = 8$, this corresponds to a p-value of 12%.

From the value of the constraints in Table 4.2 we see that the best-fit point saturates both the $R_{\nu\nu}$ and the $\tau \to \mu\gamma$ constraints. All other constraints are not saturated. The $R_{\nu\nu}$ and $\tau \to \mu\gamma$ constraints cut out the part of parameter space in which the best-fit point would lie, pushing it to their boundary. This is clear from Figure 4.12, displaying the 2σ region in the plane $(y^L_{b\tau}, y^R_{c\tau})$, assuming the other Yukawas to be at their best-fit point, as well as the region excluded by the $R_{\nu\nu}$ and $\tau \to \mu\gamma$ limits.

A comparison of Figure 4.12a and Figure 4.10a shows that the $(y^L_{b\tau}, y^R_{c\tau})$ values at the best fit are still driven by the $\mathcal{R}(D^{(*)})$ data, since they correspond to one of the two 2σ regions in the minimal coupling scenario. This is also clear by comparing Figures 4.10b and 4.12b, in which we project in the plane of the WCs of the $b \to c\tau\nu$ channel, the 2σ regions of the three Yukawa couplings on which they depend, $(y^L_{s\tau}, y^L_{b\tau}, y^R_{c\tau})$, assuming the others to be at their best-fit point. However, in the extended coupling scenario we observe that the C^L_V coupling is no longer restricted to positive values, but has instead an upper limit at around ~ 0.07 due to the $R_{\nu\nu}$ constraint.

In Figure 4.13a we display the value of the $Z\ell\ell$ couplings at the best-fit point. We see that the LQ Δ is able to improve the agreement of both the τ and the e coupling, the latter effect arising from the couplings of the LQ to the μ and via the newly included EW renormalisation, as explained above.

The better agreement with $Z\ell\ell$ data is also visible in the red bars of Figure 4.14, displaying the pulls at the best-fit point.

The coupling with the μ also implies a modification of the $\mathcal{R}_{\mu/e}(D)$ and $\mathcal{R}_{e/\mu}(D^*)$ ratios with respect to the SM, slightly worsening the agreement with experimental data. However, the nonvanishing Yukawa couplings with μ do not worsen the agreement with the angular distributions in the light lepton channels of the $B \to D^{(*)}\ell\nu$ decays. This can be seen in Figure 4.15, in which the measured binned differential rates $\Delta\Gamma/\Delta\cos\theta_D$, with θ_D defined as in Figure 3.1, is plotted together with the SM prediction and the prediction at the best-fit point.

[7]The imaginary part in the $y^L_{u\ell}$ elements originates from the phase of the CKM matrix element V_{ub}.

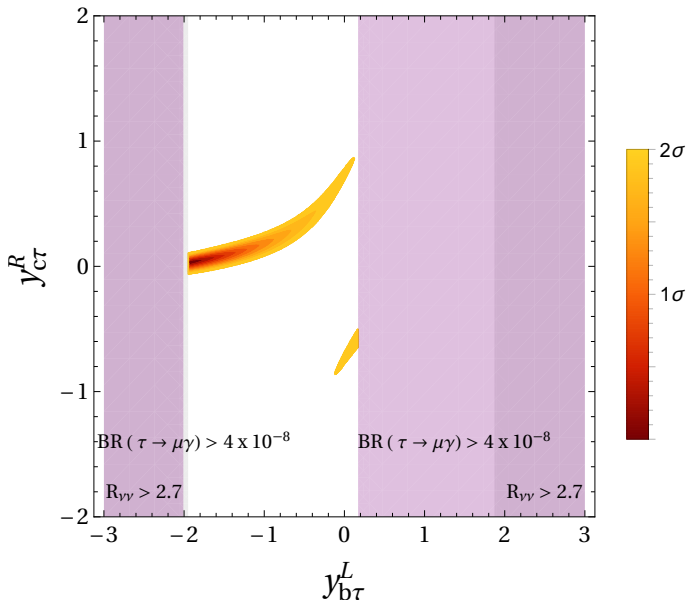

(a)

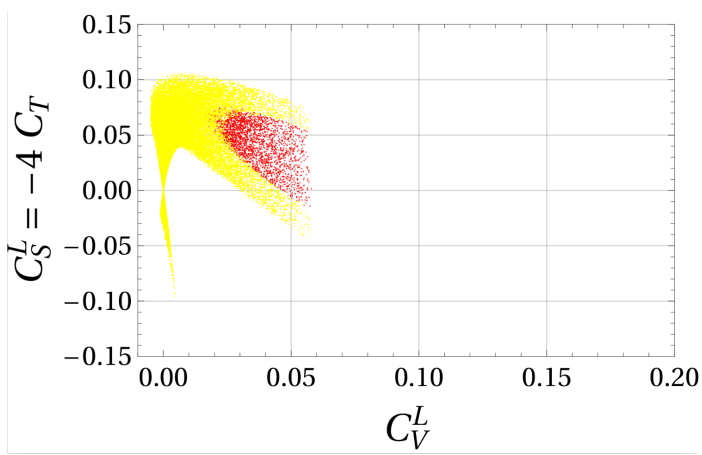

(b)

Figure 4.12: Figure (a) shows the 2σ region of the $8\mathrm{D}_{\mathrm{simple}}$ scenario in the $(y^L_{b\tau}, y^R_{c\tau})$ plane, assuming the other Yukawas to be at their best-fit point. Figure (b) shows the projection of the 1 and 2σ regions of the Yukawa couplings $(y^L_{s\tau}, y^L_{b\tau}, y^R_{c\tau})$, assuming the others to be at their best-fit point, in the Wilson Coefficients plane.

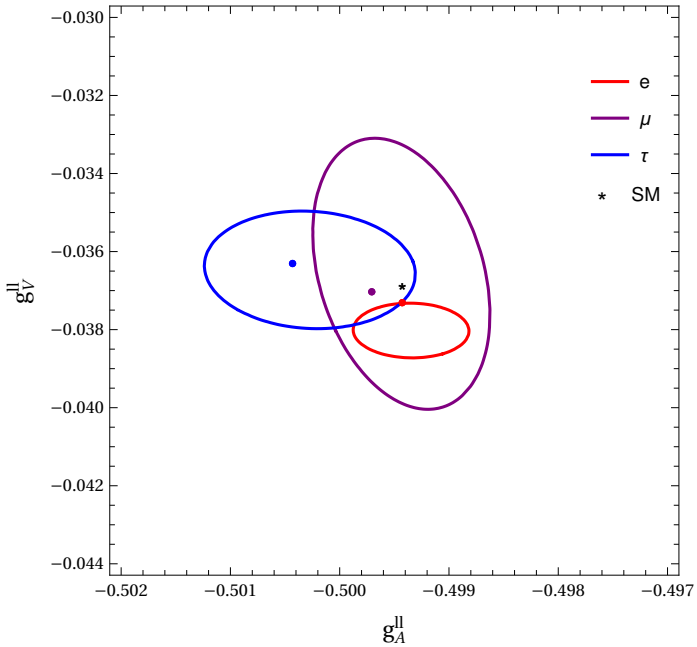

(a)

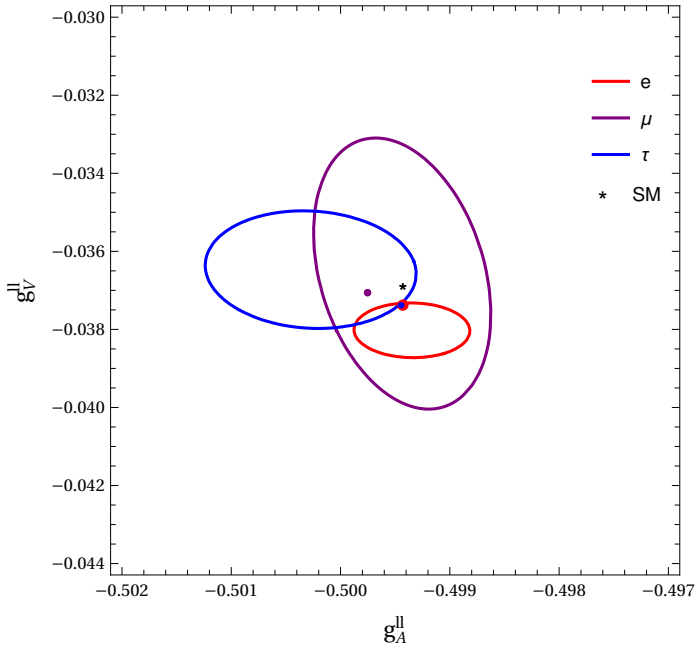

(b)

Figure 4.13: $Z\ell\ell$ couplings. The ellipses correspond to the 1σ experimental values [31], the black star to the SM prediction. The coloured dots correspond to the values at the best-fit points of the 8D scenarios. Figure (a) refers to the $8\text{D}_{\text{simple, LFU}}$ scenario and Figure (b) to the 8D_{a_μ} scenario.

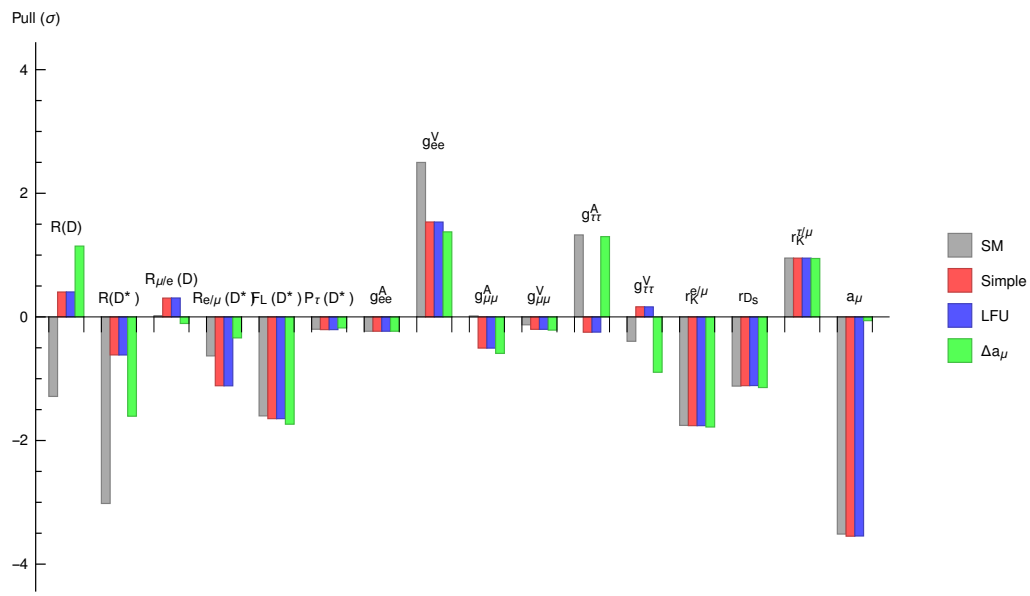

Figure 4.14: Pulls in the 8D scenario for a fit including the polarisation observables and the $Z\ell\ell$ couplings with electroweak renormalisation effects taken into account. The red, blue and green bars correspond to the $8\text{D}_{\text{simple, LFU},\Delta a_\mu}$ scenarios respectively.

Finally, in Table 4.3 we report the branching ratios of the leptonic meson decays listed in the previous section[8]. The values at the best-fit point are given together with the SM predictions and with the experimental values. We see that for $K \to \mu\nu, D_s \to \mu\nu$ and $D_s \to \tau\nu$ the difference between the SM prediction and the value at the best-fit is negligible compared to the experimental uncertainty. The only leptonic branching ratio receiving a significant contribution is $B \to \tau\nu$. The SM prediction and the prediction at the best-fit points using either V_{ub}^{incl} or V_{ub}^{excl} are reported in the two lines of Table 4.3. We observe that the prediction making use of V_{ub}^{incl} exceeds the 1σ interval of the experimental measurement. For this reason, contrary to the 2D scenario, when we relax the hypothesis about the Yukawa structure the model favours the value of V_{ub}^{excl}. The different effect on $\text{BR}(B \to \tau\nu)$ is due to the additional contribution coming from the nonvanishing Yukawa $y_{s\tau}^L$.

The marginal relevance of the effects on the branching ratio for $K \to \mu\nu, D_s \to \mu\nu$ and $D_s \to \tau\nu$ is also shown by the analysis including the LFU ratios $r_K^{e/\mu}, r_K^{\tau/\mu}, r_{D_s}^{\tau/\mu}$ in the fit, marked as 8D_{LFU} in Table 4.1. The minimum is $\chi^2 = 13$, achieved with Yukawa couplings essentially unvaried from Equation (4.36). With $N_{\text{obs}} = 15$ and $N_{\text{par}} = 8$, this corresponds to a p-value of 8%. From the pull plot in Figure 4.14 we see that at the best fit points of the $8\text{D}_{\text{simple}}$ and 8D_{LFU} scenarios, none of the observables differs significantly. From this we deduce that the only difference in the χ^2 arises from the additional contributions from the three LFU ratios whose agreement with data, however, cannot be improved significantly within this model. This is due to the fact that sizeable effects would require a large $y_{s\ell}^L$

[8]For $\text{BR}(K \to \mu\nu)$ we normalise the branching ratio to $\text{BR}(K \to e\nu)$. This allows us to include the electromagnetic corrections evaluated in Reference [127].

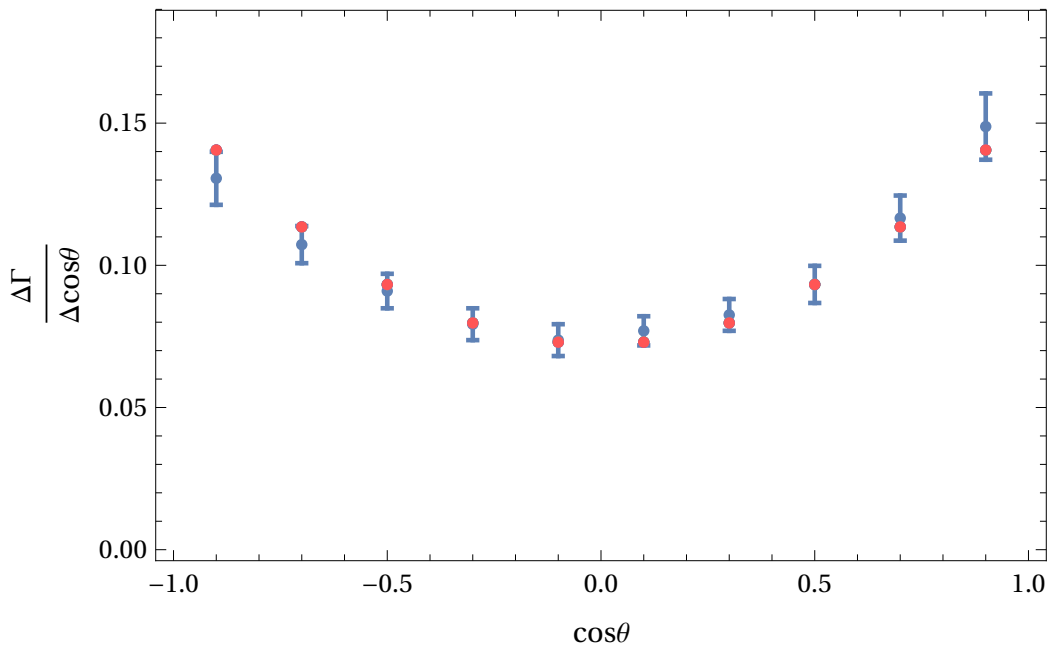

Figure 4.15: Binned differential rate $\Delta\Gamma/\Delta\cos\theta_D$ for the decay $B \to D^*\ell\nu$ with a light lepton in the final state ($\ell = \mu$ or e). The blue points with error bars represent the experimental measurements [29]. The predictions in the Standard Model and at the three best-fit points are indistinguishable, and correspond to the red points.

coupling which, however is not able to improve the agreement with the experimental values of the light meson ratios without involving too high of an effect in the $\mathcal{R}(D^{(*)})$, $\mathcal{R}_{\mu/e}(D)$ and $\mathcal{R}_{e/\mu}(D^*)$, via the CKM-related coupling $y^L_{c\ell}$.

Finally, let us come to the fit including Δa_μ. The minimum $\chi^2 = 11$ corresponds to a p-value of 5.4% for $N_{\rm obs} = 13$ and $N_{\rm par} = 8$. The minimum is achieved for the Yukawa couplings

$$y^L_{d\nu} = \begin{pmatrix} 0 & 0 & 0 \\ 0 & -5.8\times10^{-2} & -6.5\times10^{-3} \\ 0 & 1.1 & -2.8\times10^{-1} \end{pmatrix}, \qquad y^R_{u\ell} = \begin{pmatrix} 0 & 0 & 0 \\ 0 & -2.6\times10^{-2} & 4.4\times10^{-1} \\ 0 & 2.9\times10^{-3} & 2.0\times10^{-4} \end{pmatrix},$$

$$y^L_{u\ell} = V^*_{\rm CKM} y^L = \begin{pmatrix} 0 & -1.2\times10^{-2} - i4.1\times10^{-3} & (-1.8+i1.0)\times10^{-3} \\ 0 & -1.1\times10^{-2} & -1.8\times10^{-2} \\ 0 & 1.1 & -2.8\times10^{-1} \end{pmatrix}. \tag{4.36}$$

As in the other two cases, the hardest limit on the parameter space is set by the $R_{\nu\nu}$ ratio and by the limits on $\tau \to \mu\gamma$, both being saturated at the best-fit point, as can be seen in Table 4.2. In this scenario, also $B_s - \overline{B}_s$ saturates its constraint. The lower p-value is a result of the fact that a good fit to Δa_μ implies a worsening in the agreement with the

	$\frac{\mathrm{BR}(K\to e\nu)}{\mathrm{BR}(K\to\mu\nu)}$	$\mathrm{BR}(D_s\to\mu\nu)$	$\mathrm{BR}(D_s\to\tau\nu)$	$\mathrm{BR}(B\to\tau\nu)$	$\mathrm{BR}(\tau\to K\nu)$
Experimental value	$2.488(9)\times10^{-5}$	$5.50(23)\times10^{-3}$	$5.48(23)\times10^{-2}$	$1.09(24)\times10^{-4}$	$6.96(10)\times10^{-3}$
SM, V_{ub}^{excl}	2.472×10^{-5}	5.58×10^{-3}	5.44×10^{-2}	8.22×10^{-5}	6.94×10^{-5}
V_{ub}^{incl}				1.23×10^{-4}	
2D, V_{ub}^{excl}	2.472×10^{-5}	5.58×10^{-3}	5.44×10^{-2}	7.50×10^{-5}	6.94×10^{-5}
V_{ub}^{incl}				1.12×10^{-4}	
$8\mathrm{D}_{\mathrm{simple}}$	2.472×10^{-5}	5.58×10^{-3}	5.44×10^{-2}	9.19×10^{-5}	6.94×10^{-5}
V_{ub}^{incl}				1.38×10^{-4}	
$8\mathrm{D}_{\mathrm{LFU}}$	2.472×10^{-5}	5.57×10^{-3}	5.44×10^{-2}	9.19×10^{-5}	6.94×10^{-5}
V_{ub}^{incl}				1.38×10^{-4}	
$8\mathrm{D}_{a_\mu}$	2.472×10^{-5}	5.51×10^{-3}	5.44×10^{-2}	8.25×10^{-5}	6.94×10^{-5}
V_{ub}^{incl}				1.23×10^{-4}	

Table 4.3: Branching ratios for leptonic meson decays and for $\tau\to K\nu$. The values in the 8D scenario are referred to the best-fit point.

data from $\mathcal{R}(D^{(*)})$, as can be seen from the green bars of the pull plot in Figure 4.14. This is a result of an interplay between the $R_{\nu\nu}$ and $\tau\to\mu\gamma$ limits and Δa_μ, as we now briefly explain. A good agreement with Δa_μ requires a higher value of the coupling $y^R_{t\mu}$. Due to the $\tau\to\mu\gamma$ limit, a higher $y^R_{t\mu}$ requires a lower $y^L_{t\tau}$ which, up to the CKM matrix element $V_{tb}\sim 1$, implies a low $y^L_{b\tau}$. For $R_{\nu\nu}$, the limit is saturated by a cancellation of the first and second line in Equation (4.25). Since the $\tau\to\mu\gamma$ requires a low $y^L_{t\tau}$, this cancellation occurs via a fine-tuning of $y^L_{s\mu}, y^L_{s\tau}, y^L_{b\mu}$, or equivalently $y^L_{c\mu}, y^L_{c\tau}, y^L_{b\mu}$, whose value worsen the agreement with the $\mathcal{R}(D^{(*)})$ ratios. This fine-tuning effect is also shown in Figure 4.16a, displaying the 2σ region in the plane $(y^L_{b\tau}, y^R_{c\tau})$, assuming the other Yukawas to be at their best-fit point, as well as the regions excluded by the $\tau\to\mu\gamma$ and $R_{\nu\nu}$ constraints, which overlap due to the interplay just explained. Figure 4.16b displays the projection of the 1 and 2σ regions of the Yukawa couplings $(y^L_{s\tau}, y^L_{b\tau}, y^R_{c\tau})$ in the WCs plane, assuming the others to be at their best fit point. A comparison with Figure 4.12b reveals that the fit is no longer driven by the $\mathcal{R}(D^{(*)})$ data.

In addition, from Figure 4.13b we see that the agreement with the $Z\tau\tau$ couplings is worsened with respect to the other two scenarios. The Zee couplings still improve the agreement with the experimental value via the EW renormalisation effects.

Our analysis of the $8\mathrm{D}_{\mathrm{simple}}$ hence reveals that the scalar LQ with couplings to second and third generation fermions is able to accommodate the current experimental values of $\mathcal{R}(D^{(*)})$ and at the same time improve the agreement with the measured values of the $Z\tau\tau$ and Zee couplings, without significantly affecting the leptonic decays of mesons lighter than the B, an effect that could spoil the agreement with the well tested CKM unitarity. In particular, the effect on the Zee couplings is a pure result of the inclusion of the EW renormalisation effects. However, a comparison of the scenarios $8\mathrm{D}_{\mathrm{simple}}$ and $8\mathrm{D}_{a_\mu}$ shows that a simultaneous description of the experimental values of the anomalous magnetic moment of the muon Δa_μ and of the $\mathcal{R}(D^{(*)})$ ratios is challenged by the experimental constraints from other flavour observables.

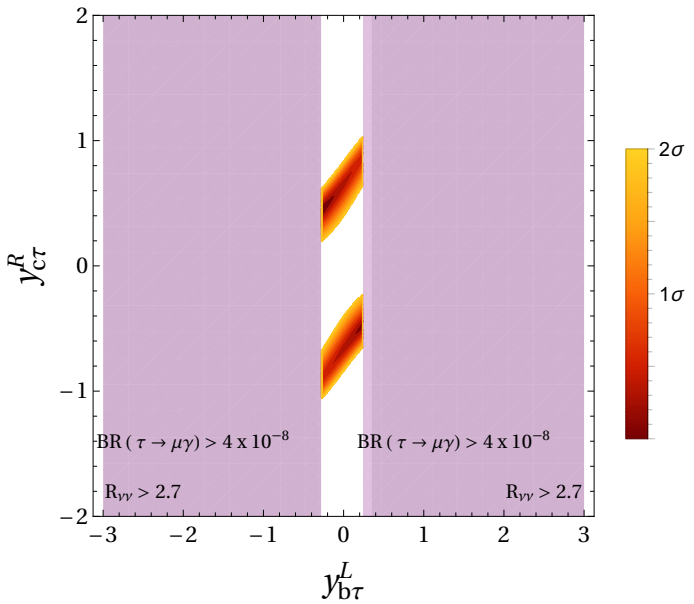

(a)

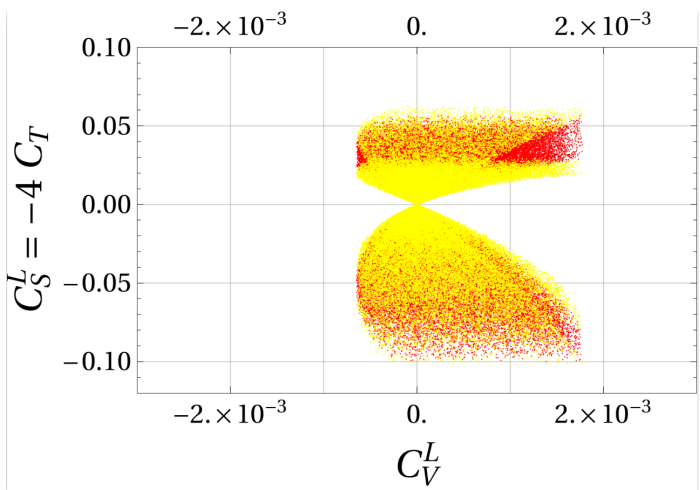

(b)

Figure 4.16: Figure (a) shows the 2σ region of the $8\mathrm{D}_{a_\mu}$ scenario in the $(y^L_{b\tau}, y^R_{c\tau})$ plane, assuming the other Yukawas to be at their best-fit point. Figure (b) shows the projection of the 1 and 2σ regions of the Yukawa couplings $(y^L_{s\tau}, y^L_{b\tau}, y^R_{c\tau})$, assuming the others to be at their best-fit point, in the Wilson coefficients plane.

Remark on $b \to s\mu\mu$

Let us comment on the interplay between the $\mathcal{R}(D^{(*)})$ and the anomalous data from $B \to K^{(*)}\mu\mu$ decays in presence of the scalar LQ Δ. Since $B \to K^{(*)}\mu\mu$ decays are not the main focus of this work, we refer the reader to Appendix B for a broader overview of these anomalies, and focus here on the details relevant for us.

The global analyses of the $b \to s\ell\ell$ data seem to favour the presence of NP effects mostly in the $b \to s\mu\mu$ channel with respect to the $b \to see$ channel [95, 128]. Among the scenarios with a single nonvanishing combination of WCs, those favoured by the data have negative contribution to the WC C_9^μ. With respect to NP solutions to the $\mathcal{R}(K^{(*)})$ anomalies, an interesting scenario is the one with nonvanishing WCs $\left(\mathcal{C}_{9(\mu)}^{\rm NP}, \mathcal{C}_{10(\mu)}^{\rm NP}\right)$, for which the global fit gives

$$\left(\mathcal{C}_{9(\mu)}^{\rm NP}, \mathcal{C}_{10(\mu)}^{\rm NP}\right) = (-0.91, 0.18). \tag{4.37}$$

Using the expressions of the WC in terms of the scalar LQ parameters [99]

$$\begin{aligned} C_{LL}^\mu &= \frac{m_t^2}{8\pi\alpha M_\Delta^2}\left|y_{t\mu}^L\right|^2 - \frac{\sqrt{2}}{64\pi\alpha G_{\rm F} M_\Delta^2}\frac{\left(y^L\cdot y^{L\dagger}\right)_{bs}\left(y^{L\dagger}\cdot y^L\right)_{\mu\mu}}{V_{tb}V_{ts}^*} \\ C_{LR}^\mu &= \frac{m_t^2}{16\pi\alpha M_\Delta^2}\left|y_{t\mu}^R\right|^2\left[\log\frac{M_\Delta^2}{m_t^2} - 1 - \frac{3}{\frac{m_t^2}{M_\Delta^2}-1}\left(\frac{\log\frac{m_t^2}{M_\Delta^2}}{\frac{m_t^2}{M_\Delta^2}-1} - 1\right)\right] + \\ &\quad - \frac{\sqrt{2}}{64\pi\alpha G_{\rm F} M_\Delta^2}\frac{\left(y^L\cdot y^{L\dagger}\right)_{bs}\left(y^{L\dagger}\cdot y^L\right)_{\mu\mu}}{V_{tb}V_{ts}^*} \end{aligned} \tag{4.38}$$

we evaluated the WC for the $b \to s\mu\mu$ couplings at the best-fit points of our 8D scenarios. Expressing them in the basis used for the $b \to s\ell\ell$ global fits,

$$\mathcal{C}_{9(\mu)}^{\rm NP} = \frac{C_{LR}^\mu + C_{LL}^\mu}{2}, \qquad \mathcal{C}_{10(\mu)}^{\rm NP} = \frac{C_{LR}^\mu - C_{LL}^\mu}{2}, \tag{4.39}$$

these correspond to

$$\begin{aligned} \left(\mathcal{C}_{9(\mu)}^{\rm NP}, \mathcal{C}_{10(\mu)}^{\rm NP}\right)_{\rm 8D_{simple,\ LFU}} &= (5.9\times10^{-2}, -5.9\times10^{-2}), \\ \left(\mathcal{C}_{9(\mu)}^{\rm NP}, \mathcal{C}_{10(\mu)}^{\rm NP}\right)_{\rm 8D_{a_\mu}} &= (2.5\times10^{-2}, -2.5\times10^{-2}). \end{aligned} \tag{4.40}$$

Although these values are small compared to the ones predicted by the global fit, we see that the couplings tend to assume opposite signs compared to the ones preferred by $b \to s\mu\mu$ data, indicating that the model is not able to resolve the tension in both $\mathcal{R}(D^{(*)})$ and $b \to s\ell\ell$ data, when all constraints are taken into account. This result is in agreement with the findings of Reference [100, 101].

4.5 Summary

In this chapter we analysed in more detail one of the single particle solutions of the $\mathcal{R}(D^{(*)})$ anomalies, namely the one involving a scalar LQ $\Delta \sim S_1^\dagger \sim (3, 1, -1/3)$. We assumed the most general Yukawa Lagrangian which does not involve contributions to the decay of the proton.

- We evaluated the virtual contributions of Δ to the coupling of Z bosons to charged leptons. Compared to previous works, our evaluation includes effects from EW renormalisation, arising from the LQ effects on the coupling with W bosons and on the photon polarisation, and hence on the Fermi constant $G_{\rm F}$ and on the electromagnetic fine-structure constant α. Fixing the relation between the EW couplings g, e and the measured quantities $G_{\rm F}, \alpha$ as the ones of the SM, gives rise to additional contributions in the Z coupling. Interestingly, these effects modify the Z coupling with a lepton even if the latter does not directly couple to the LQ via the Yukawa Lagrangian.

To analyse the interplay of the newly computed effects in the Z couplings with the $\mathcal{R}(D^{(*)})$ anomaly, we performed a fit of the Yukawa couplings of the LQ. We analysed two scenarios.

- First we assumed a simplified Yukawa structure having as nonvanishing couplings only the two required to give rise to the WC structure from Chapter 3. This scenario has the advantage that most of the contributions to the strongly constrained flavour observables are vanishing. From this analysis we concluded that the EW renormalisation effects arising from the photon polarisation are negligible. We also observed that with this Yukawa structure it is possible both to ameliorate the description of the $\mathcal{R}(D^{(*)})$ data and to improve the agreement of the theory prediction for the $Z\tau\tau$ coupling with its experimental value.
- We then extended the Yukawa structure, setting to zero only the couplings to first generation fermions. The additional couplings implied the necessity of taking several flavour constraints into account. In order to analyse the interplay between different observables, we performed three analyses, differing in the data included in the fit: a *simple* scenario, fitting only $\mathcal{R}(D^{(*)})$ and the $Z\ell\ell$ coupling, a scenario fitting also LFU ratios of light mesons and a scenario fitting also the anomalous magnetic moment of the muon, Δa_μ.
  - From the simple scenario we concluded that the extended Yukawa structure allows one to obtain a better description of $\mathcal{R}(D^{(*)})$ and of the Z couplings for both the τ and the e. In particular, the effects on the e coupling are a pure result of the newly included EW renormalisation terms. These give a nonnegligible contribution via the counterterm δg, which is nonvanishing due to the couplings of the LQ to muons.
  - At the best-fit point the effects on the leptonic decays of lighter mesons are negligible. This observation is reinforced by a comparison of the simple scenario with the scenario including LFU ratios. Since these channels are among those used for measuring the elements of the CKM matrix, we concluded that the

simple scenario does not modify significantly the agreement of the CKM unitarity with experimental data.

- Including Δa_μ in the fit implies a drastic worsening of the description of the $\mathcal{R}(D^{(*)})$ data. We conclude that the scalar LQ Δ is not able to account for both the tension in $\mathcal{R}(D^{(*)})$ and in Δa_μ.
- For all the three scenarios, the strongest constraints on the parameter space come from the decays $B \to K\nu\nu$ and $\tau \to \mu\gamma$, both saturating their experimental limit at the best-fit point. From this we conclude that our model predicts an experimental value of the branching ratios of these decays higher than their SM prediction.
- A solution of either $\mathcal{R}(D^{(*)})$ or Δa_μ in terms of the scalar LQ Δ increases the tension with the $b \to s\ell\ell$ data, hence challenging a simultaneous solution of each pair of the three anomalies in terms of Δ.

CHAPTER 5

Towards a grand unified theory

This chapter builds up on the analysis performed in the previous ones, but follows a somewhat opposite approach compared to them. While in Chapter 3 we performed an analysis of the $\mathcal{R}(D^{(*)})$ anomalies in terms of an effective field theory, and in Chapter 4 in terms of a model introducing a new physics particle *ad hoc*, in this chapter we follow a top-down approach, and specify from the beginning the UV complete model in which we want to address the $\mathcal{R}(D^{(*)})$ anomalies. We will choose the model and establish the particle content via some guiding principles that will allow us to avoid the *ad hoc* introduction of particles, since that approach would be analogous to adding these particles to the Standard Model content, as done in Chapter 4. Our guiding principles will be the requirement of unifying quarks and leptons and, on a later stage, the requirement of unifying the gauge group. We will start from the simplest extended gauge model in which quarks and leptons are unified into one representation, the Pati-Salam (PS) model [68]. After a brief introduction to the model, we will focus on the gauge sector, and see that one of the single-particle solutions to the $\mathcal{R}(D^{(*)})$ anomalies considered in Chapter 3 arises naturally. However, we will see that the constraints imposed by lepton flavour violating decays of light mesons push the mass of this particle to scales well above the one required for solving the $\mathcal{R}(D^{(*)})$ anomalies.

Having excluded the gauge sector as a solution to the anomalies, we will then focus on the scalar sector. We will assume the scalar content analysed in Reference [129], representing one of the possible minimal choices required to spontaneously break the PS group to the Standard Model with intermediate steps. This will leave us with only one viable candidate, a charged scalar, with the further feature of having couplings strictly related to the Standard Model Yukawa couplings. As we know from Chapter 3, the charged Higgs is disfavoured if $\mathrm{BR}(B_c \to \tau\nu_\tau)$ is low. In the hypothesis of a low $\mathrm{BR}(B_c \to \tau\nu_\tau)$ we will further extend the scalar sector by requiring the PS group to be an intermediate step in the spontaneous symmetry breaking (SSB) of a grand unified theory with gauge group $SO(10)$.

5.1 The Pati-Salam model

As we mentioned in the introduction, the principle guiding us in choosing the UV complete theory in which to seek for a solution to the $\mathcal{R}(D^{(*)})$ anomalies is the attempt to unify quarks and leptons by extending the gauge group of the SM. A successful attempt in this direction was done by Pati and Salam [68], who extended the gauge group to $SU(4)_\mathrm{c} \times SU(2)_\mathrm{L} \times SU(2)_\mathrm{R}$. Instead of directly analysing the features of this model, we will now briefly comment on the choice of this group.

5.1.1 Why $\mathbf{SU(4)_c \times SU(2)_L \times SU(2)_R}$?

As suggested by the title of Reference [68], the starting point of the model is the interpretation of leptons as the fourth colour. This means that of the SM gauge group $SU(3)_\mathrm{c} \times SU(2)_\mathrm{L} \times U(1)_Y$, the colour component $SU(3)_\mathrm{c}$ is regarded as a subgroup of $SU(4)_\mathrm{c}$, and the quark colour triplets are extended to fourtets by including as fourth component a lepton. The $SU(3)_\mathrm{c}$ is identified with the subgroup generated by the first eight generators, which for the fundamental representation 4 are

$$T_{1\ldots8} = \frac{1}{2}\begin{pmatrix} \lambda_{1\ldots8} & 0 \\ 0 & 0 \end{pmatrix}, \tag{5.1}$$

where $\lambda_{1\ldots8}$ represent the 3×3 Gell-Mann matrices.

Embedding quarks and leptons into the same representation implies that the naive extension to $SU(4)_\mathrm{c} \times SU(2)_\mathrm{L} \times U(1)_Y$ is unviable, since it would imply that the $SU(4)_\mathrm{c}$ part of the group commutes with the hypercharge $U(1)_Y$, a feature that is in contrast with the fact that the quarks and leptons in the same $SU(4)_\mathrm{c} \times SU(2)_\mathrm{L}$ representation have different hypercharge [130].

Another naive alternative would be to identify $U(1)_Y$ with the subgroup generated by the only generator that commutes with the $SU(3)_\mathrm{c}$ generators of Equation (5.1), namely

$$T_{15} = \frac{1}{2\sqrt{6}}\begin{pmatrix} 1 & 0 & 0 & 0 \\ 0 & 1 & 0 & 0 \\ 0 & 0 & 1 & 0 \\ 0 & 0 & 0 & -3 \end{pmatrix}. \tag{5.2}$$

However, this identification is in conflict with the hypercharge assignments in the SM. For instance, for the right-handed components, the hypercharge of the down-quarks $Y_d = -1/3$ would imply, from Equation (5.2), a hypercharge of the right-handed lepton of $Y_\ell = 1$.

These considerations show that enlarging $SU(3)_\mathrm{c}$ to $SU(4)_\mathrm{c}$ and embedding leptons into the same fundamental representation as quarks requires the need to modify the EW group as well.

The simplest choice $SU(4)_\mathrm{c} \times SU(2)_\mathrm{L} \times U(1)_R$ would already suffice to recover the correct hypercharges, whose operator could be built out of a combination of the generator in

Equation (5.2) and of the $U(1)_R$ quantum number, hence giving:

$$Y = aT_{15} + T_R. \tag{5.3}$$

The fermions are, then, introduced as

$$\begin{pmatrix} u_R & u_G & u_B & \nu \\ d_R & d_G & d_B & \ell \end{pmatrix}_L \sim (4,2)_{t_{\mathrm{L}}} \qquad \begin{matrix} \begin{pmatrix} u_R & u_G & u_B & \nu \end{pmatrix}_R \sim (4,1)_{t_{u_{\mathrm{R}}}} \\ \begin{pmatrix} d_R & d_G & d_B & \ell \end{pmatrix}_R \sim (4,1)_{t_{d_{\mathrm{R}}}} \end{matrix} \tag{5.4}$$

where the lower index t_i represents the quantum number under $U(1)_R$, i.e. the eigenvalue of T_R. The value of a and the t_i's are determined by setting the hypercharges of the particles to their SM values. For instance, acting on the right-handed down-type fermions we get

$$\begin{aligned} Y \begin{pmatrix} d_R \\ d_G \\ d_B \\ \ell \end{pmatrix} &= (aT_{15} + T_R) \begin{pmatrix} d_R \\ d_G \\ d_B \\ \ell \end{pmatrix} = (\frac{a}{2\sqrt{6}} \begin{pmatrix} 1 & 0 & 0 & 0 \\ 0 & 1 & 0 & 0 \\ 0 & 0 & 1 & 0 \\ 0 & 0 & 0 & -3 \end{pmatrix} + T_R) \begin{pmatrix} d_R \\ d_G \\ d_B \\ \ell \end{pmatrix} = \\ &= \begin{pmatrix} (\frac{a}{2\sqrt{6}} + t_{d_{\mathrm{R}}})d_R \\ (\frac{a}{2\sqrt{6}} + t_{d_{\mathrm{R}}})d_G \\ (\frac{a}{2\sqrt{6}} + t_{d_{\mathrm{R}}})d_B \\ (-\frac{3a}{2\sqrt{6}} + t_{d_{\mathrm{R}}})\ell \end{pmatrix} = \begin{pmatrix} -\frac{1}{3}d_R \\ -\frac{1}{3}d_G \\ -\frac{1}{3}d_B \\ -\ell \end{pmatrix} \Rightarrow a = \frac{\sqrt{6}}{3}, t_{d_{\mathrm{R}}} = -\frac{1}{2}. \end{aligned} \tag{5.5}$$

This leads to

$$Y = \begin{pmatrix} 1/6 & 0 & 0 & 0 \\ 0 & 1/6 & 0 & 0 \\ 0 & 0 & 1/6 & 0 \\ 0 & 0 & 0 & -1/2 \end{pmatrix} + T_{\mathrm{R}}, \tag{5.6}$$

which allows to reproduce the SM hypercharges once the fermions are assigned the following t_i charges:

$$\begin{pmatrix} u_R & u_G & u_B & \nu \\ d_R & d_G & d_B & \ell \end{pmatrix}_L \sim (4,2)_0 \qquad \begin{matrix} \begin{pmatrix} u_R & u_G & u_B & \nu \end{pmatrix}_R \sim (4,1)_{1/2} \\ \begin{pmatrix} d_R & d_G & d_B & \ell \end{pmatrix}_R \sim (4,1)_{-1/2}. \end{matrix} \tag{5.7}$$

Although $SU(4)_{\mathrm{c}} \times SU(2)_{\mathrm{L}} \times U(1)_R$ already provides the unification of quark and lepton representations, the quantum numbers in Equation (5.7) suggest that the T_{R} could be identified as the third generator of an additional $SU(2)_{\mathrm{R}}$, rather than a simple $U(1)$ generator. The advantage of $SU(4)_{\mathrm{c}} \times SU(2)_{\mathrm{L}} \times SU(2)_{\mathrm{R}}$ is that the group does not contain abelian factors $U(1)$, hence providing an explanation for the quantisation of electric charge. Furthermore, the fact that the left and right components of the gauge group are both $SU(2)$'s suggests that this analogy could be extended to a symmetry at high energies, which can be added to the PS gauge group as a discrete symmetry Z_2. However, the implementation of this

discrete symmetry is not unique, as it is the case in left-right symmetric models [131, 132]. A first way of implementing the Z_2 symmetry relating the right- and left-handed sectors is via the so-called generalised parity $\mathcal{P}$. This symmetry requires a generic spinor to transform as

$$\mathcal{P} : \Psi \to \gamma^0 \Psi, \tag{5.8}$$

implying, for the two components

$$\begin{cases} \Psi_{\mathrm{L}} = P_{\mathrm{L}}\Psi \to P_{\mathrm{L}}\gamma^0\Psi = \gamma^0 P_{\mathrm{R}}\Psi \\ \Psi_{\mathrm{R}} = P_{\mathrm{R}}\Psi \to P_{\mathrm{R}}\gamma^0\Psi = \gamma^0 P_{\mathrm{L}}\Psi \end{cases} . \tag{5.9}$$

Another possible choice is the generalised charged conjugation $\mathcal{C}$, under which a generic spinor transforms as

$$\mathcal{C} : \Psi \to \Psi^c, \tag{5.10}$$

where the charge-conjugated spinor is defined as $\Psi^c = C\overline{\Psi}^{\mathrm{T}} = i\gamma^2\gamma^0\overline{\Psi}^{\mathrm{T}}$, with

$$C = i\gamma^2\gamma^0 = \begin{pmatrix} \epsilon & 0 \\ 0 & -\epsilon \end{pmatrix} . \tag{5.11}$$

Equation (5.10) corresponds to the transformation

$$\begin{cases} \Psi_{\mathrm{L}} = P_{\mathrm{L}}\Psi \to P_{\mathrm{L}}\Psi^c = (\Psi_{\mathrm{R}})^c \\ \Psi_{\mathrm{R}} = P_{\mathrm{R}}\Psi \to P_{\mathrm{R}}\Psi^c = (\Psi_{\mathrm{L}})^c \end{cases} . \tag{5.12}$$

Let us now look at the particle content of the PS model. The fermionic sector is uniquely specified if we assume that the only additional particles are those arising from the completion of the SM representations. After the identification of T_{R} as the third generator of $SU(2)_{\mathrm{R}}$, the fermionic content of Equation (5.7) is grouped into the following representations under the PS group

$$\Psi_L = \begin{pmatrix} u_r & u_g & u_b & \nu \\ d_r & d_g & d_b & \ell \end{pmatrix}_L \sim (4,2,1) \qquad \Psi_R = \begin{pmatrix} u_r & u_g & u_b & \nu \\ d_r & d_g & d_b & \ell \end{pmatrix}_R \sim (4,1,2) \tag{5.13}$$

which require the introduction of a right-handed neutrino. The representations in Equation (5.13) refer to a single generation of fermions. As in the SM, the inclusion of all possible flavours is implemented by requiring three identical copies of these representations. The way to include the different leptons into the different quark triplets is not established a priori. In other words, one might include the electron as extension of the first, second or third generation of quarks, and analogously for the μ and τ. In the version of the model we consider, the leptons are included in the quark families following the same mass hierarchy.

The gauge boson content is uniquely determined by the gauge group. The $SU(2)_{\mathrm{L}}$ gauge bosons correspond to the $W^{\pm,3}_{\mathrm{L}\mu}$ of the SM, and analogous particles, labelled as $W^{\pm,3}_{\mathrm{R}\mu}$, are

associated to $SU(2)_\mathrm{R}$. The $SU(4)_\mathrm{c}$ gauge bosons are conveniently written in the form

$$
\begin{aligned}
G =& G^a T^a = \\
=& \frac{1}{2}\begin{pmatrix} G^3 + \frac{G^8}{\sqrt{3}} + \frac{G^{15}}{\sqrt{6}} & G^1 - iG^2 & G^4 - iG^5 & G^9 - iG^{10} \\ G^1 + iG^2 & -G^3 + \frac{G^8}{\sqrt{3}} + \frac{G^{15}}{\sqrt{6}} & G^6 - iG^7 & G^{11} - iG^{12} \\ G^4 + iG^5 & G^6 + iG^7 & -\frac{2}{\sqrt{3}}G^8 + \frac{G^{15}}{\sqrt{6}} & G^{13} - iG^{14} \\ G^9 + iG^{10} & G^{11} + iG^{12} & G^{13} + iG^{14} & -\frac{3}{\sqrt{6}}G^{15} \end{pmatrix},
\end{aligned}
\tag{5.14}
$$

in which we omitted the Lorentz index μ in order to simplify the notation. We can determine the electric charges of these gauge bosons by acting with the electric charge operator, defined as in the SM with respect to the third $SU(2)_\mathrm{L}$ generator and the hypercharge as $Q = T_\mathrm{L3} + Y = T_\mathrm{L3} + T_\mathrm{R3} + \frac{2}{\sqrt{6}}T_{15}$. The electric charges of each entry of the matrix hence read[1]

$$
\begin{pmatrix} 0 & 0 & 0 & 2/3 \\ 0 & 0 & 0 & 2/3 \\ 0 & 0 & 0 & 2/3 \\ -2/3 & -2/3 & -2/3 & 0 \end{pmatrix}. \tag{5.15}
$$

Since these gauge bosons do not carry $SU(2)_\mathrm{L}$ charge, their electric charges correspond to their hypercharges. We can rewrite the particles in Equation (5.14) by grouping them as representations under the SM group as:

$$
G = \frac{1}{2}\begin{pmatrix} \begin{pmatrix} G^a\lambda^a \end{pmatrix}_{(8,1)_0} & \begin{pmatrix} \sqrt{2}U^{+2/3} \end{pmatrix}_{(3,1)_{2/3}} \\ \begin{pmatrix} \sqrt{2}U^{-2/3} \end{pmatrix}_{(\bar{3},1)_{-2/3}} & 0 \end{pmatrix} + G_{15(1,1)_0}. \tag{5.16}
$$

The neutral particles in the 3×3 block of Equation (5.16), related to the $T_{1\ldots8}$ generators, correspond to the gluons of the SM. The gauge bosons in the off-diagonal elements of the matrix arrange themselves into a vector $SU(3)_\mathrm{c}$ triplet. The couplings of this particle with fermions can be deduced from the kinetic terms of the fermions. For instance, for the first, red-charged component of U, defined as

$$
U^{2/3} = \frac{G^9 - iG^{10}}{\sqrt{2}}, \tag{5.17}
$$

[1]The gauge bosons lie in the adjoint representation of the corresponding group. For this reason, T_{15} acts as a commutator on each gauge boson, i.e. on the matrices with a single nonvanishing element from Equation (5.14).

we get

$$D_\mu \supset -ig_4 \frac{1}{\sqrt{2}} \begin{pmatrix} 0 & 0 & 0 & U_r^{2/3} \\ 0 & 0 & 0 & 0 \\ 0 & 0 & 0 & 0 \\ 0 & 0 & 0 & 0 \end{pmatrix} \Rightarrow \overline{\Psi} i \not{D} \Psi \supset \frac{g_4}{\sqrt{2}} U_{r\mu}^{2/3} (\overline{u_r} \gamma^\mu \nu + \overline{d_r} \gamma^\mu \ell), \tag{5.18}$$

generating the vertices

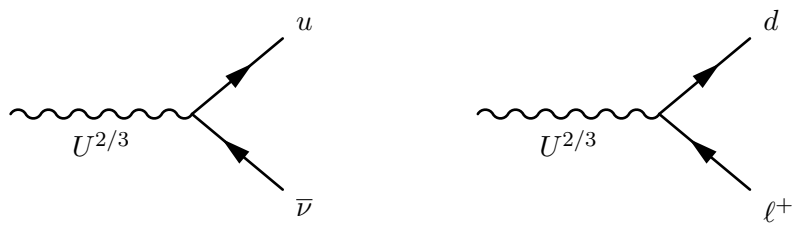

with coupling $ig_4/\sqrt{2}$. For the vertices with each component of U, the two fermions involved will always be a lepton and a quark, hence U qualifies as a vector LQ. It corresponds to the vector LQ U_1 of Chapter 3, mediating the $b \to c\tau\nu$ transition.

Contrary to the gauge sector, the scalar sector is not uniquely fixed by the gauge group. However, we will avoid the introduction of scalar particles that are not required for the SSB of the gauge group to the $U(1)_{\text{em}}$. Even then, the way the breaking PS→SM is accomplished is not unique, and as a consequence, the scalar sector is not uniquely defined. Our analysis assumes the scalar fields used in Reference [129] for breaking the PS group with intermediate breaking steps, i.e. the fields

$$\begin{aligned} \Sigma &\sim (15,1,1) \\ T_{\text{L}} \oplus T_{\text{R}} &\sim (1,3,1) \oplus (1,1,3) \\ \Phi_{\text{L}} \oplus \Phi_{\text{R}} &\sim (4,2,1) \oplus (4,1,2) \\ h &\sim (1,2,2). \end{aligned} \tag{5.19}$$

5.1.2 Pati-Salam gauge bosons and $\mathcal{R}(D^{(*)})$

In this section we analyse the effects of the gauge bosons of the PS model on the $\mathcal{R}(D^{(*)})$ ratios.

Right-handed vector current

The only possible contribution of $W_{\text{R}\mu}^{\pm,3}$ to a transition $b \to c\tau\nu$ comes from couplings identical in structure to the SM couplings with $W_{\text{L}}^{\pm}$, but with a right-handed projector. The neutrino in the final state is hence the right-handed neutrino of the $SU(2)_{\text{R}}$ doublet. This implies that the contributions originating from the coupling arising with the $W_{\text{R}}^{\pm}$

cannot interfere with the SM ones, since the particles in the final state are different. In addition, if we assume the right-handed neutrinos of the PS model to be heavy, the decay $B \to D^{(*)}\tau\nu_{\rm R}$ is kinematically forbidden. For these reason we will neglect the contribution of the $SU(2)_{\rm R}$ gauge bosons to $\mathcal{R}(D^{(*)})$.

Vector leptoquark and $\mathcal{R}(D^{(*)})$

Let us analyse the contributions of the vector LQ U arising from the $SU(4)_{\rm c}$ gauge bosons. In order to relate the couplings of Equation (5.18) to the effective couplings of Chapter 3, the interactions from the kinetic term must be rewritten in the mass basis. This change of basis introduces an additional unitary matrix for each type of fields, hence enlarging the number of parameters to be considered. As a benchmark case, we will make the hypothesis that the matrix describing the mixing of the lepton and quark generations in the U_1-mediated interactions has roughly the same structure as the CKM matrix. Under this hypothesis, the effective $b \to c\tau\nu$ interaction mediated by U_1, restricting to the case of a third generation left-handed neutrino in order to allow for interference terms with the SM contribution, reads[2]

$$\begin{aligned}\mathcal{H}_{U_1} &= \frac{g_4^2 V_{cb}}{2M_U^2}(\bar{c}\gamma^\mu\nu)(\bar{\tau}\gamma_\mu b) = \\ &= -\frac{g_4^2 V_{cb}}{2M_U^2}[(\bar{c}_{\rm L}\gamma^\mu b_{\rm L})(\bar{\tau}_L\gamma_\mu\nu_{\rm L}) - 2(\bar{c}_{\rm L}b_{\rm R})(\bar{\tau}_{\rm R}\nu_{\rm L})],\end{aligned} \tag{5.20}$$

where the CKM matrix element V_{cb} arises from the coupling of the c quark with a third generation neutrino, and where we used a Fierz rearrangement of the spinors to get from the first to the second line. This structure already suggests that if the U_1 vector LQ of Chapter 3 is to be regarded as a solution to the $\mathcal{R}(D^{(*)})$ anomalies, the underlying UV complete model is not the PS. In fact, compared to the upper-right plot of Figure 3.6, the WCs assume opposite signs with respect to the ones assumed in the 2σ region. In addition, the underlying $SU(4)_{\rm c}$ structure allows us to put strong bounds on the vector LQ effects via LFV decays of neutral mesons. The most stringent bound is set by the decay $K_{\rm L} \to \mu e$, for which the experimental limit is 2.8×10^{-5} at 90% C.L. [31]. The branching ratio for this decay reads [130, 133]

$$\mathrm{BR}(K_L \to \mu e) = \tau_K \pi \alpha_s^2(M_U)\frac{1}{M_U^4} f_K^2 m_K \left(\frac{m_K^2}{m_s + m_d}\right)^2 \left(1 - \frac{m_\mu^2}{m_K^2}\right)^2 . \tag{5.21}$$

The peculiar feature of this expression is the appearance of the strong coupling $\alpha_s = g_3^2/4\pi$, which is due to the fact that the interaction with U has the same origin as the interaction of fermions with gluons. In Equation (5.21), τ_K, f_K are the K lifetime and decay constant respectively. The coupling $g_3(M_U)$ and the quark masses $m_{s,d}(M_U)$ refer to the energy scale of the mass of the leptoquark M_U. Their values in the $\overline{\rm MS}$ scheme are obtained using the Mathematica package RunDec [134–136], assuming that there are no particles

[2] These relations are given at the LQ mass scale, and evolving them to the m_b scale implies an additional factor of roughly $\simeq 1.8$ for the scalar operator, originating as in Equation (3.10).

interacting strongly in the mass range from m_t to M_U [130]. With this procedure, the current experimental limit translates to a lower limit of $\mathcal{O}(10^3\,\text{TeV})$ on the mass of the vector LQ.

On the other hand, requiring an effective coupling of roughly $\simeq 0.08$, as suggested from the results of the EFT fit in Table 3.4, also sets the mass of the vector LQ. The $SU(4)_\text{c}$ structure implies

$$|C| = \frac{g_4^2}{2M_U^2} \simeq 0.08 \times 2\sqrt{2}G_\text{F}. \tag{5.22}$$

Using for g_4^2 the value of the strong coupling evolved to the m_b scale, this implies a mass of the vector LQ of roughly $M_U \simeq 3\,\text{TeV}$, three orders of magnitude below the limit from LFV decays.

Although some room is left from the approximations made concerning the flavour mixing matrices, covering a gap of three orders of magnitude would require a great amount of fine-tuning of the flavour parameters. We conclude that the gauge sector of the PS model is unlikely to be responsible for the $\mathcal{R}(D^{(*)})$ anomalies.

5.1.3 Pati-Salam scalars and $\mathcal{R}(D^{(*)})$

The particles coming from the scalar sector assumed in Equation (5.19) can contribute at tree-level to $b \to c\ell\overline{\nu}$ only if their Yukawa couplings with the fermions, which belong to the $(4,2,1)$ and $(4,1,2)$ representations, are allowed by gauge invariance. In other words, the tensor product of the scalar with one of the following products of two spinors

$$\begin{aligned}
&\overline{\psi}_L\psi_R : (\overline{4},2,1) \otimes (4,1,2) = (1,2,2) \oplus (15,2,2) \\
&\overline{\psi}^c_L\psi_L : (4,2,1) \otimes (4,2,1) = (10,1,1) \oplus (10,3,1) \oplus (6,1,1) \oplus (6,3,1) \\
&\overline{\psi}^c_R\psi_R : (4,1,2) \otimes (4,1,2) = (10,1,1) \oplus (10,1,3) \oplus (6,1,1) \oplus (6,1,3)
\end{aligned} \tag{5.23}$$

must contain a singlet. Comparing Equations (5.23) and (5.19) we see that the only field with nonvanishing Yukawa couplings is h. This field is usually identified with the PS completion of the SM Higgs field. The additional charged components might be identified with the scalar solution to the $\mathcal{R}(D^{(*)})$ anomalies presented in Chapter 3. However, the fact that the charged Higgs arises from the same representation of the SM Higgs implies that the couplings to this field are already constrained by the correct prediction of fermion masses and mixing within the PS model, and a solution of $\mathcal{R}(D^{(*)})$ in terms of h would hence be challenged. In addition, in Chapter 3 we pointed out that the charged Higgs solution predicts a high value of the branching ratio $\text{BR}(B_c \to \tau\nu_\tau)$. In the hypothesis that a measurement of this branching ratio gives a high value compared to its SM prediction, it will be interesting to investigate in more detail the scalar solution with the underlying PS assumption. This analysis is left for future work.

On the other hand, the measurement of a low $\text{BR}(B_c \to \tau\nu_\tau)$ implies that the scalar setup of the PS model does not allow for a solution to the $\mathcal{R}(D^{(*)})$ anomaly. This implies that

the PS alone cannot describe the current $\mathcal{R}(D^{(*)})$ data. Our search for a solution arising naturally in a PS framework requires us to go beyond this simple scenario. To do so, we will follow an additional guiding principle, which is the unification of the gauge group, as we will see in the next section.

5.1.4 An SO(10)-inspired scalar content

An interesting feature of the PS model is that it can be embedded in the breaking chain of a GUT having as gauge group the $SO(10)$ group. The latter, in turn, as well as embedding the SM gauge group in a simple group, reducing the number of gauge couplings to one, requires only one representation to describe all the fermions of a single generation. These features motivate our reconsideration of the scalar sector of the PS model under the hypothesis that the model is an intermediate step in the breaking of an $SO(10)$ GUT.

This assumption has interesting consequences on the structure of the PS gauge group, on the scalar content of the model as well as on its phenomenological predictions. We analyse these aspects separately.

Discrete symmetry

Embedding the discretely-symmetric version of the PS gauge group into $SO(10)$ implies that the discrete symmetry must be the generalised charge conjugation $\mathcal{C}$ rather than the generalised parity $\mathcal{P}$ [137]. This can be understood by analysing the fermionic representations in $SO(10)$, which are the 16. The content of this representation can be more easily understood in terms of the PS group. The *branching rule* of the $16_{SO(10)}$ in terms of $SU(4) \times SU(2) \times SU(2)$, i.e. the way the particles in the representations under the PS group are embedded into a $16_{SO(10)}$, is [138]

$$16_{SO(10)} \to (4,2,1)_{\mathrm{PS}} \oplus (\overline{4},1,2)_{\mathrm{PS}}. \tag{5.24}$$

Since the right-handed fermions are embedded as charge-conjugate representations, and since the discrete symmetry must be an element of the connected group $SO(10)$, the Z_2 symmetry cannot relate $\Psi_{\mathrm{L}} \leftrightarrow \Psi_{\mathrm{R}}$, which would be a transformation that we cannot continuously shrink to the identity. On the other hand, $\Psi_{\mathrm{L}} \leftrightarrow \Psi_{\mathrm{R}}^c$ can be achieved within $SO(10)$ since these spinors are elements of a same representation.

As discussed in References [139, 140], it is possible to break the discrete symmetry with a PS singlet, hence decoupling the breaking of the generalised parity from the breaking of PS. For this reason we will consider both the version of the PS model, with or without the generalised parity $\mathcal{C}$.

Extension of the scalar content

Extending the PS group to $SO(10)$ requires each of the representations to be regarded as the representation under the PS subgroup of a representation under $SO(10)$. This interpretation is straightforward for the fermionic content, as we saw from the branching rule

in Equation (5.24). The scalar content, instead, does not already provide the additional components needed to complete the representations, and it hence requires the introduction of additional particles. In particular, from the branching rules reported in Reference [138] we notice that the lowest-dimensional representation that allows for the embedding of the bi-doublet h is the $10_{SO(10)}$, which under the PS group decomposes as

$$10_{SO(10)} \to (1,2,2)_{\mathrm{PS}} \oplus (6,1,1)_{\mathrm{PS}}. \tag{5.25}$$

We label the additional field $F \sim (6,1,1)_{\mathrm{PS}}$, and we now analyse its properties.

The $SU(4)_{\mathrm{c}}$ sextet F transforms as the antisymmetric part of the tensor product of two fundamental representations 4, i.e. from the decomposition into irreducible representations $4 \otimes 4 = 10 \oplus 6$. Comparing this with Equation (5.25), we conclude that Yukawa terms can be built out of the field F and two fermion fields, one of them being charge-conjugated. There are two ways of writing down a Yukawa term involving F, since one can either saturate the two indices of F with each of the fermion indices directly or make use of the Levi-Civita symbol in four dimensions[3] ϵ_{ijkl}. Labelling with a tilde the terms involving the ϵ, and $\tilde{F}_{ij} = \epsilon_{ijkl} F^{kl}$, we can write

$$\mathcal{L}_F = F(A\overline{\Psi_{\mathrm{L}}}\Psi^c_{\mathrm{L}} + B\overline{\Psi_{\mathrm{R}}}\Psi^c_{\mathrm{R}}) + \tilde{F}(\tilde{A}\overline{\Psi^c_{\mathrm{L}}}\Psi_{\mathrm{L}} + \tilde{B}\overline{\Psi^c_{\mathrm{R}}}\Psi_{\mathrm{R}}) + \mathrm{h.c.} \tag{5.26}$$

Due to the antisymmetric nature of F, the Yukawa coupling matrices $A, \tilde{A}, B, \tilde{B}$ must be symmetric under the exchange of two flavour indices[4]. For instance, considering the term $A^\dagger F^\dagger \overline{\Psi^c_L} \Psi_L$, we have

$$\begin{aligned}
\mathcal{L}_F \supset A^\dagger F^\dagger \overline{\Psi^c_{\mathrm{L}}}\Psi_{\mathrm{L}} &= A^\dagger_{mn} F^\dagger \overline{\Psi^{cm}_{\mathrm{L}}}\Psi^n_{\mathrm{L}} = {A^\dagger}_{mn} F^\dagger_{\alpha\beta} \Psi_L^{\alpha iam} \epsilon_{ij}\epsilon_{ab} \Psi_L^{\beta jbn} = \\
&= -{A^\dagger}_{mn} F^\dagger_{\alpha\beta} \Psi_L^{\beta jbn} \epsilon_{ij}\epsilon_{ab} \Psi_L^{\alpha iam} = -{A^\dagger}_{mn} F^\dagger_{\beta\alpha} \Psi_L^{\alpha ian} \epsilon_{ji}\epsilon_{ba} \Psi_L^{\beta jbm} = \\
&= -{A^\dagger}_{mn} F^\dagger_{\beta\alpha} \Psi_L^{\alpha ian} \epsilon_{ij}\epsilon_{ab} \Psi_L^{\beta jbm} = {A^\dagger}_{mn} F^\dagger_{\alpha\beta} \Psi_L^{\alpha ian} \epsilon_{ij}\epsilon_{ab} \Psi_L^{\beta jbm} = \\
&= {A^\dagger}_{nm} F^\dagger_{\alpha\beta} \Psi_L^{\alpha iam} \epsilon_{ij}\epsilon_{ab} \Psi_L^{\beta jbn},
\end{aligned} \tag{5.27}$$

where the indices $(m,n), (\alpha,\beta), (i,j), (a,b)$ refer to flavour, $SU(4)_{\mathrm{c}}$, Lorentz and $SU(2)$ space respectively, while the c labels the charge-conjugated spinor. In the derivation, we used the fact that for what concerns Lorentz space, the barred charge-conjugated spinor is $\overline{\Psi^c} = \Psi^{\mathrm{T}} C$. From Equation (5.27) we deduce that the matrix A_{mn} must be symmetric, $A_{mn} = A_{nm}$; the same steps can be applied to the other matrices $\tilde{A}, B, \tilde{B}$. The requirement that the couplings to F respect the generalised charge conjugation $\mathcal{C}$ sets both the way the field F transforms and the structure of the couplings $A, B, \tilde{A}, \tilde{B}$. For instance, restricting

[3] This is allowed by the fact that the sextet is the self-conjugate representation of $SU(4)$. In other words its conjugate, obtained with the ϵ, is also a sextet.

[4] This generalises the symmetry of the z matrix of the diquark coupling of the scalar LQ S_1 of Reference [72]

to the terms involving A, B and marking with $\hat{F}$ the transformed of F we have

$$\begin{aligned}\mathcal{L}_F \supset & F(A\overline{\Psi_{\mathrm{L}}}\Psi_{\mathrm{L}}^c + B\overline{\Psi_{\mathrm{R}}}\Psi_{\mathrm{R}}^c) + F^\dagger(A^\dagger\overline{\Psi_{\mathrm{L}}^c}\Psi_{\mathrm{L}} + B^\dagger\overline{\Psi_{\mathrm{R}}^c}\Psi_{\mathrm{R}}) \rightarrow \\ \rightarrow & \hat{F}(A\overline{\Psi_{\mathrm{R}}^c}\Psi_{\mathrm{R}} + B\overline{\Psi_{\mathrm{L}}^c}\Psi_{\mathrm{L}}) + \text{h.c.}\end{aligned} \tag{5.28}$$

Requiring the Lagrangian to be invariant, i.e. setting the two lines to be equal, we get the requirements

$$\begin{cases} F \rightarrow \hat{F} = F^\dagger \\ A = B^\dagger \\ \tilde{A} = \tilde{B}^\dagger \end{cases} . \tag{5.29}$$

Expressing the sextet in terms of SM representations gives [138]

$$(6,1,1)^{\mathrm{PS}} \rightarrow (\overline{3},1)^{\mathrm{SM}}_{1/3} \oplus (3,1)^{\mathrm{SM}}_{-1/3}. \tag{5.30}$$

We see that F contains two fields transforming as the scalar leptoquark Δ considered as a solution of the $\mathcal{R}(D^{(*)})$ anomalies in Chapters 3 and 4. If we write F as the 4×4 matrix in the $SU(4)_{\mathrm{c}}$ space, this gives

$$\begin{pmatrix} 0 & -F_3^{\overline{3}} & F_2^{\overline{3}} & F_1^3 \\ F_3^{\overline{3}} & 0 & -F_1^{\overline{3}} & F_2^3 \\ -F_2^{\overline{3}} & F_1^{\overline{3}} & 0 & F_3^3 \\ -F_1^3 & -F_2^3 & -F_3^3 & 0 \end{pmatrix}, \tag{5.31}$$

where the upper indices $3, \overline{3}$ refer to the triplet and antitriplet components of Equation (5.30), while the lower indices refer to the colour $SU(3)_{\mathrm{c}}$ space.

Although these scalar LQs also arise from a completion of the bi-doublet identified as the SM Higgs, we neglect for the rest of our analysis the issue of the description of fermion masses within $SO(10)$. The reason is that, as pointed out in Reference [141], agreement with the fermionic spectrum and mixing within $SO(10)$ requires the presence of at least one more scalar representation containing components transforming as the SM Higgs doublet. A comprehensive analysis of a proper scalar sector accounting for fermion masses and mixing and simultaneously describing the $\mathcal{R}(D^{(*)})$ data is beyond the scope of this work. We focus, instead, on which Yukawa couplings would be needed to account for $\mathcal{R}(D^{(*)})$ with the 10 representation under $SO(10)$, having in mind that its couplings are not enough to account for the fermionic spectrum even without the requirement of addressing the $\mathcal{R}(D^{(*)})$ anomalies[5].

[5]The additional representations required to reproduce the fermion masses and mixings in $SO(10)$ models might also contain additional sextets, as it is the case for the 126 representation. In that case, the sextet considered here, and the corresponding Yukawa couplings, would be a linear combination of the two.

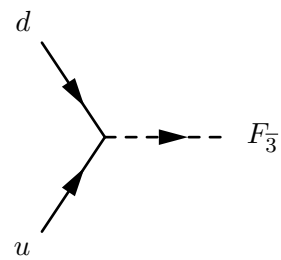

Figure 5.1: Feynman diagram for the quark-quark-$F_{\overline{3}}$ interactions arising from the *untilded* Yukawas A, B.

F-mediated proton decay

In our simplified analysis of Chapter 4 we set to zero the diquark couplings of the scalar LQ Δ in order for it not to mediate proton decay. In this section we show that these troublesome terms also arise if Δ is identified with either the triplet or the antitriplet component of F, and that setting some of the Yukawa couplings to zero does not suffice to prevent proton decay at all orders. However, proton decay can be avoided by imposing an additional symmetry to the Lagrangian.

Let us analyse separately the Yukawa interactions generated by the F^3 and $F^{\overline{3}}$ components of F, restricting to the left-handed part and analysing separately the A, B and $\tilde{A}, \tilde{B}$ terms. If we label with $\rho, \sigma = 1, 2, 3, 4$ the $SU(4)_{\rm c}$ indices and with $\alpha, \beta = 1, 2, 3$ their restriction to $SU(3)_{\rm c}$ and adopting for the other indices the same notation as in (5.27), we have

$$\begin{aligned}
\mathcal{L}_Y \supset\, & Y_{Fmn} F^\dagger_{\rho\sigma} \Psi_L^{\rho iam} \epsilon_{ij} \epsilon_{ab} \Psi_L^{\sigma jbn} = \\
&= A^\dagger_{mn} \{ F^{3\dagger}_{4\sigma} \Psi_L^{4iam} \epsilon_{ij} \epsilon_{ab} \Psi_L^{\sigma jbn} + F^{3\dagger}_{\sigma 4} \Psi_L^{\sigma iam} \epsilon_{ij} \epsilon_{ab} \Psi_L^{\sigma jbn} + F^{\overline{3}\dagger}_{\alpha\beta} \Psi_L^{\alpha iam} \epsilon_{ij} \epsilon_{ab} \Psi_L^{\beta jbn} \} = \\
&= A^\dagger_{mn} \{ 2 F^{3\dagger}_{4\sigma} \Psi_L^{4iam} \epsilon_{ij} \epsilon_{ab} \Psi_L^{\sigma jbn} + F^{\overline{3}\dagger}_{\alpha\beta} \Psi_L^{\alpha iam} \epsilon_{ij} \epsilon_{ab} \Psi_L^{\beta jbn} \} = \\
&= A^\dagger_{mn} \{ 2 F^{3\dagger}_{4\sigma} L_L^{iam} \epsilon_{ij} \epsilon_{ab} Q_L^{\sigma jbn} + F^{\overline{3}\dagger}_{\alpha\beta} Q_L^{\alpha iam} \epsilon_{ij} \epsilon_{ab} Q_L^{\beta jbn} \}.
\end{aligned} \tag{5.32}$$

We see from Equation (5.32) that in the *untilded* part of the Yukawa Lagrangian

- $F_{\overline{3}}$ only mediates quark-quark interactions, of the form shown in Figure 5.1.
- F_3 only mediates quark-lepton interactions, of the form shown in Figure 5.2.

Analogous steps show that in the *tilded* part of the Yukawa Lagrangian

- F_3 only mediates quark-quark interactions, of the form shown in Figure 5.3.
- $F_{\overline{3}}$ only mediates quark-lepton interactions, of the form shown in Figure 5.4.

Comparing the diagrams from Figures 5.1-5.4, we realise that with the most general Yukawa structure, i.e. with nonvanishing $A, B, \tilde{A}, \tilde{B}$, the field F contributes to the decay of the proton via diagrams such as that in Figure 5.5. Even assuming the tilded Yukawas to be

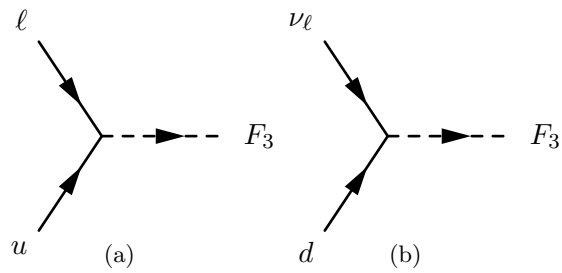

Figure 5.2: Feynman diagram for the quark-lepton-F_3 interactions arising from the *untilded* Yukawas A, B.

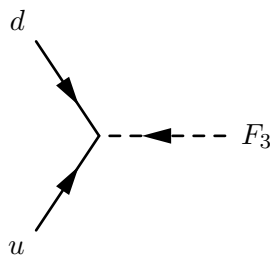

Figure 5.3: Feynman diagram for the quark-quark-F_3 interactions arising from the *tilded* Yukawas $\tilde{A}, \tilde{B}$.

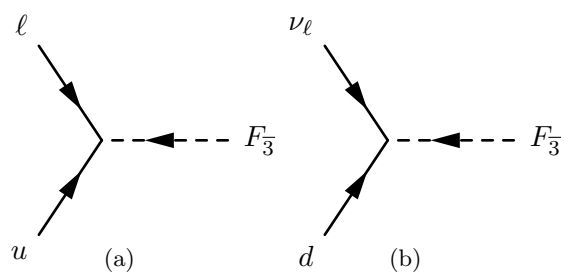

Figure 5.4: Feynman diagram for the quark-lepton-$F_{\overline{3}}$ interactions arising from the *tilded* Yukawas $\tilde{A}, \tilde{B}$.

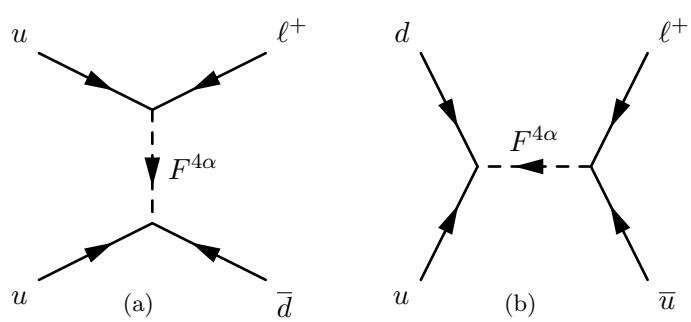

Figure 5.5: Example of tree-level contribution to the proton decay channel $p \to \ell^+ \pi^0$.

vanishing does not suffice to prevent F from mediating proton decay at higher orders. This is due to the fact that the sextet is self-conjugate, and hence all the couplings that can be built with F can be built with its conjugate $\tilde{F}$ via the use of the Levi-Civita symbol. For instance, two mass terms for F are possible, namely

$$m^2 F^\dagger_{ij} F^{ij} + \tilde{m}^2 F^{ij} F^{kl} \epsilon_{ijkl}, \tag{5.33}$$

spelling out the F components, one gets

$$2m^2 (F^{3\dagger}_\alpha F^{3\alpha} + F^{\overline{3}\dagger\alpha} F^{\overline{3}}_\alpha) - 8\tilde{m}^2 F^{3\alpha} F^{\overline{3}}_\alpha. \tag{5.34}$$

The $\tilde{m}$ mass term implies a mixing of the 3 and $\overline{3}$ components. Analogously, if any other particle couples to these fields, its virtual effects via loops effectively give rise to a mixing between the 3 and $\overline{3}$ components of F. This implies that even if the tilded Yukawa couplings vanish, i.e. even if F^3 and $F^{\overline{3}}$ give rise separately either to quark-lepton or to diquark couplings only, proton decay contributions can still arise at higher orders.

This problem can be addressed to all orders in an elegant way by introducing an additional global symmetry and assigning to F a corresponding nonzero quantum number. It is also intuitively clear why this mechanism works, since the additional charge renders the F no longer self-conjugate, hence preventing the inclusion of any term involving the Levi-Civita symbol.

For instance, assigning a charge 1 to the fermion fields implies that either the A, B or $\tilde{A}, \tilde{B}$ is nonvanishing. For nonvanishing[6] A, B the field F must have charge 2.

Up to a normalisation, this quantum number corresponds to the $3B + L$ number, where B and L stand for the baryon and lepton number respectively. Since the component of the PS group generated by the T_{15} generator of $SU(4)_\mathrm{c}$ corresponds to the $B - L$ quantum number, which is gauged in the PS model, assigning the additional $3B + L$ quantum number to each field and imposing its conservation implies thatboth the baryon and lepton number will be conserved separately. This guarantees that proton decay effects will not arise at any order.

$\mathbf{F^3 - F^{\overline{3}}}$ splitting

The additional $3B + L$ symmetry implies that each of the two LQs contained in the $SO(10)$ completion of the Higgs bi-doublet h mediates either lepton-quark transitions only, and hence contributes to $b \to c\ell\nu$, or quark-quark transitions only, contributing FCNCs. Since these fields arise from the same representation, they share the same Yukawa couplings. This implies that a fit of these couplings would require to consider simultaneously the quark-quark and quark-lepton fields. However, already with the minimal scalar content assumed above, these fields can get a significant splitting in mass at the PS breaking scale, as we now show.

We consider the field $\Sigma \sim (15, 1, 1)_\mathrm{PS}$ as responsible for the breaking of $SU(4)_\mathrm{c}$. In the $SU(4)_\mathrm{c}$ part, this representation coincides with the adjoint representation of $SU(4)_\mathrm{c}$, arising from the tensor product $4 \otimes \overline{4} = 1 \oplus 15$ and represented by a traceless 4×4 matrix Σ^j_i.

[6] The treatment for nonvanishing $\tilde{A}, \tilde{B}$ is analogous and the choice of either of the two is equivalent.

Since the product $F^\dagger F$ transforms as $\overline{6} \otimes 6 = 1 \oplus 15 \oplus 20$, the Σ can couple to two F's as

$$F^\dagger_{ij} \Sigma^j_k F^{ki}, \tag{5.35}$$

while the term coming from the $6 \otimes 6$ product is forbidden by the $3B + L$ symmetry. The field Σ performs the breaking step $SU(4)_\mathrm{c} \to SU(3)_\mathrm{c} \times U(1)_{B-L}$ if it acquires a v.e.v. with structure

$$\begin{pmatrix} v_\Sigma & 0 & 0 & 0 \\ 0 & v_\Sigma & 0 & 0 \\ 0 & 0 & v_\Sigma & 0 \\ 0 & 0 & 0 & -3v_\Sigma \end{pmatrix}. \tag{5.36}$$

Plugging Equation (5.36) into Equation (5.35) gives

$$2v_\Sigma (F^{\overline{3}\dagger\alpha} F^{\overline{3}}_\alpha - F^{3\dagger}_\alpha F^{3\alpha}). \tag{5.37}$$

From Equation (5.37) we see that, depending on the value of the $\Sigma F^\dagger F$ coupling, the PS breaking can lead to a significant splitting of the 3 and $\overline{3}$ masses. We will consider the case in which the splitting implies a light 3 component and a heavy $\overline{3}$ component, suppressing the quark-quark interactions and hence the FCNCs. Under this assumption, we will fit the Yukawas to the F^3-mediated processes only.

Let us summarise the content of this section. We showed that two copies of the scalar leptoquark Δ arise naturally as a completion of the SM Higgs representation in an $SO(10)$ GUT having as intermediate breaking step the PS group. In addition, we deduced the relations arising among the couplings of this particle from the underlying PS structure. We commented on which discrete symmetry is allowed by the $SO(10)$ structure and determined the relations that this symmetry imposes on the couplings. We showed that without any additional constraints the two scalar LQs contribute to proton decay, but that the contributions vanish at all orders if the model respects an additional global symmetry coinciding with the $3B + L$ number. Finally, we showed that the two LQs can receive a mass splitting at the PS breaking scale.

5.2 Scalar leptoquark solution to $\mathcal{R}(D^{(*)})$ within Pati-Salam

In this final section we put together the analysis of Chapter 4 and the discussion of the PS scalar sector, and perform a fit of the LQ parameters within an $SO(10)$-inspired PS model. All the phenomenological aspects, such as the way of including the different flavour observables, as well as the statistical approach, are analogous to Chapter 4. Before displaying the results of the analysis, let us summarise our assumptions as well as constraints from the PS structure.

- We assume the mass splitting of the 3 and $\overline{3}$ components of F originating at the PS breaking scale to be such that the quark-quark interactions are negligible.
- We assume a mass of the lighter LQ of $M_\Delta = M_{F^3} = 1\,\mathrm{TeV}$.

- The PS structure requires symmetric Yukawa couplings.
- The (optional) discrete symmetry $\mathcal{C}$ requires the left- and right-handed Yukawa couplings to be equal up to a hermitian conjugation, $A = B^\dagger$.

We performed the analysis with or without the inclusion of the LFU ratios and of Δa_μ, resulting in effects analogous to the inclusion of these observables in the fits discussed in Chapter 4. Concerning the LFU ratios, this confirms the marginal effects of this LQ scenario on light meson decays. Concerning Δa_μ, this confirms that the PS scalar LQ cannot account simultaneously for the $\mathcal{R}(D^{(*)})$ and Δa_μ anomalies, as expected since this was already the case in the simplified scenarios, in which the set of independent parameters is larger. Since the focus of our work are the $\mathcal{R}(D^{(*)})$ anomalies, we will only discuss the fit without Δa_μ, putting ourselves in the case in which the experimental value of this observable gets closer to its SM prediction.

Due to the symmetry of the Yukawa matrices, the PS scalar LQ scenario without discrete symmetry requires the fitting of six independent couplings, which we assume to be real. The Yukawa matrices at the best-fit point are

$$y^L_{d\nu} = \begin{pmatrix} 0 & 0 & 0 \\ 0 & 7.2\times 10^{-4} & -1.5\times 10^{-2} \\ 0 & -1.5\times 10^{-2} & -2.0 \end{pmatrix}, \qquad y^R_{u\ell} = \begin{pmatrix} 0 & 0 & 0 \\ 0 & -3.3\times 10^{-4} & 4.1\times 10^{-4} \\ 0 & 4.1\times 10^{-4} & 2.5\times 10^{-3} \end{pmatrix},$$

$$y^L_{u\ell} = V^*_{\text{CKM}} y^L = \begin{pmatrix} 0 & 1.4\times 10^{-4} + i5.5\times 10^{-5} & (-5.8 + i7.3)\times 10^{-3} \\ 0 & 9.2\times 10^{-5} & -9.7\times 10^{-2} \\ 0 & -1.5\times 10^{-2} & -2.0 \end{pmatrix}, \tag{5.38}$$

where $\chi^2_{\text{min}} = 10$, which corresponds for $N_{\text{obs}} = 12$ and $N_{\text{par}} = 6$ to a p-value of 13%.

With the inclusion of the discrete symmetry, the parameters to fit are three, and the Yukawas at the best-fit point are

$$y^L_{d\nu} = y^R_{u\ell} = \begin{pmatrix} 0 & 0 & 0 \\ 0 & -2.3\times 10^{-3} & -3.6\times 10^{-3} \\ 0 & -3.6\times 10^{-3} & -1.8 \end{pmatrix},$$

$$y^L_{u\ell} = V^*_{\text{CKM}} y^L = \begin{pmatrix} 0 & -8.1\times 10^{-4} + i1.4\times 10^{-6} & (-2.2 + i6.7)\times 10^{-3} \\ 0 & -3.6\times 10^{-3} & 7.6\times 10^{-2} \\ 0 & -2.4\times 10^{-4} & -1.8 \end{pmatrix}, \tag{5.39}$$

with $\chi_{\text{min}} = 13$ and $N_{\text{par}} = 3$, corresponding to a p-value of 15%.

The pulls of the observables at the best-fit points are visualised in Figure 5.6, the red and blue bars refer to the $\not{\mathcal{C}}$ and $\mathcal{C}$ scenarios respectively. This plot shows that the LQ scenario, when embedded within an $SO(10)$-inspired PS model without discrete symmetry, still allows the description of the $\mathcal{R}(D^{(*)})$ data, as well as improving in the description of the coupling of Z bosons with τ leptons. On the other hand, imposing the discrete symmetry worsens the agreement with both $\mathcal{R}(D^{(*)})$, although reducing the tension with the experimental

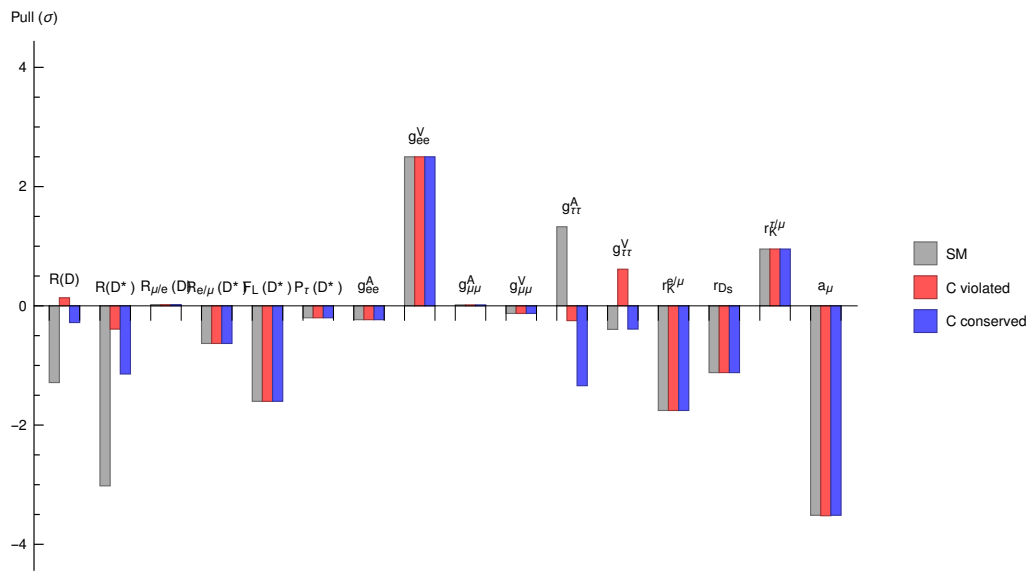

Figure 5.6: Pulls at the best-fit points of the Pati-Salam scalar leptoquark scenarios without and with $\mathcal{C}$ symmetry.

values compared to the SM, and the $Z\tau\tau$.

5.3 Summary

This chapter analysed to which extent the $\mathcal{R}(D^{(*)})$ anomalies can be regarded as a hint of the presence of a PS model as extension of the SM. After reviewing the features of the PS model, we first focused on the contributions of gauge bosons to $b \to c\tau\nu$ transitions, showing that the limits from LFV decays of light mesons exclude the possibility of solving the $\mathcal{R}(D^{(*)})$ anomalies with the PS gauge sector. We then moved to the analysis of the scalar sector, assuming the scalar sector of Reference [129], needed to perform the SSB of PS to the SM with intermediate steps. We showed that of these particles the only one mediating $b \to c\tau\nu$ transitions is the charged Higgs from the bi-doublet which includes the SM Higgs, and in the hypothesis of a low value of $\mathrm{BR}(B_c \to \tau\nu_\tau)$ we neglected this solution of the $\mathcal{R}(D^{(*)})$ anomalies. We then extended the PS scalar content by assuming PS to be an intermediate step in the SSB of a GUT with gauge group $SO(10)$. We analysed the consequences that this assumption has on the symmetry of the model and on its particle content, showing that under this assumption the model features two scalar LQs transforming as the one analysed in Chapter 4. We showed that, without any further assumption, these particles mediate proton decay, and that these effects vanish at all orders if one introduces an additional symmetry. We showed that the two LQs can receive a mass splitting at the PS breaking scale. Under the assumption that only the LQ mediating $b \to c\tau\nu$ remains light, we performed a fit of the observables modified by this particle, showing that in the PS scenario without the discrete left-right symmetry the particle is able to improve on the agreement

with data from both $\mathcal{R}(D^{(*)})$ and the $Z\tau\tau$ coupling. Requiring the discrete symmetry, which within $SO(10)$-inspired models is necessarily a generalised charge conjugation $\mathcal{C}$, worsens the agreement of both $\mathcal{R}(D^{(*)})$ and the $Z\tau\tau$ coupling compared to the PS scenario without this symmetry, but still implies a better description of the $\mathcal{R}(D^{(*)})$ ratios compared to the SM.

CHAPTER 6

Conclusion

> "It didn't work for them or me,
> But all concerned were nearer thus
> (Or so we thought) to all the fuss
> Than if we'd missed it separately. "
>
> *Philip Larkin,*
> *Sympathy in White Major (1967)*

To date, our investigation of the interactions among elementary particles indicate that the Standard Model provides an adequate description up to the energy probed at colliders. However, there are arguments indicating that the SM might be just the effective description of a theory valid in regimes that are not yet directly explored. If this is the case, we would expect the emergence of this theory as a discrepancy between the SM prediction and the experimental value of low energy observables as well, when these are measured with enough precision. This is the pattern that seems to be emerging for decays of mesons containing a b quark, for which several observables are in tension with their SM prediction. If these disagreements are confirmed when the experimental precision is increased, the natural question arising is what kind of new physics they have to be attributed to.

In this thesis we addressed this question with respect to the decays $B \to D^{(*)}\ell\nu$, for which the experimental value of the ratios $\mathcal{R}(D^{(*)})$, testing lepton flavour universality, are in tension with the SM predictions. Assuming that these anomalies are due to a NP particle with mass at the TeV scale, we used the tool of effective field theory, focusing on the data on $b \to c\tau\nu$ transitions, to infer which particle representation is more likely to be responsible for the observed discrepancies. Two interesting aspects emerge from our analysis: first of all, that if NP effects in the meson decays $B \to D^{(*)}\tau\nu$ enhance the $\mathcal{R}(D^{(*)})$ ratios with respect to the SM, as currently indicated by the experimental data, an analogous

enhancement is present in the corresponding baryon decay $\Lambda_b \to \Lambda_c \tau\nu$. To a very good approximation, this enhancement does not depend on the type of NP responsible for the anomalies, hence suggesting a measurement of $\mathcal{R}(\Lambda_c)$ as unambiguous check of whether the deviations observed in $\mathcal{R}(D^{(*)})$ are due to NP. In addition, our analysis indicates that a precise measurement of the angular distribution of the final state particles of the $B \to D^{(*)}\ell\nu$ decays, as well as a measurement of the branching ratio $\mathrm{BR}(B_c \to \tau\nu_\tau)$, will give clear indication on which particle is mediating the decay.

Although the EFT analysis constitutes a powerful model-independent tool for distinguishing NP mediators, even when the angular observables and $\mathrm{BR}(B_c \to \tau\nu_\tau)$ will allow for a ranking of NP solutions to the $\mathcal{R}(D^{(*)})$ anomalies there will still be open aspects to address. First of all, the sole fit of the $b \to c\tau\nu$ effective coupling does not allow to constrain all the parameters of the additional NP particle. A further step in this direction can be done with the use of a simplified model introducing a Lagrangian for the additional field including all the possible terms allowed by the SM symmetries, and then constraining the parameters with the data at our disposal. We performed this analysis for one of the scenarios favoured by the $b \to c\tau\nu$ effective analysis, the scalar leptoquark Δ transforming under the SM gauge group as $(3, 1, -1/3)$. Our analysis was performed reconsidering the effects of the LQ on the coupling of the Z gauge boson to charged leptons, with the novel inclusion of the $SU(2)$-related terms from the coupling to the photon and to the W boson. Even restricting the parameter space to the ones required for the $b \to c\tau\nu$ transition, the introduction of this scalar LQ allows for a better simultaneous description of the $\mathcal{R}(D^{(*)})$ ratios and of the Z coupling to τ leptons. If one relaxes the requirement of having as only nonvanishing couplings those required to address the anomalous ratios via an enhancement of the τ channel, a plethora of additional flavour observables are to be taken into account. We performed this analysis, which pointed out that once one allows for couplings to second and third generation fermions, the scalar LQ improves not only on the description of the $\mathcal{R}(D^{(*)})$ ratios and of the Z coupling to τ leptons, but also of the coupling of Z to electrons. The latter effect comes uniquely from the $SU(2)$-related effects on the W coupling, and had hence been previously neglected.

Simplified models allow for an improvement with respect to the EFT description, but they still lack an important aspect, which is the interpretation of the additional particle in terms of a bigger picture motivated by the need to address other open questions of the SM. Among the extensions of the SM, models with extended gauge symmetries and, more specifically, grand unified theories are often studied. We chose to analyse the $\mathcal{R}(D^{(*)})$ anomalies within the Pati-Salam model, which extends the SM gauge group in a way to unify quarks and leptons in the same representation. The model also provides an explanation to the quantisation of the electric charge, and can be regarded as an intermediate step in the spontaneous symmetry breaking of a GUT based on $SO(10)$. We first analysed the contributions coming from the gauge sector. We pointed out that, although the model provides a vector LQ U_1 which is a viable candidate as a solution to the $\mathcal{R}(D^{(*)})$ anomalies, the underlying PS structure relates the couplings for both $b \to c\tau\nu$ and for lepton flavour violating decays such as $K \to \mu e$ to the $SU(3)_\mathrm{c}$ coupling of the SM, hence allowing to directly relate the experimental values to the mass of the particle. Requiring the branching ratio for LFV decays to be consistent with the current experimental bounds sets a lower limit on the mass of U_1 which is three orders of magnitudes above the mass required for

resolving the tension in the $\mathcal{R}(D^{(*)})$ ratios. Unless one requires an accurate fine-tuning of the flavour structure in the PS model, this excludes the possibility that a U_1 solution to the $\mathcal{R}(D^{(*)})$ anomalies comes from the PS model. We then analysed the scalar sector under the additional assumption that PS is an intermediate step in the breaking of an $SO(10)$ GUT. Under this assumption, the model features the presence of two scalar LQs transforming as the one considered in the simplified analysis. After the introduction of an additional symmetry needed to stabilise the proton at all orders, only one of these LQs contributes to the $b \to c\ell\nu$ transitions of interest for us, while the effects of the other scalar can be neglected in light of a mass splitting occurring at the PS breaking scale. We reanalysed the scenario with the scalar LQ with the additional structure required by the $SO(10)$-inspired PS model, showing that the particle is able to address the $\mathcal{R}(D^{(*)})$ anomalies, and simultaneously improve on the description of the Z couplings to τ leptons, only if the model at the PS scale does not respect the discrete symmetry that exchanges the left and the right sectors. Imposing this symmetry still allows for an improvement on the $\mathcal{R}(D^{(*)})$ ratios, but to a lesser extent.

The anomalies in the $b \to c\ell\nu$ transitions will be probed soon to a better precision at Belle II. Meanwhile, the task for theorists that we addressed in this thesis is to get ready to interpret a possible confirmation of these anomalies, in order to shed light on the structure of the underlying NP and identify correlated ways of testing it.

APPENDIX A

Technical details about the $B \to D^{(*)}\ell\nu$ observables

In this Appendix we collect the expressions for the observables related to $B \to D^{(*)}\ell\nu$ decays, as well as review how to obtain them. We follow the treatment and notation of References [40, 65, 98, 142].

A.1 Helicity amplitudes

For the three-body decays $B \to D^{(*)}\ell\nu$, the differential decay rate is given by

$$\mathrm{d}\Gamma^{\lambda_\ell}_{\lambda_{D^{(*)}}} = \frac{1}{2m_B}\left|\sum_{i=V,SL,SR,T} \mathcal{M}_i^{\lambda_\ell\lambda_{D^{(*)}}}(q^2, \cos\theta_\ell)\right|^2 \mathrm{d}\Phi_3, \tag{A.1}$$

where λ_ℓ is the helicity of the charged lepton, $\lambda_D = s$ labels the decay rate and amplitudes of $B \to D\ell\nu$ and $\lambda_{D^*} = \pm 1, 0$ labels the helicity of D^* defined in the B rest frame. θ_ℓ is the angle between the momentum of the ℓ lepton and that of the $D^{(*)}$ meson in the rest frame of the dilepton, as depicted in Figure 3.1. The index i labels the contribution of each effective operator from Equation (3.5). The three-body phase-space is given by

$$\mathrm{d}\Phi_3 = \frac{\sqrt{Q_+Q_-}}{256\pi^3 m_B^2}\left(1 - \frac{m_\ell^2}{m_B^2}\right)\mathrm{d}q^2\mathrm{d}\cos\theta_\ell, \tag{A.2}$$

with $Q_\pm = (m_B \pm m_{D^{(*)}})^2 - q^2$. which allows to obtain the decay rate for a specific polarisation of the ℓ or of the D^*, after summing over the possible contribution and integrating

over $dq^2 \mathrm{d}\cos\theta_\ell$. Explicitly

$$\begin{aligned} \Gamma(B \to D\tau^{\lambda=\pm 1/2}\nu) &= \Gamma_s^{\pm}, \qquad \Gamma(B \to D^*\tau^{\lambda=\pm 1/2}\nu) = \sum_{\lambda_{D^*}=\pm 1,0} \Gamma_{\lambda_{D^*}}^{\pm}, \\ \Gamma(B \to D_T^*\tau\nu) &= \sum_{\lambda_\ell=\pm} \Gamma_0^{\lambda_\ell}, \qquad \Gamma(B \to D_L^*\tau\nu) = \sum_{\lambda_\ell=\pm} \sum_{\lambda_{D^*}=\pm 1} \Gamma_{\lambda_{D^*}}^{\lambda_\ell}. \end{aligned} \tag{A.3}$$

The amplitude for the decay $B \to D^{(*)}\ell\nu$ can be rewritten with the use of helicity amplitudes, which allow to separate the leptonic and the hadronic transitions. The former can easily be evaluated, while the latter can be parametrised in terms of form factors. The separation is achieved by rewriting the metric tensor(s) $g_{\mu\nu}$ in terms of a sum over polarisation vectors of a virtual vector boson. This substitution reads

$$g_{\mu\nu} \to \sum_{\lambda=\pm,0,s} \eta_\lambda \epsilon_\mu^*(\lambda)\epsilon_\nu(\lambda), \tag{A.4}$$

where $\eta_{\pm,0} = 1, \eta_s = -1$ is the metric factor and the polarisation vectors are given by

$$\epsilon_\mu(\pm) = \frac{1}{\sqrt{2}} \begin{pmatrix} 0 \\ \pm 1 \\ -i \\ 0 \end{pmatrix}, \qquad \epsilon_\mu(0) = \frac{1}{\sqrt{q^2}} \begin{pmatrix} |\boldsymbol{q}| \\ 0 \\ 0 \\ -q_0 \end{pmatrix}, \qquad \epsilon_\mu(s) = \frac{1}{\sqrt{q^2}} \begin{pmatrix} q_0 \\ 0 \\ 0 \\ -|\boldsymbol{q}| \end{pmatrix}, \tag{A.5}$$

where q_0 and $|\boldsymbol{q}|$ are the energy and momentum of the virtual vector boson in the B rest frame, and $q^2 = q_0^2 - \boldsymbol{q}^2$. With the effective couplingsin Equation (3.5), the amplitude for $B \to D^{(*)}\ell\nu$ can be written as[1]

$$\mathcal{M}^{\lambda_\ell\lambda_{D^{(*)}}} = \mathcal{M}_{\mathrm{SM}}^{\lambda_\ell\lambda_{D^{(*)}}} + \mathcal{M}_V^{\lambda_\ell\lambda_{D^{(*)}}} + \mathcal{M}_{SL}^{\lambda_\ell\lambda_{D^{(*)}}} + \mathcal{M}_{SR}^{\lambda_\ell\lambda_{D^{(*)}}} + \mathcal{M}_T^{\lambda_\ell\lambda_{D^{(*)}}}. \tag{A.6}$$

Separating the contributions of each effective operator and using the substitution of Equation (A.4) for all the metric tensors, we can separate the leptonic and the hadronic ampli-

[1] We are assuming the flavour of the neutrino to be aligned with the one produced in a $\ell\nu W$ vertex.

tudes as

$$
\begin{aligned}
\mathcal{M}_V^{\lambda_\ell \lambda_{D^{(*)}}} =& \frac{G_F}{\sqrt{2}} V_{cb} C_V^L g^{\mu\nu} \langle \ell(p_\ell, \lambda_\ell)\overline{\nu}(p_\nu)| \, \overline{\ell}\gamma_\mu(1-\gamma_5)\nu \, |0\rangle \, \langle D^{(*)}(p_{D^{(*)}}, \lambda_{D^{(*)}})| \, \overline{c}\gamma_\nu(1-\gamma_5)b \, |\overline{B}(p_B)\rangle \\
=& \frac{G_F}{\sqrt{2}} V_{cb} C_V^L \sum_{\lambda=\pm,0,s} \eta_\lambda H_{V,\lambda} L_\lambda^{\lambda_\ell}, \\
\mathcal{M}_{SL}^{\lambda_\ell \lambda_{D^{(*)}}} =& \frac{G_F}{\sqrt{2}} V_{cb} C_S^L \, \langle \ell(p_\ell, \lambda_\ell)\overline{\nu}(p_\nu)| \, \overline{\ell}(1-\gamma_5)\nu \, |0\rangle \, \langle D^{(*)}(p_{D^{(*)}}, \lambda_{D^{(*)}})| \, \overline{c}(1-\gamma_5)b \, |\overline{B}(p_B)\rangle \\
=& -\frac{G_F}{\sqrt{2}} V_{cb} C_S^L H_{SL} L^{\lambda_\ell}, \\
\mathcal{M}_{SR}^{\lambda_\ell \lambda_{D^{(*)}}} =& \frac{G_F}{\sqrt{2}} V_{cb} C_S^R \, \langle \ell(p_\ell, \lambda_\ell)\overline{\nu}(p_\nu)| \, \overline{\ell}(1-\gamma_5)\nu \, |0\rangle \, \langle D^{(*)}(p_{D^{(*)}}, \lambda_{D^{(*)}})| \, \overline{c}(1+\gamma_5)b \, |\overline{B}(p_B)\rangle \\
=& -\frac{G_F}{\sqrt{2}} V_{cb} C_S^R H_{SR} L^{\lambda_\ell}, \\
\mathcal{M}_T^{\lambda_\ell \lambda_{D^{(*)}}} =& \frac{G_F}{\sqrt{2}} V_{cb} C_T g^{\mu\nu} g^{\rho\sigma} \, \langle \ell(p_\ell, \lambda_\ell)\overline{\nu}(p_\nu)| \, \overline{\ell}\sigma_{\mu\rho}(1-\gamma_5)\nu \, |0\rangle \, \langle D^{(*)}(p_{D^{(*)}}, \lambda_{D^{(*)}})| \, \overline{c}\sigma_{\nu\sigma}(1-\gamma_5)b \, |\overline{B}(p_B)\rangle \\
=& -\frac{G_F}{\sqrt{2}} V_{cb} C_T \sum_{\lambda,\lambda'=\pm,0,s} H_{T,\lambda\lambda'} L_{\lambda\lambda'}^{\lambda_\ell},
\end{aligned}
\tag{A.7}
$$

with leptonic amplitudes

$$
\begin{aligned}
L_\lambda^{\lambda_\ell} =& \epsilon^\mu(\lambda) \, \langle \ell(p_\ell, \lambda_\ell)\overline{\nu}(p_\nu)| \, \overline{\ell}\gamma_\mu(1-\gamma_5)\nu \, |0\rangle \, , \\
L^{\lambda_\ell} =& \langle \ell(p_\ell, \lambda_\ell)\overline{\nu}(p_\nu)| \, \overline{\ell}(1-\gamma_5)\nu \, |0\rangle \, , \\
L_{\lambda\lambda'}^{\lambda_\ell} =& -i\epsilon^\mu(\lambda)\epsilon^\rho(\lambda') \, \langle \ell(p_\ell, \lambda_\ell)\overline{\nu}(p_\nu)| \, \overline{\ell}\sigma_{\mu\rho}(1-\gamma_5)\nu \, |0\rangle \, ,
\end{aligned}
\tag{A.8}
$$

and hadronic amplitudes for $B \to D\ell\nu$

$$\begin{aligned}
H_{V,\lambda}^{\lambda_{D^{(*)}}} &= \epsilon^{*\nu}(\lambda) \langle D(p_{D^{(*)}}, \lambda_{D^{(*)}}) | \, \overline{c}\gamma_\nu(1-\gamma_5)b \, | \overline{B}(p_B) \rangle \, , \\
H_{SL}^{\lambda_{D^{(*)}}} &= \langle D(p_{D^{(*)}}, \lambda_{D^{(*)}}) | \, \overline{c}(1-\gamma_5)b \, | \overline{B}(p_B) \rangle \, , \\
H_{SR}^{\lambda_{D^{(*)}}} &= \langle D(p_{D^{(*)}}, \lambda_{D^{(*)}}) | \, \overline{c}(1+\gamma_5)b \, | \overline{B}(p_B) \rangle \, , \\
H_{T,\lambda}^{\lambda_{D^{(*)}}} &= i\epsilon^{*\nu}\epsilon^{*\sigma}(\lambda) \langle D(p_{D^{(*)}}, \lambda_{D^{(*)}}) | \, \overline{c}\sigma_{\nu\sigma}(1-\gamma_5)b \, | \overline{B}(p_B) \rangle \, .
\end{aligned} \tag{A.9}$$

The leptonic amplitudes are functions of q^2, θ_ℓ and can be calculated with the usual QFT techniques, writing down the spinors in the $q^2 = 0$ reference frame. The hadronic amplitudes are functions of q^2 only, and cannot be evaluated perturbatively.

A.2 Form factors

In this section we summarise our choice of form factors for $B \to D^{(*)}\ell\nu$.

A.2.1 $B \to D\ell\nu$

The hadronic amplitudes for $B \to D\ell\nu$ can be rewritten in terms of the form factors $F_{0,1,T}(q^2)$, as in Equation (11) of Reference [98]. For the scalar (F_0) and vector (F_1) form factors we use the results from Reference [8], in which the BGL parametrisation [143][2] is fitted to lattice data points. For the tensor form factor (F_T), we use the ratio F_T/F_1 from Reference [10], which makes use of HQET up to order (Λ_{QCD}) and (α_s) to parametrise the form factors for both $B \to D^{(*)}\ell\nu$. We use the fit results in which the parameters are constrained by QCD sum rules and only lattice points are used for the fitting.

A.2.2 $B \to D^*\ell\nu$

The hadronic amplitudes for $B \to D^*\ell\nu$ can be rewritten in terms of the form factors $A_{0,1,2}(q^2), V(q^2), T_{1,2,3}(q^2)$. For $A_{1,2}(q^2), V(q^2)$ we use the result of Reference [12], where the CLN parametrisation[3] is fitted to $B \to D^*e\nu$ and $B \to D^*\mu\nu$ data. For $A_0, T_{1,2,3}$, as for F_T, we take the fit of the ratios $A_0, T_{1,2,3}/A1$ from Reference [10], in which the (Λ_{QCD}), (α_s) parametrisation is fitted to lattice points with constraints from QCD sum rules.

[2]This parametrisation is based on dispersion relations and unitarity conditions, and does not make use of HQET.

[3]This parametrisation is based on dispersion relations, unitarity conditions and makes use of HQET.

APPENDIX B

Summary of $b \to s\ell\ell$ data

In this Appendix we analyse some aspects of the data on $b \to s\ell\ell$ transitions, reviewing why this transition gained interest as a channel displaying the presence of NP. Then, following References [56, 95, 128], we review the interpretation of these data in terms of an EFT describing NP effects.

The decay $b \to s\ell\ell$ is mediated by a FCNC. Since FCNCs are suppressed in the SM, this decay constitutes a good channel for probing the presence of NP. When considered in bound states, this quark-level process mediates the decays $B \to K^{(*)}\ell\ell$. The interest in these decays increased when the authors of References [144–146] proposed for the decay $B \to K^*\ell\ell$ a set of *optimized* observables, as a compromise between the accessibility at experiments and the cleanness of their SM theoretical prediction, originating from the reduced dependence on the form factors. When these observables were measured by the LHCb Collaboration [147], the channel with muons displayed some deviations with respect to the SM predictions, the largest one appearing for the q^2 bins of the so-called P_5' angular observable. The global analysis of $b \to s\mu\mu$ data performed in Reference [148] first pointed out that these discrepancies were consistent with a simple NP pattern, as we now briefly explain.

The global analysis is performed by parametrising the short-distance SM and NP contributions via the WCs $\mathcal{C}_i = \mathcal{C}_i^{\rm SM} + \mathcal{C}_i^{\rm NP}$, where the index i labels the coefficients of the following tensorial structures

$$\begin{aligned} O_7^{(\prime)} &= \tfrac{e}{16\pi^2} m_b \left(\bar{s}\sigma_{\mu\nu}P_{\rm R(L)}b\right) F^{\mu\nu}, \\ O_9^{(\prime)} &= \tfrac{e^2}{16\pi^2} \left(\bar{s}\gamma_\mu P_{\rm L(R)}b\right) \left(\bar{\mu}\gamma^\mu\mu\right), \\ O_{10}^{(\prime)} &= \tfrac{e^2}{16\pi^2} \left(\bar{s}\gamma_\mu P_{\rm L(R)}b\right) \left(\bar{\mu}\gamma^\mu\gamma_5\mu\right). \end{aligned} \tag{B.1}$$

The only nonnegligible SM effects arise in the WCs $(C_7^{\rm SM}, C_9^{\rm SM}, C_{10}^{\rm SM}) = (-0.29, 4.07, -4.31)$,

where the values are given at the factorisation scale $\mu_b = 4.8\,\text{GeV}$. The authors performed a fit of the NP part of the WCs, including the optimised observables for $B \to K^*\mu\mu$ as well as data from radiative and dileptonic B decays with muons in the final state, and considering separately scenarios with one or two nonvanishing WCs. These fits all showed a preference of the data for the scenarios with a nonvanishing $\mathcal{C}_9^{\text{NP}} \simeq -1$, relatively large and with opposite sign compared to the corresponding SM part $\mathcal{C}_9^{\text{SM}} = 4.07$.

Later on, the data on the $b \to s\ell\ell$ attracted even more attention due to the tension in the LFU ratios

$$\mathcal{R}(K^{(*)}) \equiv \frac{\text{BR}(B \to K^{(*)}\mu\mu)}{\text{BR}(B \to K^{(*)}ee)}, \tag{B.2}$$

whose SM prediction is also particularly clean due to the reduced dependence on the form factors. The most striking discrepancies appeared in some of the bins of the dilepton invariant mass q^2, expressed in GeV. For these bins, the SM predictions give [149, 150]

$$\begin{aligned} \mathcal{R}_{\text{SM}}^{[1.1,6.0]}(K) &= 1.00 \pm 0.01, \\ \mathcal{R}_{\text{SM}}^{[0.045,1.1]}(K^*) &= 0.92 \pm 0.02, \\ \mathcal{R}_{\text{SM}}^{[1.1,6.0]}(K^*) &= 1.00 \pm 0.01, \end{aligned} \tag{B.3}$$

while the results from Belle [151] and LHCb [152, 153] give

$$\begin{aligned} \mathcal{R}_{\text{LHCb}}^{[1.1,6.0]}(K) &= 0.846^{+0.060+0.016}_{-0.054-0.014}, \\ \mathcal{R}_{\text{LHCb}}^{[0.045,1.1]}(K^*) &= 0.66^{+0.11}_{-0.07} \pm 0.03, \qquad \mathcal{R}_{\text{Belle}}^{[0.045,1.1]}(K^*) = 0.90^{+0.27}_{-0.21} \pm 0.10, \\ \mathcal{R}_{\text{LHCb}}^{[1.1,6.0]}(K^*) &= 0.69^{+0.11}_{-0.07} \pm 0.05, \qquad \mathcal{R}_{\text{Belle}}^{[1.1,6.0]}(K^*) = 1.18^{+0.52}_{-0.32} \pm 0.10. \end{aligned} \tag{B.4}$$

The tension between the SM predictions and the experimental values is consistent with the picture of a nonvanishing LFNU contribution to the WC C_9 for the muon channel [95, 128].

The latest global fit to $b \to s\ell\ell$ observables [128] identifies several patterns of NP that are preferred by the data, also exploring the possibility of LFNU effects accompanied by universal ones. Of all the scenarios analysed in this reference, the one relevant for the analysis performed in Chapter 4 is the two-dimensional scenario with nonvanishing WC for the muon channel $\left(\mathcal{C}_{9(\mu)}^{\text{NP}}, \mathcal{C}_{10(\mu)}^{\text{NP}}\right)$, for which the best-fit point is at $(-0.91, 0.18)$, with a p-value of 68.7%.

Bibliography

[1] M. Blanke, A. Crivellin, S. de Boer, M. Moscati, U. Nierste, I. Nišandžić, and T. Kitahara, "Impact of polarization observables and $B_c \to \tau\nu$ on new physics explanations of the $b \to c\tau\nu$ anomaly," *Phys. Rev.* **D99** (2019) 075006, `arXiv:1811.09603 [hep-ph]`.

[2] M. Blanke, A. Crivellin, T. Kitahara, M. Moscati, U. Nierste, and I. Nišandžić, "Addendum to "Impact of polarization observables and $B_c \to \tau\nu$ on new physics explanations of the $b \to c\tau\nu$ anomaly"," *Phys. Rev.* **D100** no. 3, (2019) 035035, `arXiv:1905.08253 [hep-ph]`.

[3] Y. Grossman, "Introduction to flavor physics," in *Flavianet School on Flavour Physics Karlsruhe, Germany, September 7-18, 2009*, pp. 111–144. 2014. `arXiv:1006.3534 [hep-ph]`. [,73(2014)].

[4] S. Fajfer, J. F. Kamenik, and I. Nišandžić, "On the $B \to D^* \tau \bar{\nu}_\tau$ Sensitivity to New Physics," *Phys. Rev.* **D85** (2012) 094025, `arXiv:1203.2654 [hep-ph]`.

[5] D. Bigi and P. Gambino, "Revisiting $B \to D\ell\nu$," *Phys. Rev.* **D94** no. 9, (2016) 094008, `arXiv:1606.08030 [hep-ph]`.

[6] **MILC** Collaboration, J. A. Bailey *et al.*, "$B \to D\ell\nu$ form factors at nonzero recoil and —V_{cb}— from 2+1-flavor lattice QCD," *Phys. Rev.* **D92** no. 3, (2015) 034506, `arXiv:1503.07237 [hep-lat]`.

[7] **HPQCD** Collaboration, H. Na, C. M. Bouchard, G. P. Lepage, C. Monahan, and J. Shigemitsu, "$B \to Dl\nu$ form factors at nonzero recoil and extraction of $|V_{cb}|$," *Phys. Rev.* **D92** no. 5, (2015) 054510, `arXiv:1505.03925 [hep-lat]`. [Erratum: Phys. Rev.D93,no.11,119906(2016)].

[8] S. Aoki *et al.*, "Review of lattice results concerning low-energy particle physics," *Eur. Phys. J.* **C77** no. 2, (2017) 112, `arXiv:1607.00299 [hep-lat]`.

[9] D. Bigi, P. Gambino, and S. Schacht, "$R(D^*)$, $|V_{cb}|$, and the Heavy Quark Symmetry relations between form factors," *JHEP* **11** (2017) 061, `arXiv:1707.09509 [hep-ph]`.

[10] F. U. Bernlochner, Z. Ligeti, M. Papucci, and D. J. Robinson, "Combined analysis of semileptonic B decays to D and D^*: $R(D^{(*)})$, $|V_{cb}|$, and new physics," *Phys. Rev.* **D95** no. 11, (2017) 115008, `arXiv:1703.05330 [hep-ph]`. [Erratum: Phys. Rev.D97,no.5,059902(2018)].

[11] S. Jaiswal, S. Nandi, and S. K. Patra, "Extraction of $|V_{cb}|$ from $B \to D^{(*)}\ell\nu_\ell$ and the Standard Model predictions of $R(D^{(*)})$," *JHEP* **12** (2017) 060, `arXiv:1707.09977 [hep-ph]`.

[12] **HFLAV** Collaboration, Y. Amhis *et al.*, "Averages of b-hadron, c-hadron, and τ-lepton properties as of summer 2016," *Eur. Phys. J.* **C77** no. 12, (2017) 895, `arXiv:1612.07233 [hep-ex]`. Updated average of $R(D)$ and $R(D^*)$ for Spring 2019 at `https://hflav-eos.web.cern.ch/hflav-eos/semi/spring19/html/RDsDsstar/RDRDs.html`.

[13] **LHCb** Collaboration, R. Aaij *et al.*, "Measurement of the ratio of branching fractions $\mathcal{B}(\bar{B}^0 \to D^{*+}\tau^-\bar{\nu}_\tau)/\mathcal{B}(\bar{B}^0 \to D^{*+}\mu^-\bar{\nu}_\mu)$," *Phys. Rev. Lett.* **115** no. 11, (2015) 111803, `arXiv:1506.08614 [hep-ex]`. [Erratum: Phys. Rev. Lett.115,no.15,159901(2015)].

[14] **Belle** Collaboration, Y. Sato *et al.*, "Measurement of the branching ratio of $\bar{B}^0 \to D^{*+}\tau^-\bar{\nu}_\tau$ relative to $\bar{B}^0 \to D^{*+}\ell^-\bar{\nu}_\ell$ decays with a semileptonic tagging method," *Phys. Rev.* **D94** no. 7, (2016) 072007, `arXiv:1607.07923 [hep-ex]`.

[15] **Belle** Collaboration, S. Hirose *et al.*, "Measurement of the τ lepton polarization and $R(D^*)$ in the decay $\bar{B} \to D^*\tau^-\bar{\nu}_\tau$," *Phys. Rev. Lett.* **118** no. 21, (2017) 211801, `arXiv:1612.00529 [hep-ex]`.

[16] **LHCb** Collaboration, R. Aaij *et al.*, "Measurement of the ratio of the $B^0 \to D^{*-}\tau^+\nu_\tau$ and $B^0 \to D^{*-}\mu^+\nu_\mu$ branching fractions using three-prong τ-lepton decays," *Phys. Rev. Lett.* **120** no. 17, (2018) 171802, `arXiv:1708.08856 [hep-ex]`.

[17] **Belle** Collaboration, S. Hirose *et al.*, "Measurement of the τ lepton polarization and $R(D^*)$ in the decay $\bar{B} \to D^*\tau^-\bar{\nu}_\tau$ with one-prong hadronic τ decays at Belle," *Phys. Rev.* **D97** no. 1, (2018) 012004, `arXiv:1709.00129 [hep-ex]`.

[18] **LHCb** Collaboration, R. Aaij *et al.*, "Test of Lepton Flavor Universality by the measurement of the $B^0 \to D^{*-}\tau^+\nu_\tau$ branching fraction using three-prong τ decays," *Phys. Rev.* **D97** no. 7, (2018) 072013, `arXiv:1711.02505 [hep-ex]`.

[19] **Belle** Collaboration, A. Abdesselam *et al.*, "Measurement of $\mathcal{R}(D)$ and $\mathcal{R}(D^*)$ with a semileptonic tagging method," `arXiv:1904.08794 [hep-ex]`.

[20] **BaBar** Collaboration, J. P. Lees *et al.*, "Evidence for an excess of $\bar{B} \to D^{(*)}\tau^-\bar{\nu}_\tau$ decays," *Phys. Rev. Lett.* **109** (2012) 101802, `arXiv:1205.5442 [hep-ex]`.

[21] **BaBar** Collaboration, J. P. Lees *et al.*, "Measurement of an Excess of $\bar{B} \to D^{(*)}\tau^-\bar{\nu}_\tau$ Decays and Implications for Charged Higgs Bosons," *Phys. Rev.* **D88** no. 7, (2013) 072012, `arXiv:1303.0571 [hep-ex]`.

[22] **Belle** Collaboration, M. Huschle *et al.*, "Measurement of the branching ratio of $\bar{B} \to D^{(*)}\tau^-\bar{\nu}_\tau$ relative to $\bar{B} \to D^{(*)}\ell^-\bar{\nu}_\ell$ decays with hadronic tagging at Belle," *Phys. Rev.* **D92** no. 7, (2015) 072014, `arXiv:1507.03233 [hep-ex]`.

[23] M. Bordone, M. Jung, and D. van Dyk, "Theory determination of $\bar{B} \to D^{(*)}\ell^-\bar{\nu}$ form factors at $\mathcal{O}(1/m_c^2)$," `arXiv:1908.09398 [hep-ph]`.

[24] T. Kitahara, "Theory status and implications of $R(D^{(*)})$ and polarization observables." Talk at *18th International Conference on B-Physics at Frontier Machines (BEAUTY2019)*, Ljubljana, Slovenia, 3 Oct 2019, 2019.

[25] A. J. Buras, "Weak Hamiltonian, CP violation and rare decays," in *Probing the standard model of particle interactions. Proceedings, Summer School in Theoretical Physics, NATO Advanced Study Institute, 68th session, Les Houches, France, July 28-September 5, 1997. Pt. 1, 2*, pp. 281–539. 1998. `arXiv:hep-ph/9806471 [hep-ph]`.

[26] A. A. Petrov and A. E. Blechman, *Effective Field Theories*. WSP, 2016. `http://www.worldscientific.com/worldscibooks/10.1142/8619`.

[27] K. Melnikov, "Eft spring 2017." `https://sites.google.com/site/eftspring2017/lectures`. Lecture notes.

[28] **Belle** Collaboration, R. Glattauer *et al.*, "Measurement of the decay $B \to D\ell\nu_\ell$ in fully reconstructed events and determination of the Cabibbo-Kobayashi-Maskawa matrix element $|V_{cb}|$," *Phys. Rev.* **D93** no. 3, (2016) 032006, `arXiv:1510.03657 [hep-ex]`.

[29] **Belle** Collaboration, A. Abdesselam *et al.*, "Precise determination of the CKM matrix element $|V_{cb}|$ with $\bar{B}^0 \to D^{*+}\ell^-\bar{\nu}_\ell$ decays with hadronic tagging at Belle," `arXiv:1702.01521 [hep-ex]`.

[30] **Belle** Collaboration, A. Abdesselam *et al.*, "Measurement of CKM Matrix Element $|V_{cb}|$ from $\bar{B} \to D^{*+}\ell^-\bar{\nu}_\ell$," `arXiv:1809.03290 [hep-ex]`.

[31] **Particle Data Group** Collaboration, M. Tanabashi *et al.*, "Review of particle physics," *Phys. Rev. D* **98** (Aug, 2018) 030001. `https://link.aps.org/doi/10.1103/PhysRevD.98.030001`.

[32] **CMS** Collaboration, A. M. Sirunyan *et al.*, "Search for leptoquarks coupled to third-generation quarks in proton-proton collisions at $\sqrt{s} = 13$ TeV," *Phys. Rev. Lett.* **121** no. 24, (2018) 241802, `arXiv:1809.05558 [hep-ex]`.

[33] B. Grzadkowski, M. Iskrzynski, M. Misiak, and J. Rosiek, "Dimension-Six Terms in the Standard Model Lagrangian," *JHEP* **10** (2010) 085, `arXiv:1008.4884 [hep-ph]`.

[34] V. Cirigliano, J. Jenkins, and M. Gonzalez-Alonso, "Semileptonic decays of light quarks beyond the Standard Model," *Nucl. Phys.* **B830** (2010) 95–115, `arXiv:0908.1754 [hep-ph]`.

[35] R. Alonso, B. Grinstein, and J. Martin Camalich, "Lepton universality violation and lepton flavor conservation in B-meson decays," *JHEP* **10** (2015) 184, `arXiv:1505.05164 [hep-ph]`.

[36] O. Catà and M. Jung, "Signatures of a nonstandard Higgs boson from flavor physics," *Phys. Rev.* **D92** no. 5, (2015) 055018, `arXiv:1505.05804 [hep-ph]`.

[37] J. Aebischer, A. Crivellin, M. Fael, and C. Greub, "Matching of gauge invariant dimension-six operators for $b \to s$ and $b \to c$ transitions," *JHEP* **05** (2016) 037, `arXiv:1512.02830 [hep-ph]`.

[38] S. Fajfer, J. F. Kamenik, I. Nišandžić, and J. Zupan, "Implications of Lepton Flavor Universality Violations in B Decays," *Phys. Rev. Lett.* **109** (2012) 161801, `arXiv:1206.1872 [hep-ph]`.

[39] Y. Sakaki and H. Tanaka, "Constraints on the charged scalar effects using the forward-backward asymmetry on $B \to D^{(*)}\tau\overline{\nu}_\tau$," *Phys. Rev.* **D87** no. 5, (2013) 054002, `arXiv:1205.4908 [hep-ph]`.

[40] M. Tanaka and R. Watanabe, "New physics in the weak interaction of $\bar{B} \to D^{(*)}\tau\bar{\nu}$," *Phys. Rev.* **D87** no. 3, (2013) 034028, `arXiv:1212.1878 [hep-ph]`.

[41] D. Bečirević, N. Košnik, and A. Tayduganov, "$\bar{B} \to D\tau\bar{\nu}_\tau$ vs. $\bar{B} \to D\mu\bar{\nu}_\mu$," *Phys. Lett.* **B716** (2012) 208–213, `arXiv:1206.4977 [hep-ph]`.

[42] A. Datta, M. Duraisamy, and D. Ghosh, "Diagnosing New Physics in $b \to c\,\tau\,\nu_\tau$ decays in the light of the recent BaBar result," *Phys. Rev.* **D86** (2012) 034027, `arXiv:1206.3760 [hep-ph]`.

[43] M. Duraisamy and A. Datta, "The Full $B \to D^*\tau^-\bar{\nu_\tau}$ Angular Distribution and CP violating Triple Products," *JHEP* **09** (2013) 059, `arXiv:1302.7031 [hep-ph]`.

[44] R. Dutta, A. Bhol, and A. K. Giri, "Effective theory approach to new physics in $b \to u$ and $b \to c$ leptonic and semileptonic decays," *Phys. Rev.* **D88** no. 11, (2013) 114023, `arXiv:1307.6653 [hep-ph]`.

[45] M. Duraisamy, P. Sharma, and A. Datta, "Azimuthal $B \to D^*\tau^-\bar{\nu_\tau}$ angular distribution with tensor operators," *Phys. Rev.* **D90** no. 7, (2014) 074013, `arXiv:1405.3719 [hep-ph]`.

[46] Y. Sakaki, M. Tanaka, A. Tayduganov, and R. Watanabe, "Probing New Physics with q^2 distributions in $\bar{B} \to D^{(*)}\tau\bar{\nu}$," *Phys. Rev.* **D91** no. 11, (2015) 114028, `arXiv:1412.3761 [hep-ph]`.

[47] M. Freytsis, Z. Ligeti, and J. T. Ruderman, "Flavor models for $\bar{B} \to D^{(*)}\tau\bar{\nu}$," *Phys. Rev.* **D92** no. 5, (2015) 054018, `arXiv:1506.08896 [hep-ph]`.

[48] A. K. Alok, D. Kumar, S. Kumbhakar, and S. U. Sankar, "D^* polarization as a probe to discriminate new physics in $\bar{B} \to D^*\tau\bar{\nu}$," *Phys. Rev.* **D95** no. 11, (2017) 115038, `arXiv:1606.03164 [hep-ph]`.

[49] R. Alonso, A. Kobach, and J. Martin Camalich, "New physics in the kinematic distributions of $\bar{B} \to D^{(*)}\tau^-(\to \ell^-\bar{\nu}_\ell\nu_\tau)\bar{\nu}_\tau$," *Phys. Rev.* **D94** no. 9, (2016) 094021, `arXiv:1602.07671 [hep-ph]`.

[50] D. Bardhan, P. Byakti, and D. Ghosh, "A closer look at the R_D and R_{D^*} anomalies," *JHEP* **01** (2017) 125, `arXiv:1610.03038 [hep-ph]`.

[51] S. Bhattacharya, S. Nandi, and S. K. Patra, "Looking for possible new physics in $B \to D^{(*)}\tau\nu_\tau$ in light of recent data," *Phys. Rev.* **D95** no. 7, (2017) 075012, `arXiv:1611.04605 [hep-ph]`.

[52] A. Celis, M. Jung, X.-Q. Li, and A. Pich, "Scalar contributions to $b \to c(u)\tau\nu$ transitions," *Phys. Lett.* **B771** (2017) 168–179, `arXiv:1612.07757 [hep-ph]`.

[53] A. K. Alok, D. Kumar, J. Kumar, S. Kumbhakar, and S. U. Sankar, "New physics solutions for R_D and R_{D^*}," *JHEP* **09** (2018) 152, `arXiv:1710.04127 [hep-ph]`.

[54] R. Dutta, "Exploring R_D, R_{D^*} and $R_{J/\Psi}$ anomalies," `arXiv:1710.00351 [hep-ph]`.

[55] A. Azatov, D. Bardhan, D. Ghosh, F. Sgarlata, and E. Venturini, "Anatomy of $b \to c\tau\nu$ anomalies," `arXiv:1805.03209 [hep-ph]`.

[56] S. Bifani, S. Descotes-Genon, A. Romero Vidal, and M.-H. Schune, "Review of Lepton Universality tests in B decays," `arXiv:1809.06229 [hep-ex]`.

[57] Z.-R. Huang, Y. Li, C.-D. Lu, M. A. Paracha, and C. Wang, "Footprints of New Physics in $b \to c\tau\nu$ Transitions," `arXiv:1808.03565 [hep-ph]`.

[58] P. Asadi, M. R. Buckley, and D. Shih, "Asymmetry Observables and the Origin of $R_{D^{(*)}}$ Anomalies," `arXiv:1810.06597 [hep-ph]`.

[59] Q.-Y. Hu, X.-Q. Li, and Y.-D. Yang, "$b \to c\tau\nu$ Transitions in the Standard Model Effective Field Theory," `arXiv:1810.04939 [hep-ph]`.

[60] F. Feruglio, P. Paradisi, and O. Sumensari, "Implications of scalar and tensor explanations of $R_{D^{(*)}}$," `arXiv:1806.10155 [hep-ph]`.

[61] A. Angelescu, D. Bečirević, D. A. Faroughy, and O. Sumensari, "Closing the window on single leptoquark solutions to the B-physics anomalies," *JHEP* **10** (2018) 183, `arXiv:1808.08179 [hep-ph]`.

[62] S. Iguro, Y. Omura, and M. Takeuchi, "Test of the $R(D^{(*)})$ anomaly at the LHC," `arXiv:1810.05843 [hep-ph]`.

[63] S. Bhattacharya, S. Nandi, and S. Kumar Patra, "$b \to c\tau\nu_\tau$ Decays: A Catalogue to Compare, Constrain, and Correlate New Physics Effects," `arXiv:1805.08222 [hep-ph]`.

[64] J. Aebischer, J. Kumar, P. Stangl, and D. M. Straub, "A Global Likelihood for Precision Constraints and Flavour Anomalies," `arXiv:1810.07698 [hep-ph]`.

[65] D. Becirevic, S. Fajfer, I. Nisandzic, and A. Tayduganov, "Angular distributions of $\bar{B} \to D^{(*)}\ell\bar{\nu}_\ell$ decays and search of New Physics," `arXiv:1602.03030 [hep-ph]`.

[66] D. Bečirević, M. Fedele, I. Nišandžić, and A. Tayduganov, "Lepton Flavor Universality tests through angular observables of $\overline{B} \to D^{(*)}\ell\overline{\nu}$ decay modes," `arXiv:1907.02257 [hep-ph]`.

[67] **Belle** Collaboration, A. Abdesselam *et al.*, "Measurement of the D^{*-} polarization in the decay $B^0 \to D^{*-}\tau^+\nu_\tau$," in *10th International Workshop on the CKM Unitarity Triangle (CKM 2018) Heidelberg, Germany, September 17-21, 2018*. 2019. `arXiv:1903.03102 [hep-ex]`.

[68] J. C. Pati and A. Salam, "Lepton Number as the Fourth Color," *Phys. Rev.* **D10** (1974) 275–289. [Erratum: Phys. Rev.D11,703(1975)].

[69] H. Georgi, "The State of the Art—Gauge Theories," *AIP Conf. Proc.* **23** (1975) 575–582.

[70] H. Georgi and S. L. Glashow, "Unity of All Elementary Particle Forces," *Phys. Rev. Lett.* **32** (1974) 438–441.

[71] H. Fritzsch and P. Minkowski, "Unified Interactions of Leptons and Hadrons," *Annals Phys.* **93** (1975) 193–266.

[72] I. Doršner, S. Fajfer, A. Greljo, J. F. Kamenik, and N. Košnik, "Physics of leptoquarks in precision experiments and at particle colliders," *Phys. Rept.* **641** (2016) 1–68, `arXiv:1603.04993 [hep-ph]`.

[73] i. González-Alonso, J. Martin Camalich, and K. Mimouni, "Renormalization-group evolution of new physics contributions to (semi)leptonic meson decays," *Phys. Lett.* **B772** (2017) 777–785, `arXiv:1706.00410 [hep-ph]`.

[74] R. Alonso, E. E. Jenkins, A. V. Manohar, and M. Trott, "Renormalization Group Evolution of the Standard Model Dimension Six Operators III: Gauge Coupling Dependence and Phenomenology," *JHEP* **04** (2014) 159, `arXiv:1312.2014 [hep-ph]`.

[75] **LHCb** Collaboration, R. Aaij *et al.*, "Measurement of the ratio of branching fractions $\mathcal{B}(B_c^+ \to J/\psi\tau^+\nu_\tau)/\mathcal{B}(B_c^+ \to J/\psi\mu^+\nu_\mu)$," *Phys. Rev. Lett.* **120** no. 12, (2018) 121801, `arXiv:1711.05623 [hep-ex]`.

[76] V. V. Kiselev, "Exclusive decays and lifetime of B_c meson in QCD sum rules," `arXiv:hep-ph/0211021 [hep-ph]`.

[77] I. P. Gouz, V. V. Kiselev, A. K. Likhoded, V. I. Romanovsky, and O. P. Yushchenko, "Prospects for the B_c studies at LHCb," *Phys. Atom. Nucl.* **67** (2004) 1559–1570, `arXiv:hep-ph/0211432 [hep-ph]`. [Yad. Fiz.67,1581(2004)].

[78] M. A. Ivanov, J. G. Korner, and P. Santorelli, "Exclusive semileptonic and nonleptonic decays of the B_c meson," *Phys. Rev.* **D73** (2006) 054024, `arXiv:hep-ph/0602050 [hep-ph]`.

[79] E. Hernandez, J. Nieves, and J. M. Verde-Velasco, "Study of exclusive semileptonic and non-leptonic decays of B_c - in a nonrelativistic quark model," *Phys. Rev.* **D74** (2006) 074008, `arXiv:hep-ph/0607150 [hep-ph]`.

[80] C.-T. Tran, M. A. Ivanov, J. G. Körner, and P. Santorelli, "Implications of new physics in the decays $B_c \to (J/\psi, \eta_c)\tau\nu$," *Phys. Rev.* **D97** no. 5, (2018) 054014, `arXiv:1801.06927 [hep-ph]`.

[81] T. D. Cohen, H. Lamm, and R. F. Lebed, "Model-independent bounds on $R(J/\psi)$," *JHEP* **09** (2018) 168, `arXiv:1807.02730 [hep-ph]`.

[82] C. W. Murphy and A. Soni, "Model-Independent Determination of $B_c^+ \to \eta_c\, \ell^+\, \nu$ Form Factors," `arXiv:1808.05932 [hep-ph]`.

[83] T. D. Cohen, H. Lamm, and R. F. Lebed, "Precision Model-Independent Bounds from Global Analysis of $b \to c\ell\nu$ Form Factors," `arXiv:1909.10691 [hep-ph]`.

[84] K. Hagiwara, A. D. Martin, and D. Zeppenfeld, "Tau Polarization Measurements at LEP and SLC," *Phys. Lett.* **B235** (1990) 198–202.

[85] M. Tanaka and R. Watanabe, "Tau longitudinal polarization in $B \to D\tau\nu$ and its role in the search for charged Higgs boson," *Phys. Rev.* **D82** (2010) 034027, `arXiv:1005.4306 [hep-ph]`.

[86] **BELLE** Collaboration, S. Hirose, "First Measurement of the τ Lepton Polarization in the Decay $\bar{B} \to D^*\tau^-\bar{\nu}_\tau$ at Belle," *PoS* **KMI2017** (2017) 054.

[87] R. Alonso, B. Grinstein, and J. Martin Camalich, "Lifetime of B_c^- Constrains Explanations for Anomalies in $B \to D^{(*)}\tau\nu$," *Phys. Rev. Lett.* **118** no. 8, (2017) 081802, `arXiv:1611.06676 [hep-ph]`.

[88] C. McNeile, C. T. H. Davies, E. Follana, K. Hornbostel, and G. P. Lepage, "Heavy meson masses and decay constants from relativistic heavy quarks in full lattice QCD," *Phys. Rev.* **D86** (2012) 074503, `arXiv:1207.0994 [hep-lat]`.

[89] **LHCb** Collaboration, R. Aaij *et al.*, "Measurement of the $B^\pm$ production cross-section in pp collisions at $\sqrt{s} = 7$ and 13 TeV," *JHEP* **12** (2017) 026, `arXiv:1710.04921 [hep-ex]`.

[90] A. G. Akeroyd and C.-H. Chen, "Constraint on the branching ratio of $B_c \to \tau\bar{\nu}$ from LEP1 and consequences for $R(D^{(*)})$ anomaly," *Phys. Rev.* **D96** no. 7, (2017) 075011, `arXiv:1708.04072 [hep-ph]`.

[91] M. L. Mangano and S. R. Slabospitsky, "The Contribution of $B_{(c)}$ mesons to the search for $B \to \tau^+\nu_\tau$ decays at LEP," *Phys. Lett.* **B410** (1997) 299–303, `arXiv:hep-ph/9707248 [hep-ph]`.

[92] T. Konstantin, "Spectroscopy and production of B_c mesons in ATLAS." Talk at *18th International Conference on B-Physics at Frontier Machines (BEAUTY2019)*, Ljubljana, Slovenia, 30 Sept 2019, 2019.

[93] M. Beneke and G. Buchalla, "The B_c Meson Lifetime," *Phys. Rev.* **D53** (1996) 4991–5000, `arXiv:hep-ph/9601249 [hep-ph]`.

[94] A. Greljo, J. Martin Camalich, and J. D. Ruiz-Álvarez, "The Mono-Tau Menace: From B Decays to High-p_T Tails," *Phys. Rev. Lett.* **122** no. 13, (2019) 131803, `arXiv:1811.07920 [hep-ph]`.

[95] S. Descotes-Genon, L. Hofer, J. Matias, and J. Virto, "Global analysis of $b \to s\ell\ell$ anomalies," *JHEP* **06** (2016) 092, `arXiv:1510.04239 [hep-ph]`.

[96] D. Bečirević, I. Doršner, S. Fajfer, N. Košnik, D. A. Faroughy, and O. Sumensari, "Scalar leptoquarks from grand unified theories to accommodate the B-physics anomalies," *Phys. Rev.* **D98** no. 5, (2018) 055003, `arXiv:1806.05689 [hep-ph]`.

[97] W. Detmold, C. Lehner, and S. Meinel, "$\Lambda_b \to p\ell^-\bar{\nu}_\ell$ and $\Lambda_b \to \Lambda_c\ell^-\bar{\nu}_\ell$ form factors from lattice QCD with relativistic heavy quarks," *Phys. Rev.* **D92** no. 3, (2015) 034503, `arXiv:1503.01421 [hep-lat]`.

[98] Y. Sakaki, M. Tanaka, A. Tayduganov, and R. Watanabe, "Testing leptoquark models in $\bar{B} \to D^{(*)}\tau\bar{\nu}$," *Phys. Rev.* **D88** no. 9, (2013) 094012, `arXiv:1309.0301 [hep-ph]`.

[99] M. Bauer and M. Neubert, "Minimal Leptoquark Explanation for the $\mathrm{R}_{D^{(*)}}$, R_K , and $(g-2)_g$ Anomalies," *Phys. Rev. Lett.* **116** no. 14, (2016) 141802, `arXiv:1511.01900 [hep-ph]`.

[100] D. Bečirević, N. Košnik, O. Sumensari, and R. Zukanovich Funchal, "Palatable Leptoquark Scenarios for Lepton Flavor Violation in Exclusive $b \to s\ell_1\ell_2$ modes," *JHEP* **11** (2016) 035, `arXiv:1608.07583 [hep-ph]`.

[101] Y. Cai, J. Gargalionis, M. A. Schmidt, and R. R. Volkas, "Reconsidering the One Leptoquark solution: flavor anomalies and neutrino mass," *JHEP* **10** (2017) 047, `arXiv:1704.05849 [hep-ph]`.

[102] A. Crivellin and F. Saturnino, "Correlating Tauonic B Decays to the Neutron EDM via a Scalar Leptoquark," `arXiv:1905.08257 [hep-ph]`.

[103] P. Arnan, D. Becirevic, F. Mescia, and O. Sumensari, "Probing low energy scalar leptoquarks by the leptonic W and Z couplings," *JHEP* **02** (2019) 109, `arXiv:1901.06315 [hep-ph]`.

[104] L. Di Luzio and M. Nardecchia, "What is the scale of new physics behind the B-flavour anomalies?," *Eur. Phys. J.* **C77** no. 8, (2017) 536, `arXiv:1706.01868 [hep-ph]`.

[105] **SINDRUM II** Collaboration, W. H. Bertl *et al.*, "A Search for muon to electron conversion in muonic gold," *Eur. Phys. J.* **C47** (2006) 337–346.

[106] A. Denner, H. Eck, O. Hahn, and J. Kublbeck, "Feynman rules for fermion number violating interactions," *Nucl. Phys.* **B387** (1992) 467–481.

[107] A. Denner, H. Eck, O. Hahn, and J. Kublbeck, "Compact Feynman rules for Majorana fermions," *Phys. Lett.* **B291** (1992) 278–280.

[108] R. Mertig, M. Bohm, and A. Denner, "FEYN CALC: Computer algebraic calculation of Feynman amplitudes," *Comput. Phys. Commun.* **64** (1991) 345–359.

[109] V. Shtabovenko, R. Mertig, and F. Orellana, "New Developments in FeynCalc 9.0" *Comput. Phys. Commun.* **207** (2016) 432–444, `arXiv:1601.01167 [hep-ph]`.

[110] H. H. Patel, "Package-X: A Mathematica package for the analytic calculation of one-loop integrals," *Comput. Phys. Commun.* **197** (2015) 276–290, `arXiv:1503.01469 [hep-ph]`.

[111] **MuLan** Collaboration, D. M. Webber *et al.*, "Measurement of the Positive Muon Lifetime and Determination of the Fermi Constant to Part-per-Million Precision," *Phys. Rev. Lett.* **106** (2011) 041803, `arXiv:1010.0991 [hep-ex]`. [Phys. Rev. Lett.106,079901(2011)].

[112] A. Denner, "Techniques for calculation of electroweak radiative corrections at the one loop level and results for W physics at LEP-200," *Fortsch. Phys.* **41** (1993) 307–420, `arXiv:0709.1075 [hep-ph]`.

[113] M. Ciuchini, E. Franco, S. Mishima, and L. Silvestrini, "Electroweak Precision Observables, New Physics and the Nature of a 126 GeV Higgs Boson," *JHEP* **08** (2013) 106, `arXiv:1306.4644 [hep-ph]`.

[114] A. Lenz, U. Nierste, J. Charles, S. Descotes-Genon, A. Jantsch, C. Kaufhold, H. Lacker, S. Monteil, V. Niess, and S. T'Jampens, "Anatomy of New Physics in $B - \bar{B}$ mixing," *Phys. Rev.* **D83** (2011) 036004, `arXiv:1008.1593 [hep-ph]`.

[115] D. King, A. Lenz, and T. Rauh, "B_s mixing observables and —$\mathrm{V}_{td}/\mathrm{V}_{ts}$— from sum rules," *JHEP* **05** (2019) 034, `arXiv:1904.00940 [hep-ph]`.

[116] **ETM** Collaboration, N. Carrasco *et al.*, "B-physics from $N_f = 2$ tmQCD: the Standard Model and beyond," *JHEP* **03** (2014) 016, `arXiv:1308.1851 [hep-lat]`.

[117] **HPQCD** Collaboration, E. Gamiz, C. T. H. Davies, G. P. Lepage, J. Shigemitsu, and M. Wingate, "Neutral B Meson Mixing in Unquenched Lattice QCD," *Phys. Rev.* **D80** (2009) 014503, `arXiv:0902.1815 [hep-lat]`.

[118] Y. Aoki, T. Ishikawa, T. Izubuchi, C. Lehner, and A. Soni, "Neutral B meson mixings and B meson decay constants with static heavy and domain-wall light quarks," *Phys. Rev.* **D91** no. 11, (2015) 114505, `arXiv:1406.6192 [hep-lat]`.

[119] **Fermilab Lattice, MILC** Collaboration, A. Bazavov *et al.*, "$B^0_{(s)}$-mixing matrix elements from lattice QCD for the Standard Model and beyond," *Phys. Rev.* **D93** no. 11, (2016) 113016, `arXiv:1602.03560 [hep-lat]`.

[120] **Flavour Lattice Averaging Group** Collaboration, S. Aoki *et al.*, "FLAG Review 2019," `arXiv:1902.08191 [hep-lat]`.

[121] R. J. Dowdall, C. T. H. Davies, R. R. Horgan, G. P. Lepage, C. J. Monahan, J. Shigemitsu, and M. Wingate, "Neutral B-meson mixing from full lattice QCD at the physical point," `arXiv:1907.01025 [hep-lat]`.

[122] W. Altmannshofer, A. J. Buras, D. M. Straub, and M. Wick, "New strategies for New Physics search in $B \to K^* \nu\bar{\nu}$, $B \to K\nu\bar{\nu}$ and $B \to X_s \nu\bar{\nu}$ decays," *JHEP* **04** (2009) 022, `arXiv:0902.0160 [hep-ph]`.

[123] **Belle** Collaboration, J. Grygier *et al.*, "Search for $\boldsymbol{B \to h\nu\bar{\nu}}$ decays with semileptonic tagging at Belle," *Phys. Rev.* **D96** no. 9, (2017) 091101, `arXiv:1702.03224 [hep-ex]`. [Addendum: Phys. Rev.D97,no.9,099902(2018)].

[124] A. J. Buras, J. Girrbach-Noe, C. Niehoff, and D. M. Straub, "$B \to K^{(*)} \nu\bar{\nu}$ decays in the Standard Model and beyond," *JHEP* **02** (2015) 184, `arXiv:1409.4557 [hep-ph]`.

[125] **BaBar** Collaboration, B. Aubert *et al.*, "Searches for Lepton Flavor Violation in the Decays $\tau^\pm \to e^\pm \gamma$ and $\tau^\pm \to \mu^\pm \gamma$," *Phys. Rev. Lett.* **104** (2010) 021802, `arXiv:0908.2381 [hep-ex]`.

[126] R. Mandal and A. Pich, "Constraints on scalar leptoquarks from lepton and kaon physics.".

[127] V. Cirigliano and I. Rosell, "Two-loop effective theory analysis of $\pi(K) \to e\overline{\nu}_e[\gamma]$ branching ratios," *Phys. Rev. Lett.* **99** (2007) 231801, `arXiv:0707.3439 [hep-ph]`.

[128] M. Algueró, B. Capdevila, A. Crivellin, S. Descotes-Genon, P. Masjuan, J. Matias, and J. Virto, "Emerging patterns of New Physics with and without Lepton Flavour Universal contributions," *Eur. Phys. J.* **C79** no. 8, (2019) 714, `arXiv:1903.09578 [hep-ph]`.

[129] F. Hartmann, W. Kilian, and K. Schnitter, "Multiple Scales in Pati-Salam Unification Models," *JHEP* **05** (2014) 064, `arXiv:1401.7891 [hep-ph]`.

[130] G. Valencia and S. Willenbrock, "Quark - lepton unification and rare meson decays," *Phys. Rev.* **D50** (1994) 6843–6848, `arXiv:hep-ph/9409201 [hep-ph]`.

[131] L. Vale Silva, *Phenomenology of Left-Right Models in the quark sector*. PhD thesis, Orsay, IPN, 2016. `arXiv:1611.08187 [hep-ph]`.

[132] V. Tello, *Connections between the high and low energy violation of Lepton and Flavor numbers in the minimal left-right symmetric model*. PhD thesis, SISSA, Trieste, 2012. `http://hdl.handle.net/1963/6272`.

[133] N. G. Deshpande and R. J. Johnson, "Experimental limit on $SU(4)_C$ gauge boson mass," *Phys. Rev.* **D27** (1983) 1193.

[134] K. G. Chetyrkin, J. H. Kuhn, and M. Steinhauser, "RunDec: A Mathematica package for running and decoupling of the strong coupling and quark masses," *Comput. Phys. Commun.* **133** (2000) 43–65, `arXiv:hep-ph/0004189 [hep-ph]`.

[135] B. Schmidt and M. Steinhauser, "CRunDec: a C++ package for running and decoupling of the strong coupling and quark masses," *Comput. Phys. Commun.* **183** (2012) 1845–1848, `arXiv:1201.6149 [hep-ph]`.

[136] F. Herren and M. Steinhauser, "Version 3 of RunDec and CRunDec," *Comput. Phys. Commun.* **224** (2018) 333–345, `arXiv:1703.03751 [hep-ph]`.

[137] A. Maiezza, M. Nemevsek, F. Nesti, and G. Senjanovic, "Left-Right Symmetry at LHC," *Phys. Rev.* **D82** (2010) 055022, `arXiv:1005.5160 [hep-ph]`.

[138] R. Slansky, "Group Theory for Unified Model Building," *Phys. Rept.* **79** (1981) 1–128.

[139] D. Chang, R. N. Mohapatra, and M. K. Parida, "Decoupling Parity and SU(2)-R Breaking Scales: A New Approach to Left-Right Symmetric Models," *Phys. Rev. Lett.* **52** (1984) 1072.

[140] D. Chang, R. N. Mohapatra, and M. K. Parida, "A New Approach to Left-Right Symmetry Breaking in Unified Gauge Theories," *Phys. Rev.* **D30** (1984) 1052.

[141] K. S. Babu, B. Bajc, and S. Saad, "Yukawa Sector of Minimal SO(10) Unification," *JHEP* **02** (2017) 136, `arXiv:1612.04329 [hep-ph]`.

[142] J. G. Korner and G. A. Schuler, "Exclusive Semileptonic Decays of Bottom Mesons in the Spectator Quark Model," *Z. Phys.* **C38** (1988) 511. [Erratum: Z. Phys.C41,690(1989)].

[143] C. G. Boyd, B. Grinstein, and R. F. Lebed, "Constraints on form-factors for exclusive semileptonic heavy to light meson decays," *Phys. Rev. Lett.* **74** (1995) 4603–4606, `arXiv:hep-ph/9412324 [hep-ph]`.

[144] J. Matias, F. Mescia, M. Ramon, and J. Virto, "Complete Anatomy of $\bar{B}_d \to \bar{K}^{*0}(\to K\pi)l^+l^-$ and its angular distribution," *JHEP* **04** (2012) 104, `arXiv:1202.4266 [hep-ph]`.

[145] S. Descotes-Genon, J. Matias, M. Ramon, and J. Virto, "Implications from clean observables for the binned analysis of $B \to K * \mu^+\mu^-$ at large recoil," *JHEP* **01** (2013) 048, `arXiv:1207.2753 [hep-ph]`.

[146] S. Descotes-Genon, T. Hurth, J. Matias, and J. Virto, "Optimizing the basis of $B \to K^* ll$ observables in the full kinematic range," *JHEP* **05** (2013) 137, `arXiv:1303.5794 [hep-ph]`.

[147] **LHCb** Collaboration, R. Aaij *et al.*, "Measurement of Form-Factor-Independent Observables in the Decay $B^0 \to K^{*0}\mu^+\mu^-$," *Phys. Rev. Lett.* **111** (2013) 191801, `arXiv:1308.1707 [hep-ex]`.

[148] S. Descotes-Genon, J. Matias, and J. Virto, "Understanding the $B \to K^*\mu^+\mu^-$ Anomaly," *Phys. Rev.* **D88** (2013) 074002, `arXiv:1307.5683 [hep-ph]`.

[149] B. Capdevila, S. Descotes-Genon, L. Hofer, and J. Matias, "Hadronic uncertainties in $B \to K^* \mu^+ \mu^-$: a state-of-the-art analysis," *JHEP* **04** (2017) 016, `arXiv:1701.08672 [hep-ph]`.

[150] M. Bordone, G. Isidori, and A. Pattori, "On the Standard Model predictions for R_K and R_{K^*}," *Eur. Phys. J.* **C76** no. 8, (2016) 440, `arXiv:1605.07633 [hep-ph]`.

[151] **Belle** Collaboration, A. Abdesselam *et al.*, "Test of lepton flavor universality in $B \to K^* \ell^+ \ell^-$ decays at Belle," `arXiv:1904.02440 [hep-ex]`.

[152] **LHCb** Collaboration, R. Aaij *et al.*, "Test of lepton universality with $B^0 \to K^{*0} \ell^+ \ell^-$ decays," *JHEP* **08** (2017) 055, `arXiv:1705.05802 [hep-ex]`.

[153] **LHCb** Collaboration, R. Aaij *et al.*, "Search for lepton-universality violation in $B^+ \to K^+ \ell^+ \ell^-$ decays," *Phys. Rev. Lett.* **122** no. 19, (2019) 191801, `arXiv:1903.09252 [hep-ex]`.